# Development of a Wall Climbing Inspection Robot with High Mobility on Complex Shaped Walls

---

A thesis submitted in partial fulfilment of the requirements for

the Degree

of Master of Engineering in Mechanical Engineering

in the University of Canterbury

by Yuan Chang

University of Canterbury

2015

---

# Acknowledgements

Firstly I would like to express my sincere gratitude to my supervisor, Professor Xiaoqi Chen, who provided me continuous support throughout my thesis research. I attribute the level of my Master degree to his patience, encouragement, motivation and immense knowledge.

My sincere thanks also go to my fellow labmates for their stimulating conversations and great help.

Last but not the least, I would like to thank my family for supporting me spiritually throughout writing this thesis and my life in general.

# Contents

# List of Figures:

# List of Tables:

Deputy Vice-Chancellor's Office
Postgraduate Office

UNIVERSITY OF CANTERBURY
*Te Whare Wānanga o Waitaha*
CHRISTCHURCH NEW ZEALAND

# Co-Authorship Form

This form is to accompany the submission of any thesis that contains research reported in co-authored work that has been published, accepted for publication, or submitted for publication. A copy of this form should be included for each co-authored work that is included in the thesis. Completed forms should be included at the front (after the thesis abstract) of each copy of the thesis submitted for examination and library deposit.

Please indicate the chapter/section/pages of this thesis that are extracted from co-authored work and provide details of the publication or submission from the extract comes:

*Chapter 3 (Pages:47-63) and Chapter 4 (Pages:64-86) of the thesis are extracted from following co-authored work:*

1. Yuan Chang, Xiao-Qi Chen. "Design of A Scalable Wall Climbing Robot for Inter-Plane Traversing," The 4th International Conference on Robotic Welding, Intelligence and Automation (RWIA'2014), Shanghai, China, Oct. 25-27, 2014.
2. Chang Y., Chen, X.Q. (2015), "Design of a Scalable Wall Climbing Robot for Inter-Plane Traversing", Robotic Welding, Intelligence and Automation, Advances in Intelligent System, Computing, Vol. 363, Springer Verlag, Editors: Tarn, T.-J., Chen S.B., Chen, X.Q, ISBN 978-3-319-18997-0, DOI 10.1007/978-3-319-18997-0, pp.145-158.

Please detail the nature and extent (%) of contribution by the candidate:

*The candidate is the lead author who wrote the text. 70% above co-authored published work is contributed by the candidate.*

**Certification by Co-authors:**

If there is more than one co-author then a single co-author can sign on behalf of all

The undersigned certifys that:

- The above statement correctly reflects the nature and extent of the PhD candidate's contribution to this co-authored work
- In cases where the candidate was the lead author of the co-authored work he or she wrote the text

Name: *Xiaoqi Chen* Signature: *XIAOQi CHEN* Date: *28/09/2015*

# Abstract

Wall-climbing robots have been widely used in fields of inspection, building cleaning, welding, and so on. These robots can freely move on surfaces with various inclinations, e.g. vertical walls and ceilings. In addition to fundamental locomotion (e.g. wheels, tracks and legs) for robot mobility, a wall-climbing robot must counter the force of gravity for firmly adhering to the inclined work surface by employing adhesion mechanisms (e.g. vacuum suction, magnetic adhesion, etc). In the past decades, various adhesion and locomotion mechanisms have been developed for wall-climbing robots. In practical applications, one of the greatest challenges for wall-climbing robots is to develop optimum adhesion and locomotion mechanisms which enable wall-climbing robots to freely move on various types of complex shaped structure surfaces with various inclined walls, such as milk tanks, ventilation ducts, and so on.

This study aims to design and develop a compact and reliable wall-climbing robot with high mobility on complex shaped walls, such as passing 90° convex and concave obstacles with any inclination regarding the gravity, for the inspections of ducts, tanks, bridges, etc.

Firstly an overview of the state-of-the-art of the research and development of wall-climbing robots around the world is given. The advantages and disadvantages of various adhesion and locomotion mechanisms are comprehensively discussed for wall-climbing robots for different applications.

A modular wall-climbing inspection robot is proposed. The modular design allows the robot to be easily scaled by changing the number of wheeled modules to be joined together. The active joint is able to fold the robot modules to pass various obstacles. General-purpose vacuum suction is employed to enable robot to adhere to various (e.g. metal, wood, glasses, concrete and plastics) structure surfaces. A two-module wall-climbing robot prototype was developed by using SolidWorks. Mechanic design and kinetics analysis of a two-module robot are presented. Comprehensive simulations

demonstrate that the proposed wall-climbing robot is capable of freely moving on complex shaped walls.

Furthermore, for ferromagnetic structures (such as ships, bridges, steel tanks, and so on), the modular wall-climbing robot with magnetic adhesion is investigated. Compared with general-purpose vacuum suction, magnetic adhesion offers an energy-saving and reliable adhesion solution. Mechanical design and kinetics analysis of a two-module robot with built-in electromagnetic adhesion are given. Simulations validate such an alternative robot design.

The major contributions of this thesis include:

- A modular wall-climbing inspection robot is proposed. The advantages of the proposed robot include high mobility on complex shaped walls, simple structure, easy control, good reliability, low cost, and being scalable.
- Two types of two-module wall-climbing robot prototypes with different adhesion mechanisms are designed and developed. The robot with general-purpose vibration adhesion mechanism is applicable to the climbing of various structure walls, while the robot with electromagnetic adhesion mechanism offers an optimal climbing device for ferromagnetic walls.
- Comprehensive design, kinematic analysis and simulations of the two-module wall-climbing robots are successfully completed.

# Chapter 1 Introduction

## 1.1 Motivation

The purpose of this work is to investigate and develop a wall-climbing robot for applications of duct inspection, bridge maintenance, etc.

Wall-climbing robots, which have been developed in the last few decades, are mainly employed for the tasks that are dangerous or costly when performed by a human operator in the harsh environment. As shown in Figure 1, these tasks include wall cleaning of high buildings, remote maintenance of large storage tanks, inspection of large concrete structures such as bridge pylons, cooling towers or dams and in-pipe inspections.


**Figure 1: Applications of wall-climbing robot [1]**

An overview of applications of wall-climbing robots will be presented in the following section.

## 1.2 Applications of Wall-Climbing Robots

A number of wall-climbing robots have been developed in the past decades, which have already been widely used in following applications:

a) Inspection

Inspection robots are used to detect defects of various structures. Kalra, et al. [2] built an autonomous wall-climbing robot, which can climb along the external wall of oil storage tanks and carry out inspection independently with an ultrasonic sensor. Shao et al. [3] built a wall-climbing robot with gecko features which can be used to inspect and maintain high conical towers for wind power generators. The climbing robot CROMSCI is developed to carry out inspection of large concrete structures, such as bridge pylons, cooling towers or dams [4]. An "insect" inspired autonomous wall-climbing robot ROMA [5] is developed to inspect a complex 3D metallic-based bridge structure. A remote-controlled robot with single suction cup is built to perform ultrasonic inspection of nuclear storage tanks [6]. Climbing robots can also be used to detect defects of reservoirs tanks and pipelines, such as pinholes, cracks and thickness reduction [7]. Luk et al. [8] developed a climbing robot, SADIE, which is used to perform inspection of various welds in the main reactor cooling gas ducts at Sizewell 'A' nuclear Power Station. Sattar et al. [9] built a ring formation climbing robot which is capable of inspecting defects on wind turbine blades. A small size climbing robot is capable of performing the detection of welds porosity, lack of root penetration and internal cracks on the hull of ship is given by Mondal et al.[10]. A micro biped robot for aircraft structure inspection is reported in [11]. A tracked robot is developed to perform diary container inspection in [12]. Ariga et al. [13] developed a pantograph-type structural wall-climbing robot that can move and inspect within narrow space, such as sewer pipe. Tache et al. [14] developed a two-wheeled robot used for inspecting complex shaped pipe environments.

b) Cleaning

An auto-climbing robot is designed for cleaning the spherical surface of the National

Grand Theatre in China [15]. A underwater cleaning robot adopting flexible crawling mechanism is presented in [16]. A robot named Skycleaner is developed for cleaning glass walls of high-rise buildings [17]. A heavy-load wall climbing robot with ultra high pressure water jetting equipment for ship rust removal is reported in [18].

c) Security

The City-Climber robot is used in urban environments for search and rescue, weapon or tool delivery, inspection and reconnaissance purposes [19]. Guo et al. [20] developed an anti-terrorist purpose wall-climbing robot, which has six legs and a low-noise vacuum adhesion mechanism.

d) Welding

Wu et al. [21] developed a welding robot using magnetic adhesion mechanism. Taylor et al. [22] built a climbing welding robot named TigBot, which adopts vacuum suction.

e) Grit Blasting or Painting

A climbing robot is built for grit blasting operations in shipyards [23]. A wall-climbing robot adopting two magnetic tracks is developed for hull painting [24].

## 1.3 Essential Elements of Wall-Climbing Robot

In addition to fundamental locomotion (e.g. wheels, tracks and legs) for robot mobility, a wall-climbing robot must be able to carry functional instrumentations and counter the force of gravity for firmly adhering to the inclined structure surfaces by employing adhesion mechanisms (e.g. vacuum suction, magnetic adhesion, etc.). In practical applications, one of the greatest challenges for wall-climbing robots is to freely move on various types of complex shaped structure surfaces, such as passing 90° convex and concave obstacles with any inclination regarding the gravity. Adhesion and locomotion mechanisms are the two essential elements of wall-climbing robots. Each adhesion or locomotion mechanism has its own strengths and weaknesses.

### 1.3.1 Adhesion Mechanisms

One essential element of wall-climbing robot is the adhesion mechanism, which can generate pressure to secure the robot on walls. The adhesion mechanisms of wall-climbing robots can mainly be categorized into:

1) Vacuum adhesion, or negative pressure suction;
2) Magnetic adhesion;
3) Dry adhesion or Van Der Waals force adhesion;
4) Electrostatic adhesion.

Vacuum adhesion, or negative pressure adhesion, is widely employed in wall-climbing robots, as it has several eminent advantages, such as simple structure, general-purpose adhesion to various types of surfaces, which include ferromagnetic and non-ferromagnetic surfaces. Vibration suction is also reported as a new kind of negative pressure (or vacuum adhesion) suction, where negative pressure can be generated and strengthened through the vibration of the suction cup. Compared with conventional vacuum adhesions using suction actuator or engine, vibration suction has the advantages of lower power consumption, higher stability in suction force and relatively lower noise. However, the vacuum adhesion is usually not robust against dusty or rough surfaces; air leakage and the consequently the loss of negative pressure often occur when robot moves.

Although magnetic adhesion using permanent magnets or/and electromagnets is not applicable to many types of surfaces (e.g. wood, concrete or glass), it is a very reliable adhesion solution for wall-climbing robots attaching on ferromagnetic structures in terms of energy efficiency and robust adhesion.

Dry adhesion, also known as Van Der Waals force, is based on nanofabrication technique inspired by creatures such as geckos. The principle of this mechanism is to generate Van der Waals forces between the surface and the microscopic fibril tape attached on robot. This technology has shown great potential in industry application due to its low power consumption. However, the mechanism often fails on dusty and moist surfaces, and its elastomeric materials tend to lose the adhesion force after being repeatedly used [12, 25].

Electrostatic adhesion has been developed recently. It is capable of adhering to wall surfaces made of a wide range of materials, such as wood, glass, metal and many other construction materials. The advantages of such adhesion mechanism include electrically controllable adhesion, low power consumption, and being capable of working on dusty and wet surfaces. However, reported drawbacks of this mechanism include: 1) its adhesion force will decrease on damp concrete surfaces; 2) it can only work over a short distance as the adhesion surface usually becomes clogged.

### 1.3.2 Locomotion Mechanisms

Another crucial element of wall-climbing robot is locomotion mechanism for mobility. Optimum locomotion should be selected regarding the given tasks and the operation environment. The most common locomotion mechanisms of the wall-climbing robot include legged locomotion, tracked locomotion, and wheeled locomotion.

Legged locomotion is predominately used, as legged robots can step over obstacles and have relatively high mobility on discontinuous surfaces. However, the design and development of legged locomotion involves complex mechanical structure design and multi-degree-of-freedom gait control, and this gait in turn will result in low moving velocity of legged robots.

Tracked locomotion is relatively fast and less complex. Consequently, it is often used in applications such as inspection and maintenance of large tanks. However, the robots using tracked locomotion mechanism often have difficulty in passing over large steps or obstacles.

Compared to the tracked locomotion, wheeled locomotion is more flexible in steering. It can be of simple mechanical structure, and does not need multi-degree-of-freedom control. Similar to tracked locomotion, wheeled locomotion is also inferior in negotiating obstacles.

## 1.4 Development of Wall-Climbing Inspection Robots

For various inspection tasks, it is often a challenging job to design and develop agile wall-climbing robots which can freely move on various complex shaped structures, such as

ventilation ducts, milk tanks, bridges, and so on. In this thesis, the research study is dedicated to develop a compact and reliable wall-climbing inspection robot with high mobility on complex shaped walls, such as passing 90° convex and concave obstacles with any inclination conquering the gravity. Compared with the reported robots [19, 25-26], the proposed robots have the advantages of compact size, simple structure and reliable performance. This robot is developed for the inspections of ducts, tanks, bridges, etc.

## 1.5 Organization of the Thesis

This thesis is organized as follows:

- Chapter 1 gives a brief introduction to the motivation of this research study;
- Chapter 2 presents an overview of the state-of-the-art of the research and development of wall-climbing robots around the world;
- Chapter 3 presents the design of the proposed modular wall-climbing wheeled robot for general-purpose inspection, which employs vacuum suction mechanism;
- Chapter 4 presents kinetics analysis of a proposed the two-module wall-climbing robot prototype. Comprehensive simulations are carried out to verify the proposed design;
- Chapter 5 presents the design of the proposed modular wall-climbing robot for specific inspection (such as steel vessels), which employs built-in electromagnetic adhesion;
- Chapter 6 draws conclusions and discusses promising future work.

# Chapter 2 Literature Review

This literature review investigates state-of-the-art research work on wall-climbing robots. It mainly involves the advances of various adhesion and locomotion mechanisms for wall-climbing robots, and also discusses various wall-climbing robots' mobility.

## 2.1 Adhesion Mechanism

Adhesion mechanisms for wall-climbing robots primarily include vacuum adhesion (or negative pressure suction), magnetic adhesion, dry adhesion (or Van Der Waals force adhesion) and electrostatic adhesion.

### 2.1.1 Vacuum Adhesion

Vacuum adhesion, or negative pressure suction, is considered the most commonly used adhesion method for wall-climbing robots. Its advantages include simple structure and good adaptability to various types of surfaces (including non-ferromagnetic surface). Negative pressure suction cup or chamber is the common vacuum adhesion mechanisms for wall-climbing robot in practical applications.

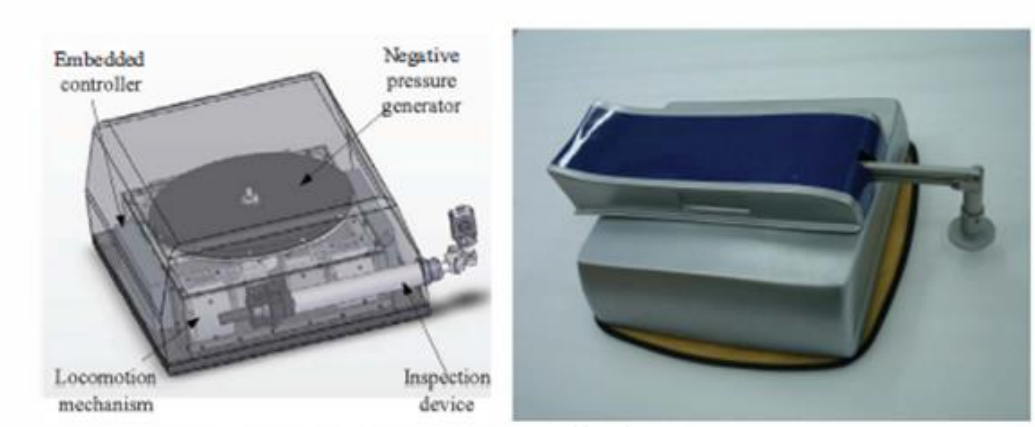


**Figure 2: An example of wall-climbing robot which uses cavity body as suction cup [27] .**

Negative pressure suction cups are usually implemented in several ways: 1) the cavity body of the robot [6, 27-28] acts as the suction cup (shown in Figure 2) ; 2) suction cups

are mounted at the tips of locomotion legs [11, 20, 28-29]; 3) suction cups are installed on the feet of a caterpillar robot [30] (shown in Figure 3); 4) suction cups are installed on the tracks [31-32]; 4) cups are mounted under the chassis of the main body [12, 19].

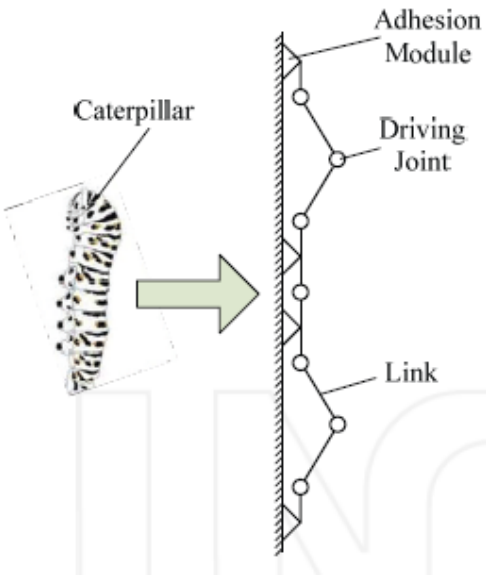


**Figure 3: A caterpillar robot using feet as suction cup[30] .**

The negative pressure can be generated by using various devices: 1) suction engine [4, 33]; 2) vacuum generator with pipes [29]; 3) an hydraulic generator connected to the robot by a hose in the tether link [16]; 4) a plunger pump which is driven by a DC motor [20] (shown in Figure 4); 5) spinning-motor driven centrifugal impeller [6, 27, 34-35] (shown in Figure 5); 6) common passive suction cups [36]; 7) vibration mechanism [37].

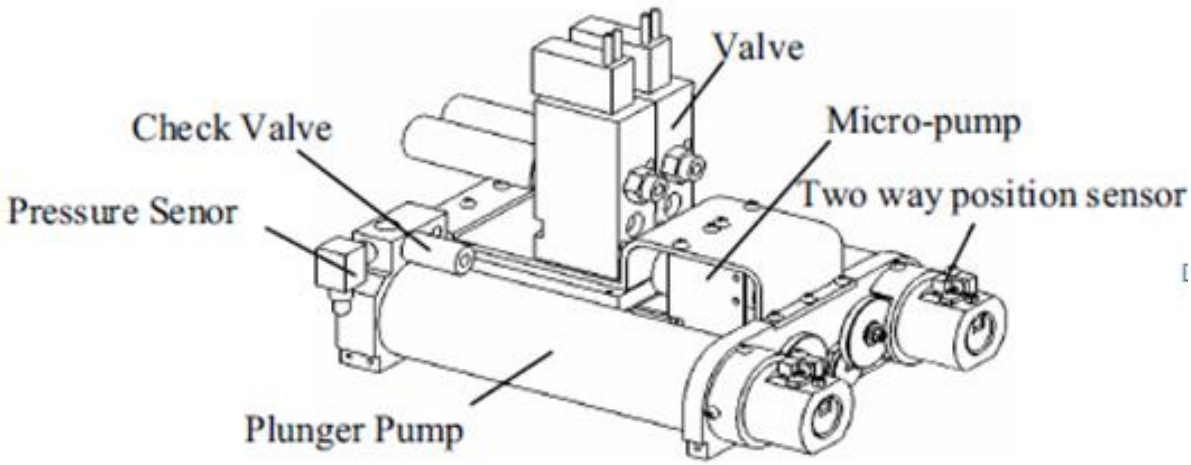


**Figure 4: A plunger pump used in a six-legged robot to generate negative pressure [20] .**

The vibration mechanism is also known as Vibration Suction [30, 37-41] (shown in Figure 6), which is reported as a new kind of negative pressure suction method. Negative pressure is generated through the vibration of the suction cup, and can be strengthened by increasing the amplitude and frequency of the vibration. This way has the advantages of low power consumption, high stability in suction and relatively low noise. Moreover, compared with the vacuum pump based adhesion mechanisms, the vibration mechanism is relatively light and compact.

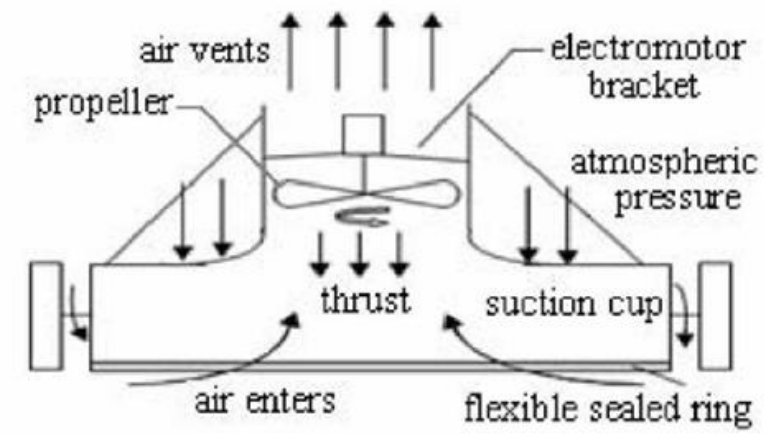


**Figure 5: A centrifugal impeller is used as suction system [34].**

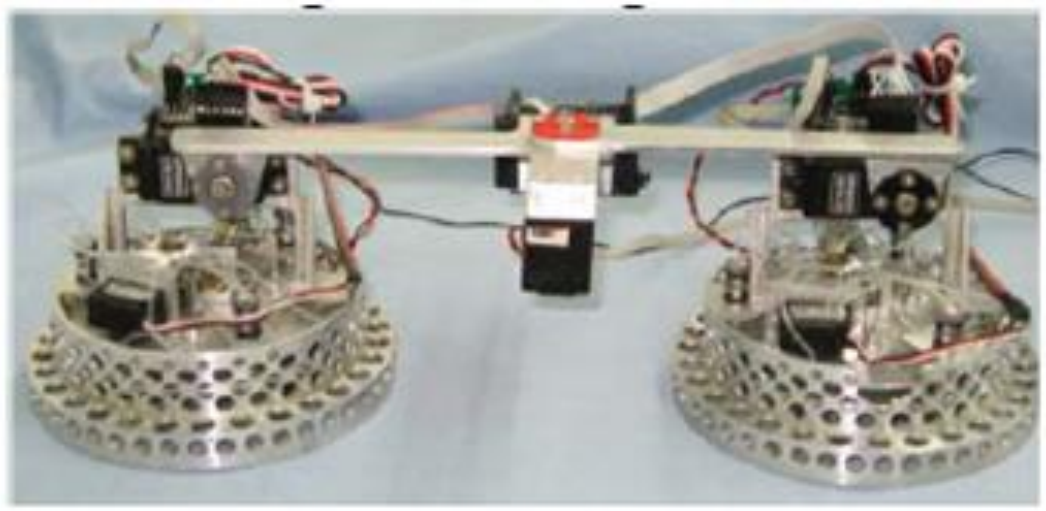

**Figure 6: A biped robot using vibration suction[38].**

However, the vacuum adhesion is often not robust against dusty or rough surfaces, because the suction cups are designed with certain degree of stiffness and may not well attach on a rough surface, thus causes air leakage, and in turn, the loss of negative pressure.

The material and stiffness of the suction cup may affect the properties of the robot in several aspects: 1) the elasticity of the cups could determine its sealing property; 2) the soft cups tend to have low sliding ability and can easily stick to surfaces, but are prone to wear; 3) suction cups made from low friction coefficient material may reduce the energy consumption of driving.

### 2.1.2 Magnetic Adhesion

Although a magnet adhesion using permanent magnets or/and electromagnets is not applicable to concrete or glass surfaces, it offers the best solution to ferromagnetic structure adhesion in terms of energy efficiency, adhesive force and reliability. It has been adopted by many wall-climbing robots for clinging to steel structures.

The adhesion force of a magnetic mechanism can be determined by the magnetic property of the magnet it used, the ferromagnetic characteristics of the surface and the distance between suction mechanism and the surface.

There are several types of magnetic mechanisms in practical applications: 1) permanent magnets or electromagnets fixed at the end of legs [42-43]; 2) tracks equipped with multiple integrated magnets [2-3, 44-45] (shown in Figure 7 to Figure 9); 3) magnetic wheels [7, 46-47]. Figure 10 shows a new type of variable permanent magnet wheel [48], which contains an inner wheel and a coaxially assembled outer wheel. The magnetic force can be adjusted by rotating the outer wheel.

**Figure 7: An robot with tracks equipped with multiple integrated magnets [2].**

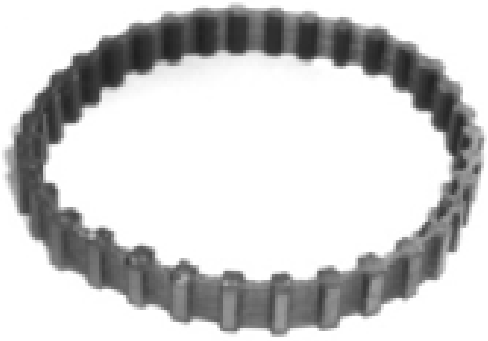

**Figure 8: Track with multiple integrated magnets [44].**

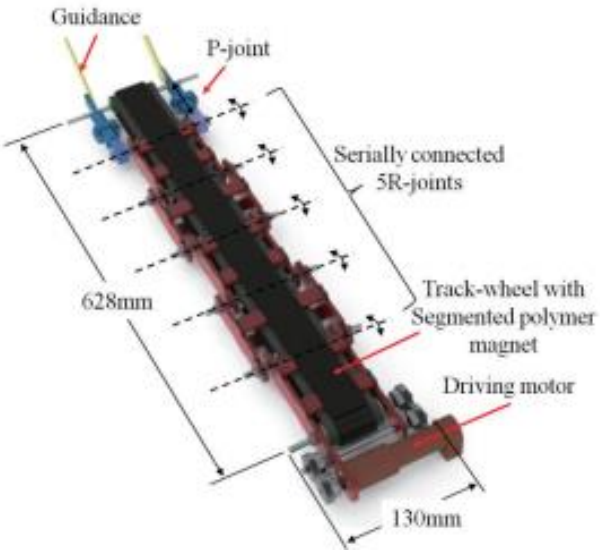


**Figure 9: A caterpillar robot with compliant magnetic track [45].**

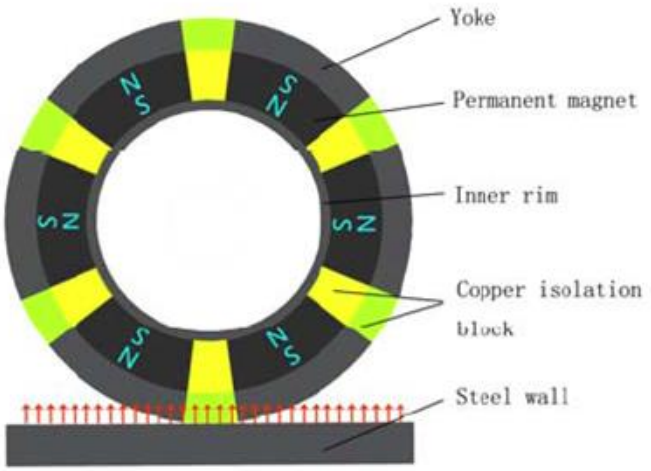


**Figure 10: Structure of variable magnetic force wheel [48].**

Compared with the magnetic track, the magnetic wheel often takes lower energy-efficiency due to its smaller load area. To facilitate wheeled locomotion, magnets can be installed under the robot body in a non-contact manner [21, 49]. An example of magnetic sucker is shown in Figure 11.

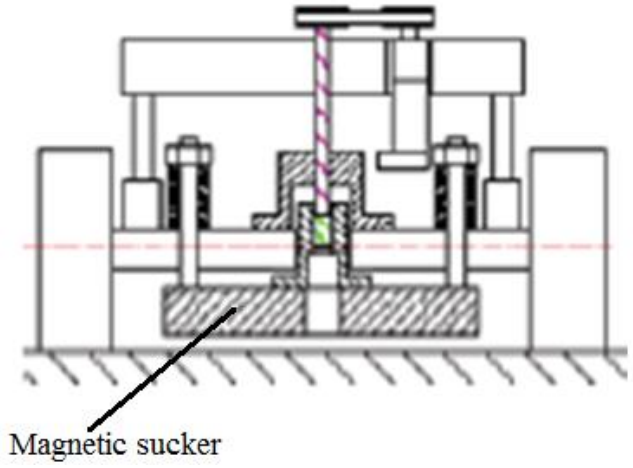


**Figure 11: Structure of a magnetic sucker [21].**

### 2.1.3 Dry Adhesion

Dry adhesion, also known as Van Der Waals force, is based on nanofabrication technique inspired by creatures such as geckos. Dry adhesion mechanism can generate Van der Waals forces between the surface and the microscopic fibril tape attached on the robot.

Dry adhesion has been applied in wall-climbing robots to achieve a sticking and releasing mechanism similar to gecko feet. The operation of such mechanism commonly consists of three phases: attaching, preloading (to increase adhesion force) and peeling (to remove the adhesive on the Surface and make robot move to another position).

Examples of robots adopting dry adhesion mechanism are shown in Figure 12. These robots include: 1) a gecko inspired robot with four legs [50-51]; 2) a tracked locomotion climbing robot with mushroom-shape nanotechnology setae on the belts[52]; 3) a tracked robot with flat sticky polymer (pressure-sensitive Vytaflex-10 Smooth-on Inc.) on belts[26]; 4) a leg-wheeled robot consisting of four legs and a passive wheel [53]; 5) a multi-spoke structural wheeled-legs locomotion robot with the pressure-sensitive adhesive fibres

attached on each spoke [54-56]; 6) a six-legged robot with Polydimethylsiloxane (PDMS) attached on feet [57].

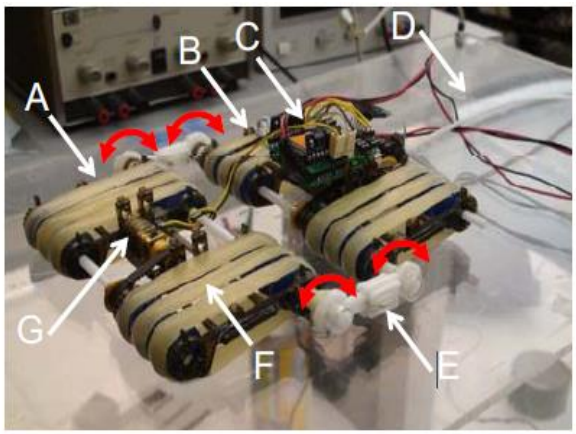


**(a) [26]**

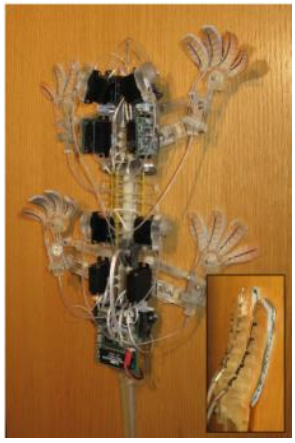

**(b) [50]**

**(c) [52]**

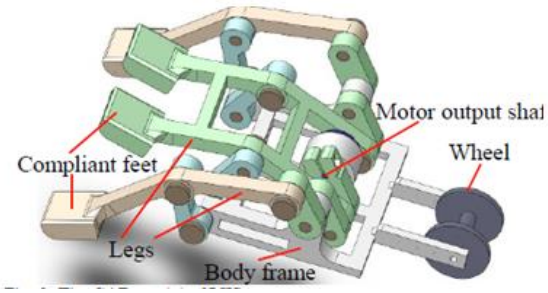


**(d) [53]**

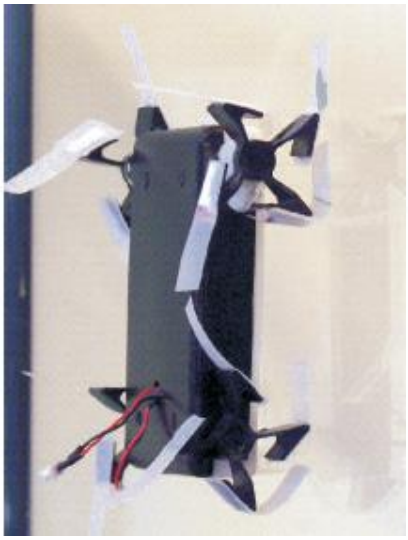

**(e) [54]**

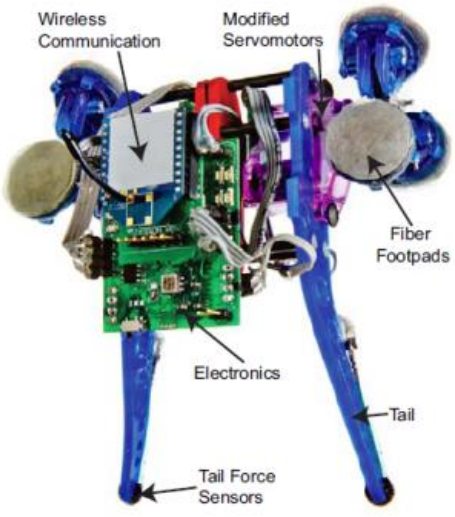


**(f) [55]**

**Figure 12: Examples of wall-climbing robot with dry adhesion mechanism.**

Previous studies indicate that dry adhesion force will increase with the contact area of the adhesive material and the preloading on this area. It is also reported that the geometry property of the setae can influence the micro-scale adhesion [58].

Some wall-climbing robots using no-energy-consumption dry adhesions have shown great potential in industry applications. However, the previous study shows that dust and moisture on the wall may cause this adhesion mechanism to lose its adhesion force. The adhesion may also decrease after being repeatedly used. Another restriction of such mechanism for practical applications is due to the high manufacturing cost of the nanotechnology setae.

### 2.1.4 Electrostatic Adhesion

Electrostatic adhesion has been developed recently. It has the capability of working on a wide range of materials, including fibre cloth, wood, glass, metal and some common construction materials [59]. The fundamental principle behind such mechanism is that - when an adhesive pad is placed near a wall surface, the electrostatic adhesion voltage of the robot can generate electrostatic charges on the pad whilst induce opposite charges on the wall surface, thus will produce electrostatic adhesion between the adhesive pad and the wall surface.

The advantages of the mechanism include low power consumption, simple structure, lightweight, low noise and capability of working on dusty and wet surfaces. However, it is reported that the electrostatic adhesion is inferior in attaching on damp concrete surfaces [59]. Another drawback is that this adhesion mechanism currently is only suitable for short-distance working as the adhesion surface is apt to become clogged.

Figure 13 presents three examples of robots which adopt electrostatic adhesion. Figure 13(a) shows a tracked locomotion wall-climbing robot, which uses lithium batteries to drive two DC motors and excite the electrostatic adhesion force on the compliant interdigital electrode panel [60]. Figure 13(b) shows a four-leg robot which has a structure and climbing gait similar to a real gecko [61]. Figure 13(c) shows a thin inchworm type climbing robot [62].

(a)[60]

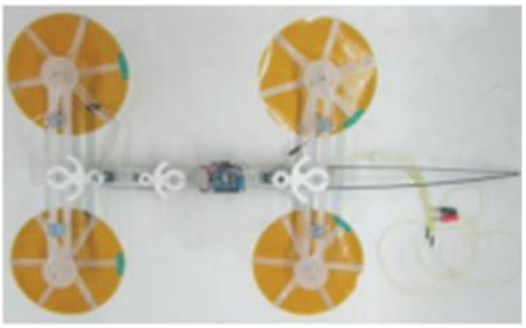

(b) [61]

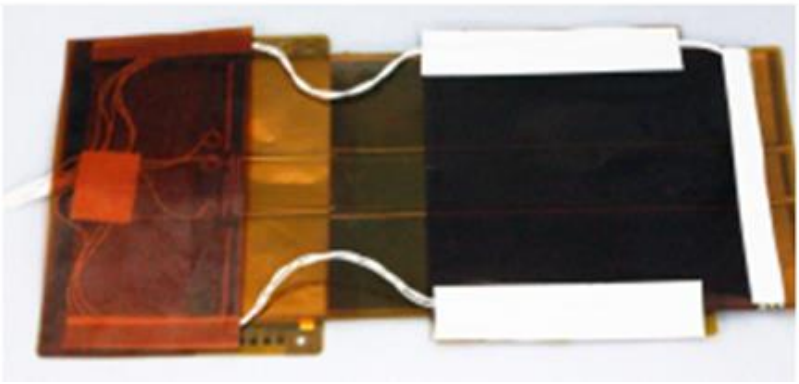

(c) [62]

**Figure 13: Robots adopting electrostatic adhesion.**

The electrostatic adhesion force is determined by several factors, such as the applied electrostatic voltages, the electric conductivity of the wall surface, the geometrical properties of the electrostatic pad, and the working environment.

### 2.1.5 Other Adhesion Mechanisms

Besides the four adhesion mechanisms described above, several other adhesion mechanisms are available for wall-climbing robots, such as

**Hot Melt Adhesion**: Osswald et al. [63] developed a climbing robot that uses hot melt adhesion mechanism for attaching. The material used in this adhesion mechanism is temperature-dependent, which means it can repeatedly transform between fluid and solid states by controlling the temperature. Although hot melt adhesion mechanism can provide

robust attach–detach processes, it is relatively slow, and may leave residue on the path when the robot moves.

**Claw**: A four-leg climbing robot CLIBO has been developed by Sintov, et al. [64]. Specially designed claws are attached on each leg, which enables the robot to navigate on the rough wall and to move in any direction. The claw device is shown in Figure 14.

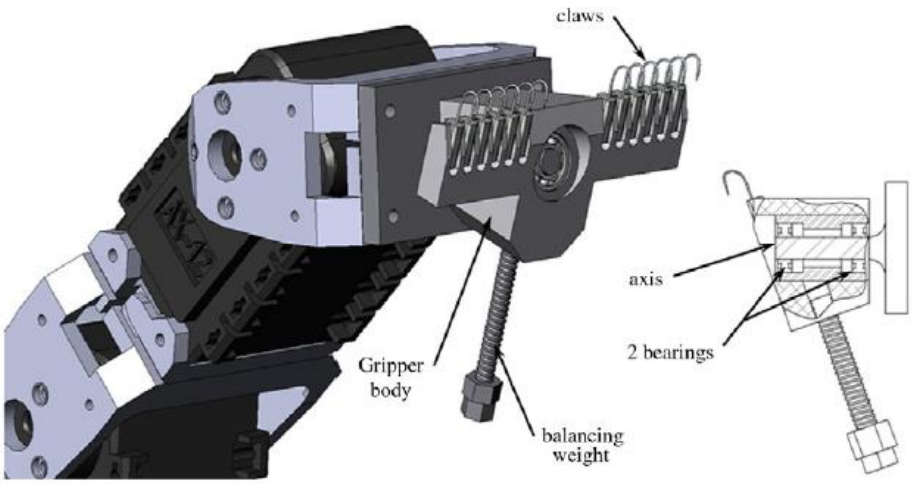


**Figure 14: The claw device of a robot [64].**

**Gripper:** ROMA I is a robot which has two grippers fixed at the end of two arms [5]. The grippers can perform various actions, such as grasping and releasing.

**Figure 15: ROMA I [5].**

## 2.2 Locomotion Mechanism

Another crucial element of wall climbing robot is locomotion mechanism, which determines the motion capability of the robot. The current locomotion mechanisms of the wall-climbing robot can mainly be categorized into legged, tracked, wheeled and sliding locomotion mechanisms.

### 2.2.1 Legged Locomotion

Among all the wall-climbing robots, legged locomotion is predominately used.

Depending on the individual task, different legged wall-climbing robots have been designed. These robots include biped robot containing several controllable active joints [11, 37, 57, 65], four-legged robot [50, 64] and six-legged robot [20, 43]. Figure 16 presents three types of legged locomotion robots. Legged robots usually are designed with multi-degree of freedom for enhancing their mobility.

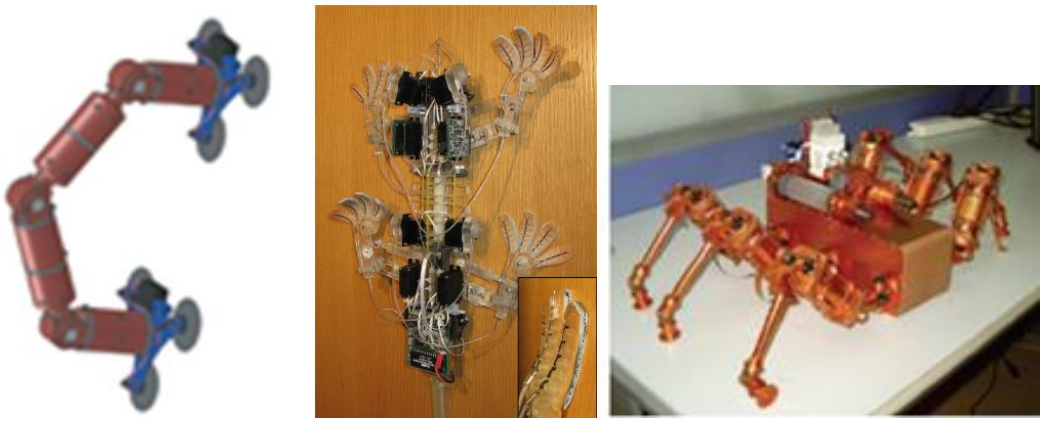

**(a)[66]** **(b)[50]** **(c)[20]**

**Figure 16: Legged locomotion robots.**

Legged robots motions, including walking, negotiating obstacles and making plane transitions, are archived through alternatively attaching one (group) foot to the working surface and releasing another one (group). Commonly, the legs of the robot are separated into two groups; when one suction group attaches to the working surface to support the robot, the other suction group moves to a target position and adheres to the wall; the former suction group then releases the adhesion and moves to a new position.

To make the robot efficiently and safely perform these motions, it is important to design the gait. As a result, many studies of the legged robot have focused on the gait planning. For example, a six-legged robot which has an optimal gait has been built by Boscariol et al. [57]. This robot is considered to have higher safety on vertical walls because only one leg detaches to the working surface when it moves, as shown in Figure 17. Another example is a fuzzy multi-sensor data fusion system developed by Xiao et al.[67]. By applying this intelligent control system, robot can effectively synthesize sensory information, then plan the actions and control the motions.

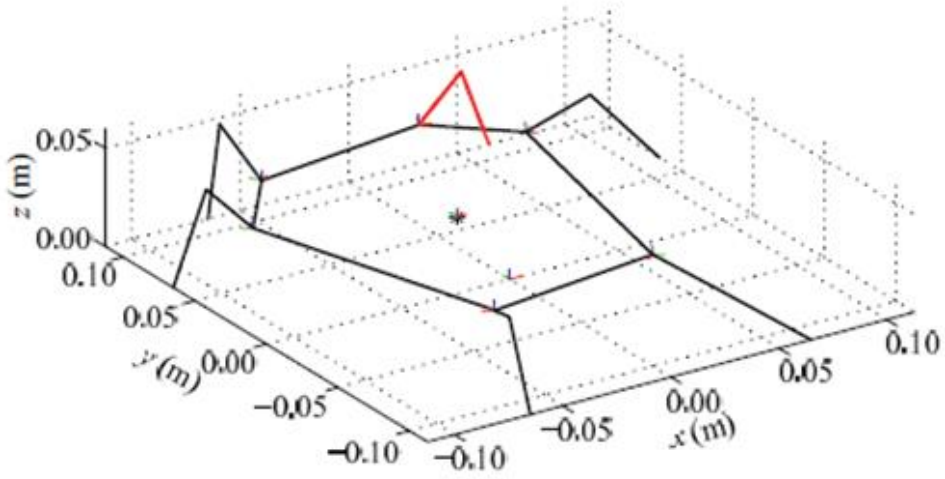


**Figure 17: Optimal posture for a vertical wall: leg 1 is lifted [57].**

Legged locomotion is good at moving on discontinuous surfaces, stepping over obstacles and making plane transitions than other locomotion. However, it is argued that this mechanism is complex in structure and control, due to the gait planning and multi-degree of freedom. Furthermore, compare with other locomotion, the moving velocity of this system is relatively low because the alternative running of two suction groups leads to a discontinuous and slow movement. Therefore, they are seldom employed by robots moving on large-scale structure surface.

### 2.2.2 Tracked Locomotion

Tracked locomotion is relatively faster and less complex. It is also commonly used in applications such as inspection and maintenance of large tanks.

Some tracked robots use magnetic adhesion mechanism [2-3, 18, 44-45].

As shown in Figure 18, a robot with four tracks is built by Shao et al. [3]. This device has two modules connected with joints, and each module contains two tracks where steel segmented magnets are integrated. The robot body is compliant and can fit conical curved surfaces.

**Figure 18: Four magnetic tracked robot [3].**

Autonomous wall-climbing robot adopting two tracked belts with segmented magnets have also been developed [2, 18]. Figure 19 shows a wall-climbing robot for ship rust removal. The robot is able to make turns by driving two tracks separately.

**Figure 19: A wall-climbing root with two magnetic tracks [18].**

Figure 20(a) presents another double-tracked robot [44]. Two triangular magnetic tracks are mounted on both sides of the robot main body. The triangular configuration enables the robot to make inner plane transitions, as shown in figure 20(b). In addition, by driving the two tracks separately, this robot is steerable and can make on spot turning.

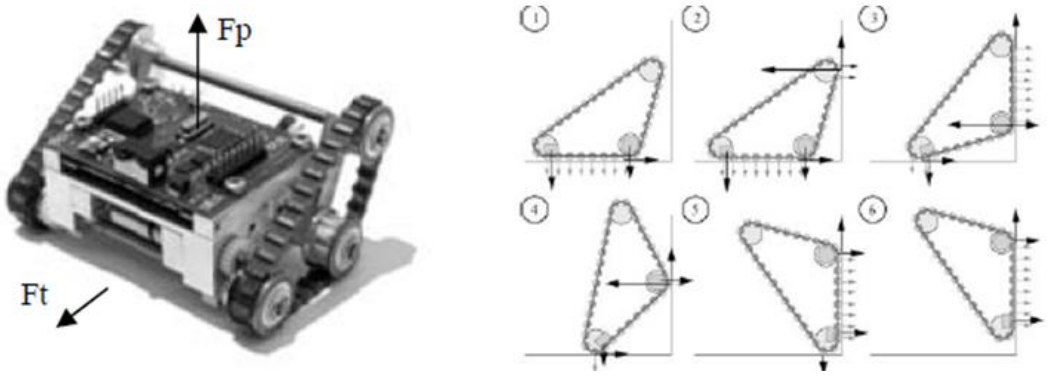


**(a): The robot** **(b):Plan transition stages**

**Figure 20: Triangular magnetic tracks robot [44].**

Some tracked climbing robots utilize dry adhesion [26, 52]. The track belts are made of sticky nanometre materials rather than the magnet units mentioned above. Some other double-tracked robots adopt negative pressure mechanism [12], as shown in Figure 21. Some double-tracked robots also utilizes electrode panels as the adhesion mechanism [68].

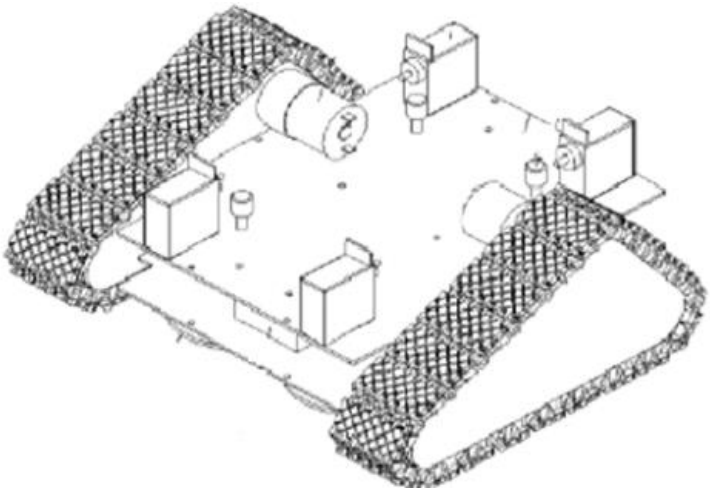

**Figure 21: A double-track robot using negative pressure mechanism [12].**

One major drawback of tracked robots is that they often have difficulty in negotiating large steps or obstacles.

### 2.2.3 Wheeled Locomotion

Similar to tracked robots, wheeled robots do not need multi-degree-of-freedom and gaits control. Wheeled robots usually have simple mechanical structure and need easy control, as shown in Figure 22.

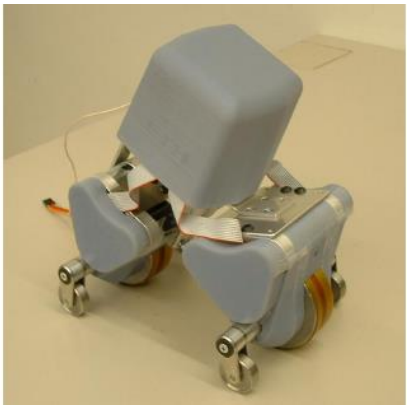

**(a)[14]**

**(b)[47]**

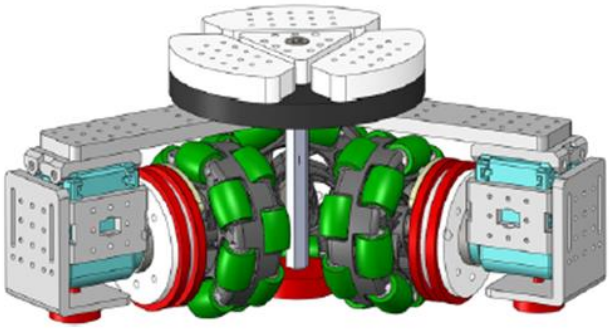

**(c) [69]**

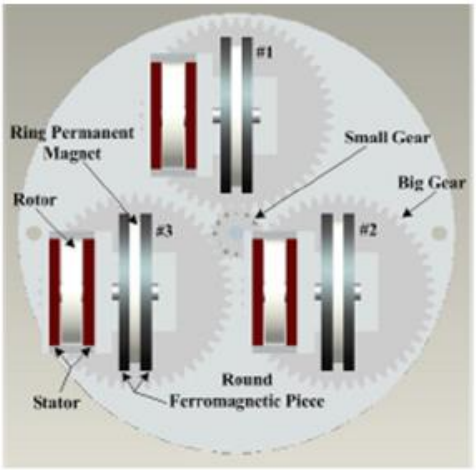


**(d) [70]**

**Figure 22: Wheeled wall-climbing robots with magnetic wheels.**

Some wheeled wall-climbing robots use magnetic wheels as both adhesion and locomotion mechanisms [14, 46-48, 69-71]. Figure 22(a) presents a compact robot with two magnetic wheels in a bicycle configuration [14]. This robot is used to inspect the inner casing of pipes with complex-shaped structures.

Some wheeled robots adopt uncoupled locomotion and adhesion mechanisms, shown in Figure 23. Figure 23(b) shows a robot with six wheels [21]. Rather than using the magnetic wheels, the robot adopts magnet suckers, which are mounted under the main platform, to provide a non-contact permanent magnetic adhesion. Figure 23(a) and (c) give two examples of wheeled locomotion robot adopting vacuum suction mechanism [4, 72]. Both robots have three wheels mounted on a round chassis in Y-type configuration.

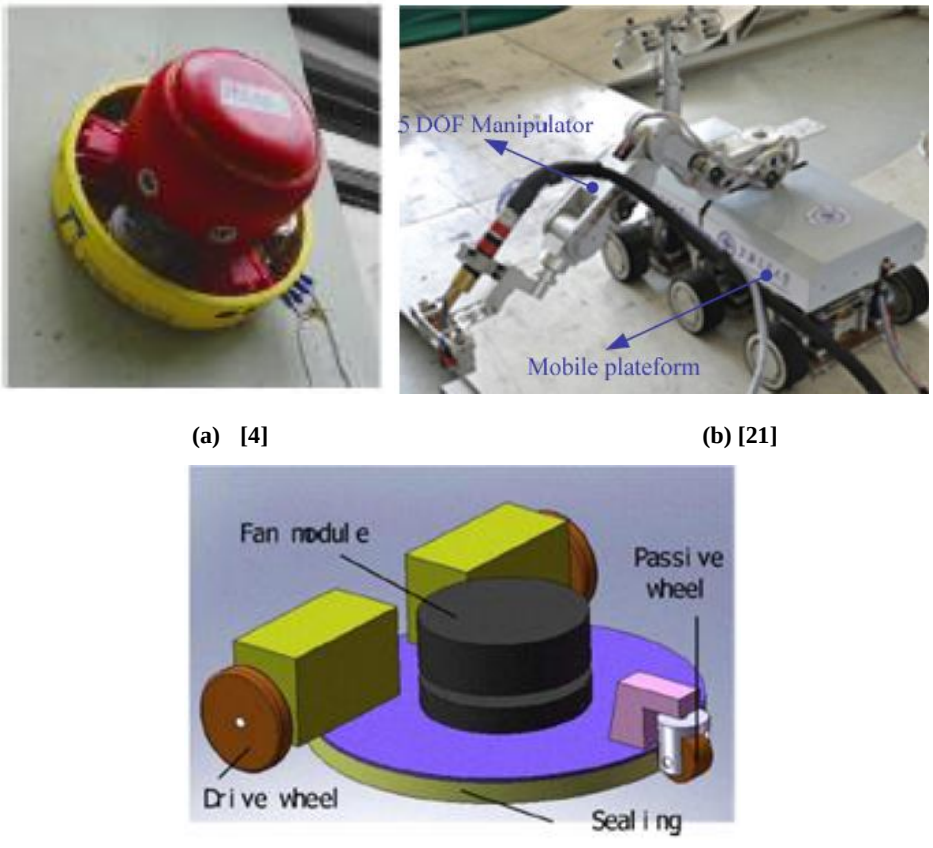


**(a) [4]** **(b) [21]**

**(c) [72]**

**Figure 23: Wheeled robots which have independent adhesion mechanism and locomotion mechanism.**

As shown in Figure 24, a ring robot prototype is designed for inspecting offshore wind turbine blades [9]. The locomotion mechanism contains three wheels in trisection Y-type configuration. The wheels depend on spring forces to grip around and climb on the tower.

The innovation of the robot is that its adhesive forces are provided entirely by springs rather than conventional adhesion methods (such as vacuum suction, magnetic force and dry adhesions).

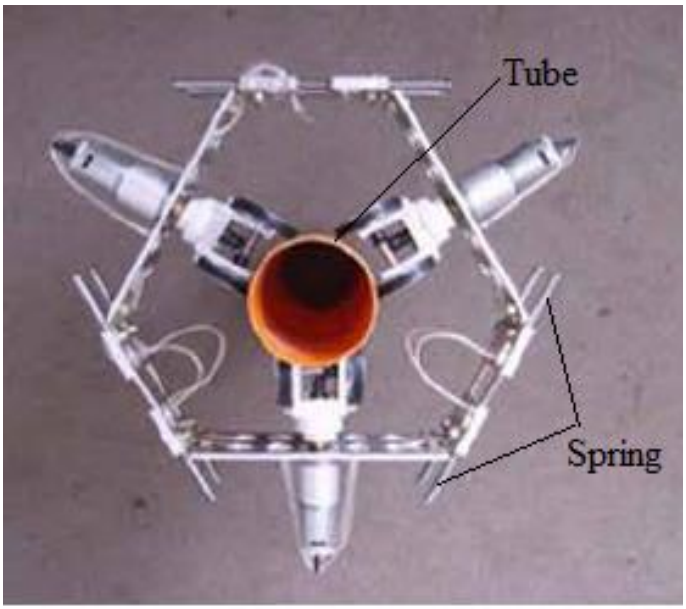


**Figure 24: A ring robot prototype [9].**

Compared with the tracked locomotion, wheeled locomotion is more flexible in steering. However, if the adhesion mechanism is integrated with the locomotion mechanism, the contact area of magnetic wheels may shrink. Therefore magnetic wheels may produce weaker adhesion than the magnetic belts or magnetic legs do. Wheeled locomotion is also inferior in stepping over obstacles and making inter-plane transitions.

### 2.2.4 Sliding Locomotion

Sliding frame mechanism is another commonly used locomotion mechanism [8, 15, 73-74]. Figure 25 (a) presents a new kind of auto-climbing robot, which is used for cleaning the spherical surface of the National Grand Theatre in China [15]. This robot uses clutches for griping on the tracks of the construction.

Another example of sliding locomotion is shown in Figure 25(b). It is a grit blasting robot which uses permanent magnetic adhesion mechanism[23].

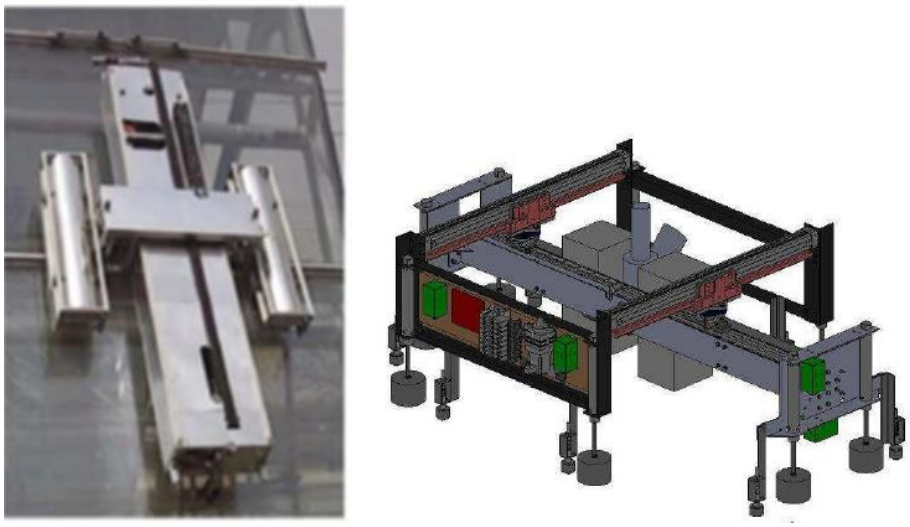

(a) **[15]** **(b) [23]**

**Figure 25: Sliding frame robots.**

Sliding locomotion mechanism often contains two frames which can make linear or rotational relative movements. Each frame is equipped with independent adhesion unit, such as suction cups or magnets. Consequently, a sliding frame robot can move in the desired direction by lifting and moving one frame while attaching the other frame on the working surface. Sliding frame robots usually have simple mechanical structure and reliable adhesion. However, the drawbacks of this mechanism include slow moving speed, discontinuous stick-move-stick movement, and relative large size.

## 2.3 Inter-Plane Transition Ability

The adhesion and locomotion methods of wall-climbing robots should be designed in accordance with the specific applications. Some tasks and application environments involve complex structures such as steps, obstacles and different inclined planes. The robot should be able to negotiate obstacles and make inter-plane transitions. The inter-plane transition is one of the most challenging tasks for wall-climbing robots. The crucial factor for the transition is to ensure the robot safe and stable in the whole process.

Some wall-climbing robots make inter-plane transitions by manipulating the suction mechanism to adhere to the new plane and detach the robot from previous plane alternatively. Wall-climbing robots with inter-plane transition capability can be categorized

into three types:

1) Legged robots. Examples are bipedal robots [37, 42, 65] and six-legged robots[20] .

These robots commonly adopt active joints to connect the modules of each leg, so that the legs can rotate to desired degrees under control.

The transition motions are illustrated in Figure 26 and 27. It can be seen from the figures that the legs, and also the suction mechanism on them, are separated into two groups. One suction group attaches on the working surface to support the robot, while the other suction group moves to a desired surface and adheres to it. The former suction group then releases the adhesion and moves to a new position.

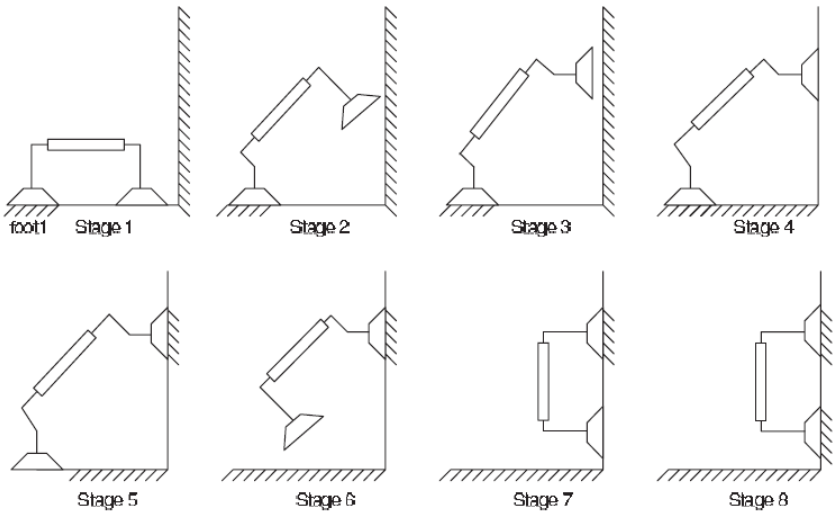


.

**Figure 26: Locomotion sequence to transit from a ground to a vertical wall [67].**

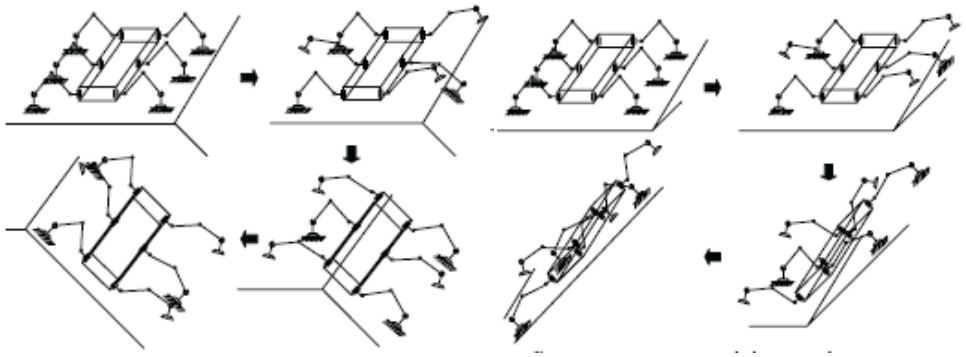

**(a)Concave transition gait.** **(b) Convex transition gait.**

**Figure 27: Locomotion sequence to make plane transitions [20].**

However, such type of robot is often designed with multi-degree-of-freedom, and its walking and plane transition motions involve gait planning. Therefore legged robots need complicated design and control.

2) Magnetic wheeled robots [14] or compliant magnetic track-wheeled robots[44-45].

When making inter-plane transitions, magnetic wheels may simultaneously adhere to both planes of an inner corner and have difficulty in moving forward. To solve such problem, Tache et al. have designed a adapted magnetic wheel unit with two lateral wheels [14]. As shown in Figure 28, when the robot encounters an inner corner with the magnetic wheels attaching on both plane surfaces, the lateral wheels will be actuated to allow the magnetic wheels to be slightly lifted and leave the unwanted surface.

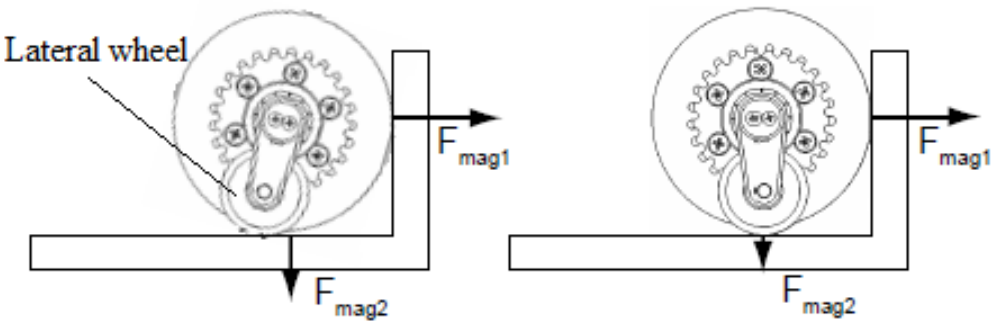


**Figure 28: The lateral wheels slightly lift the wheel and decrease the unwanted force $F_{mag2}$ [14].**

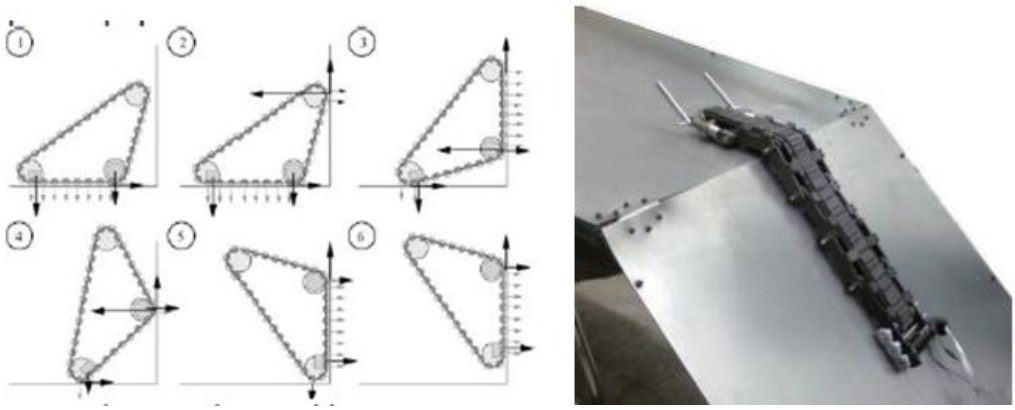

**(a) [44]** **(b) [45]**

**Figure 29: Plane transitions.**

Figure 29 presents plane transition stages of two magnetic track-wheeled robots. It can be seen from Figure 29(a) that its triangular configuration tracks help the robot be lifted

from the previous surface and attach to the next one[44]. A compliant tracked robot is shown in figure 29(b), torsion springs are used at body joints to help robot perform external and internal transitions [45].

Unlike legged robots, magnetic tracked or magnetic wheeled robots do not involve multiple-degree-of-freedom locomotion and only need simple and reliable control.

3) Robots adopting dry adhesion.

Figure 12 shows a two-module robot with dry adhesion [26, 52, 56], and Figure 30 illustrates one-module robot with tail [54]. Such type of robots may utilize active body joints [52, 56], compliant body joint with torsion springs and active tail [26], or compliant foot ankles with torsion springs [54] to accomplish the plane transitions. Figure 30 shows the plane transition stages of the robot Mini-Whegs, where the torsion springs in foot ankles are activated to implement transitions. Figure 31 presents the transition stages of the robot TBCP-II [52], the active joints are driven to implement transitions. Active joints mechanisms have been proven to be especially valid for two-module wall-climbing robots to make inter-plane transitions.

**(a) Internal plane transition stages.**

**(b) External plane transition stages.**

**Figure 30: Internal and external plane transitions [54] .**

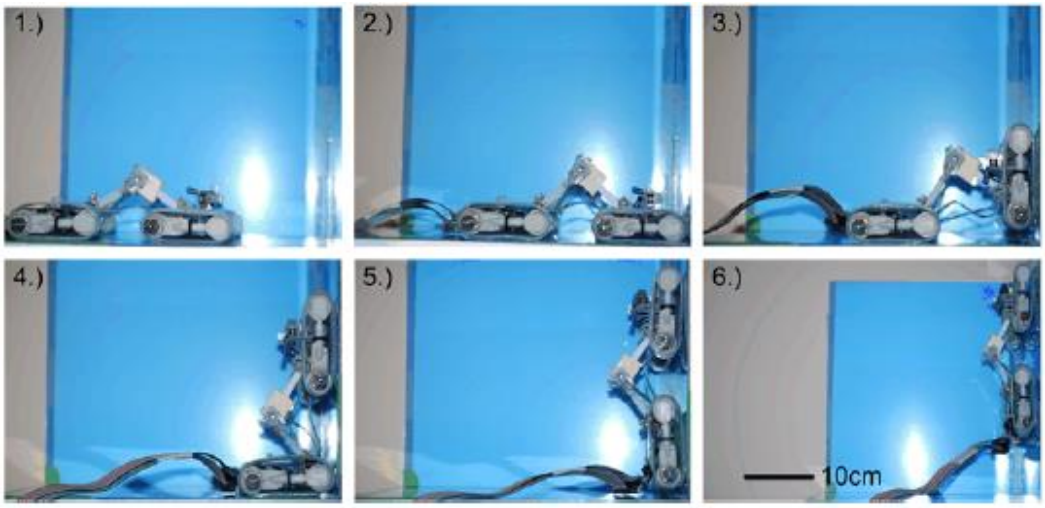


**(a) Inside corner transition stages.**

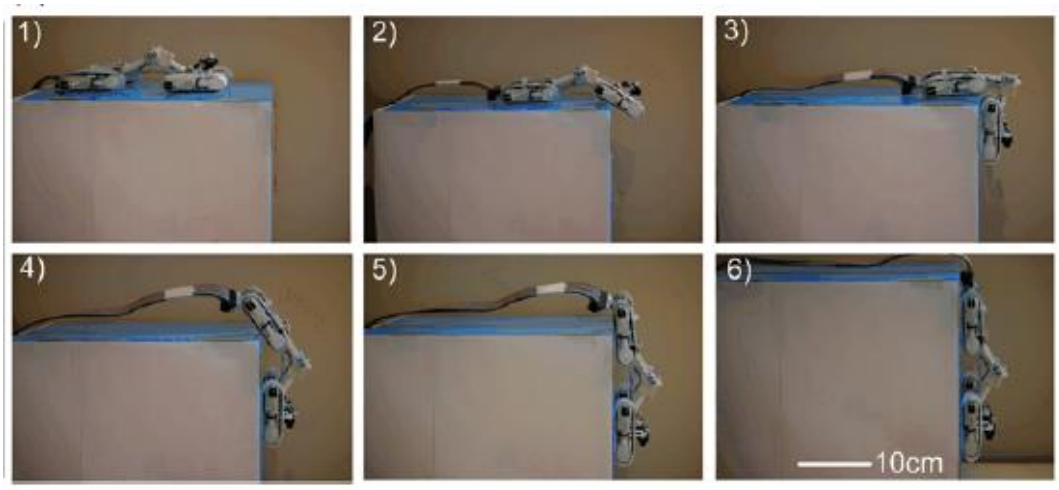


**(b) Outside corner transition stages.**

**Figure 31: Transition stages of TBCP-II [52].**

## 2.4 In-Pipe Inspection Robots

This thesis study is to develop a robot which is used for in-pipe inspection. The previous duct inspection robots can be classified into several categories:

- Wheeled robots without adhesion mechanism have been developed for inspection applications [75-76]. These robots can only move on horizon ducts but are not able to climb on vertical ducts. An example of pipe inspection robot is presented in Figure 32.
- Secondly, to enable the robot to attach to a duct, one of the most common solutions

is to make elastic arms with spring mechanism [77-79]. Figure 33 shows two wheel-type structure inspection robots. By pushing the arms to the duct, the wheels can obtain friction force to make the robot move up and down the duct.

**Figure 32: Duct inspection robot without adhesion (internet).**

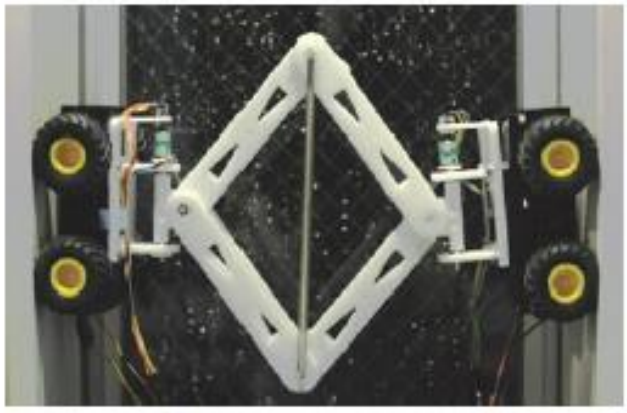

**(a) [77]**

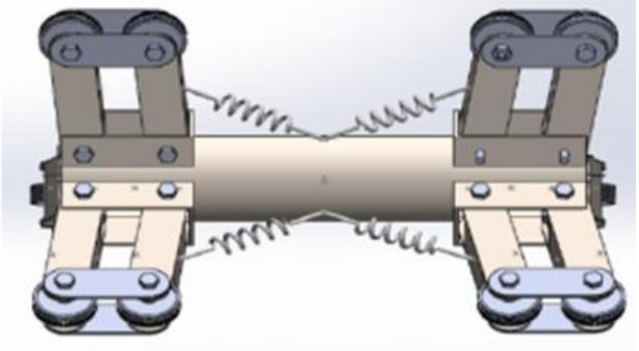

**(b) [79]**

**Figure 33: Wheel-type structure robot.**

- The third type is called Screw type robot. An example of screw type inspection robot which utilize springs, is shown in Figure 34 [78]. When the robot climbs on a vertical pipe, it can revolve around z-axis on a helical trajectory.
- The fourth type is Caterpillar wheel robot [80-81] . Examples of caterpillar wheel inspection robot are shown in Figure 35. Compared to the common wheeled mechanism, the caterpillar wheel is more compliant on uneven surface, which allows the wheels to continuously contact the pipe with larger contact area and higher friction.

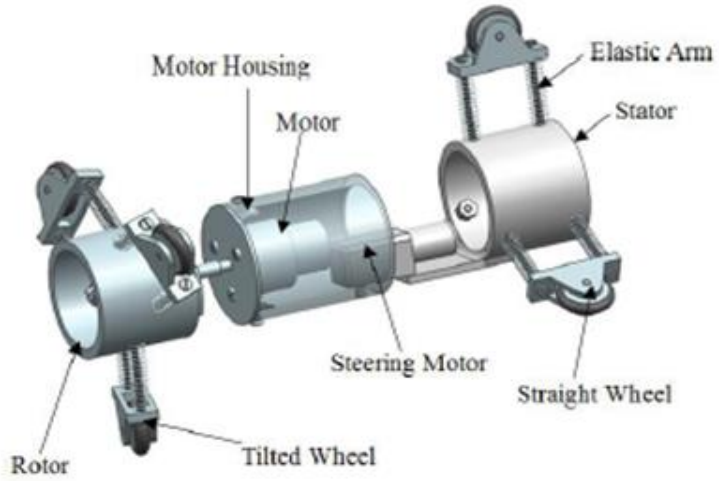


**Figure 34: Screw type robot [78].**

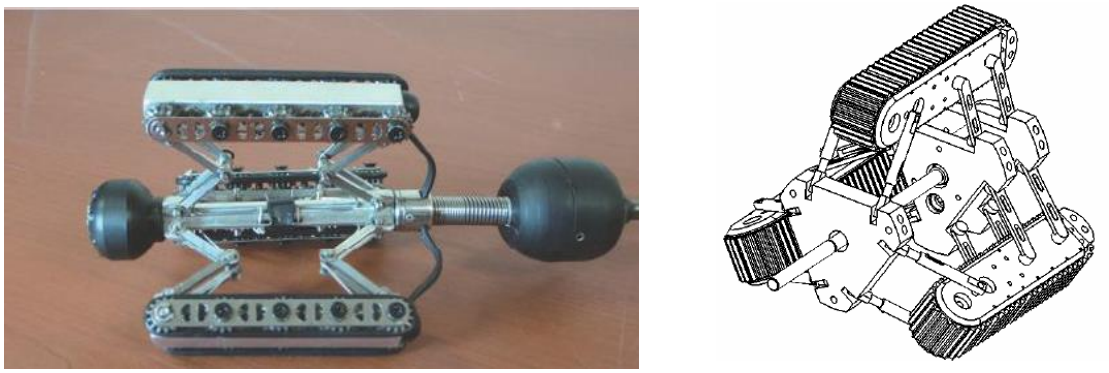

**(a) [80]** **(b) [81]**

**Figure 35: Caterpillar wheel robot.**

- The fifth type is called Caterpillar robot. Figure 36[82] and 37[83] show two Caterpillar inspection robots. This type of robot is capable of attaching and

climbing in the pipe with wheels by rocking its body to stretch across the pipe. The rocking actions are archived by using active joints.

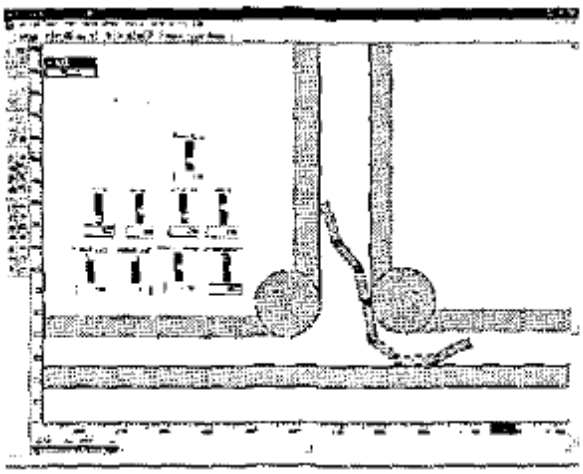

**Figure 36: Snake robot negotiating at t-branches [82] .**

**Figure 37: Caterpillar robot [83].**

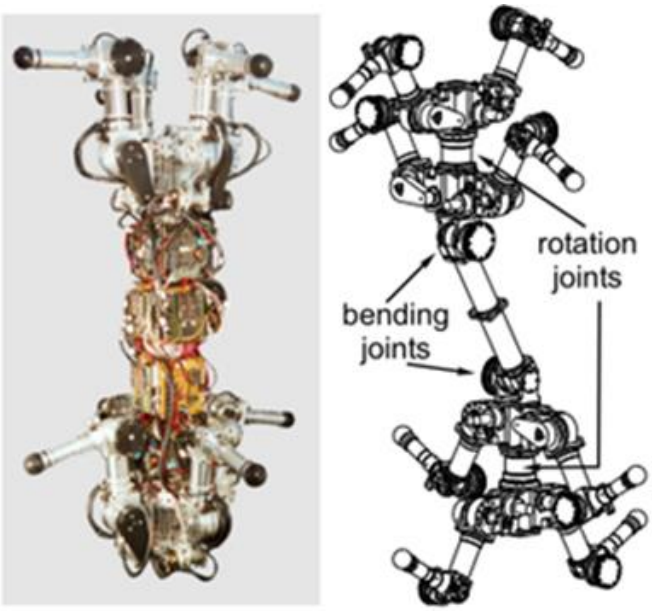


**Figure 38: MORITZ [84].**

- Legged robots are also developed to inspect inner casing of pipes. Figure 38 presents a legged inspection robot called MORITZ[84]. Similar to the caterpillar robots above, this robot also uses active joints to manipulate legs to get adhesion friction force.

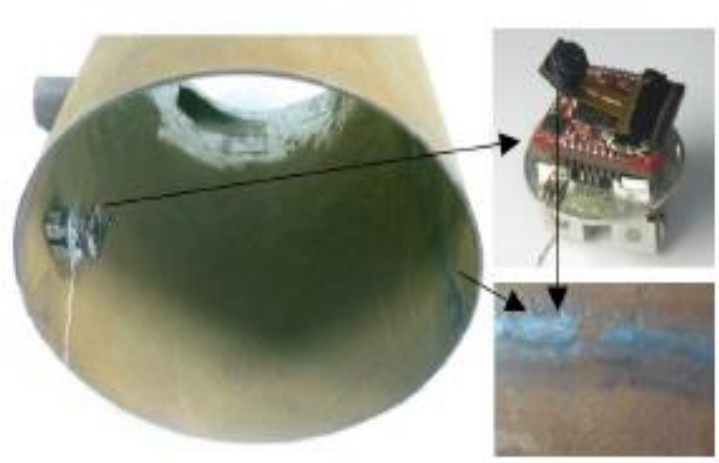

**(a) [70]**

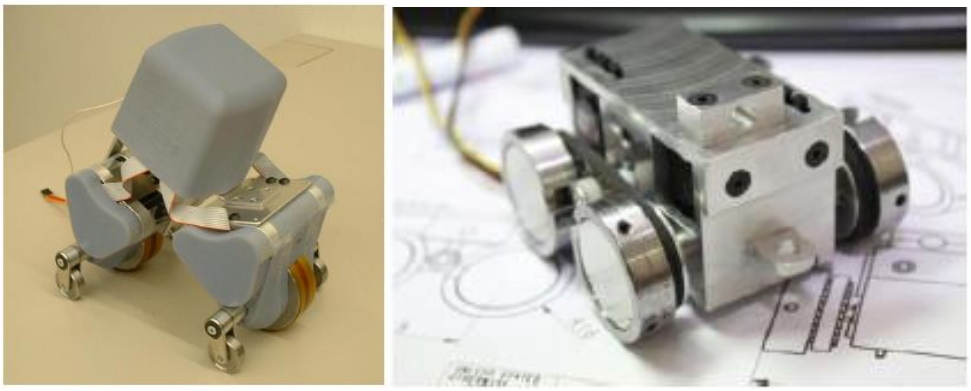

**(b) [14]** **(c) [85]**

**Figure 39: Magnetic wheeled robots.**

Although considerable inspection robots have been developed, it is almost impossible to provide a universal solution to the optimal design of in-pipe inspection robots. Pipes, such as gas or oil pipelines, air-condition duct and drain pipes, often are narrow, contaminated by sewage and/or dust, and in complex shapes with sectional dimension changes and pipe intersections. Consequently the in-pipe inspection robots often should possess small size

body, environment-adaptive adhesion mechanism, and high mobility on complex-shape walls (such as negotiating obstacles and making inter-plane transitions). For examples, some robots mentioned above have good mobility on the inner wall of ducts, such as negotiating duct intersections [78, 83-84], but they may have complex structure, large size body, or not robust against dust and dampness, etc.; magnetic wheels robots shown in Figure 39 are only fit for ferromagnetic pipe inspection [14, 46, 70, 85].

Taking above factors into consideration, this thesis will investigate feasible designs of wall-climbing robots for duct inspection (such as milk tanks, ventilation ducts, and so on), which feature in simple structure, compact size, easy control, good reliability, low cost, and high mobility on complex shaped walls.

## 2.5 Summary

Wall-climbing robots comprise two essential elements - adhesion mechanism and locomotion mechanism. The developments of common adhesion and locomotion mechanisms, which include vacuum adhesion, magnetic adhesion, dry adhesion, electrostatic adhesion, legged locomotion, tracked locomotion, wheeled locomotion, and sliding locomotion, are comprehensively investigated in this chapter. The advantages and disadvantage of each adhesion/locomotion mechanism are discussed in terms of its reliability, flexibility, and complexity.

Furthermore, the impacts of mobility of wall-climbing robots (especially inter-plane transition ability) on the design of adhesion and locomotion methods are highlighted.

At last, the in-pipe inspection robots are explored to facilitate the development of wall-climbing robots for duct inspection.

.

# Chapter 3 Modular Wall-Climbing Inspection Robot

For different inspection tasks, it is often a challenging job to design and develop agile wall-climbing robots which can freely move on various complex shaped structures in harsh environment, such as ventilation ducts, milk tanks, bridges, and so on. In this Chapter, a modular wall-climbing inspection wheeled robot is developed. The robot will be able to have high mobility on complex structures such as steps, obstacles and surfaces with different inclinations. A two-module robot prototype and a three-module robot prototype with general-purpose vibration adhesion mechanism are designed and investigated.

## 3.1 A Two-Module Wall-Climbing Wheeled Robot

Figure 40 presents a two-module wall-climbing wheeled robot, which is suitable for general-purpose inspection applications, such as narrow duct inspection and bridge maintenance. It is an un-tethering device, and can carry remote controlled inspection equipment, such as camcorder, radio signal sender and receiver. The proposed robot is of simple structure, compact size, reliable performance and flexible scalability.

The two modules are connected by an active joint, which enables the robot to be folded from -90° to 90° degree, thus facilitating the robot to make inter-plane transitions. The proposed robot can make inter-plane transitions by folding the two jointed modules. A balance tail is also joined to the rear module. The active joint between the rear module and the balance tail utilizes a torsion spring to provide a preload for firm adhesion and prevent the robot from rolling over during its inter-plane transitions. The modular design enables the robot to flexibly arrange its shape and distribute its weight, and to be easily scaled by changing the number of jointed modules.

The modular robot employs wheeled locomotion which contains three pairs of wheels. The front and rear wheels are driven by two separated motors respectively. The wheeled locomotion has the advantages of simple structure, easy control and high reliability.

Vibration suction pads are installed under every module to provide adhesion force for the

robot to counter the gravity. Vibration suction often has lower power consumption, higher suction force stability, relatively simple structure and less noise. It also can offer general-purpose adhesion to various types of surfaces (including ferromagnetic and non-ferromagnetic surfaces).

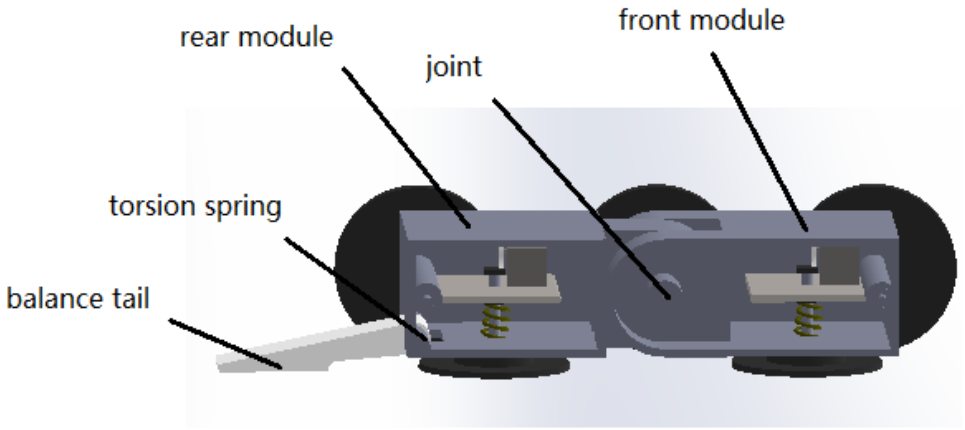


**Figure 40: CAD model of robot.**

## 3.2 General-Purpose Adhesion Mechanism Design

This section illustrates the detail of general-purpose vibration adhesion (*i.e.* vacuum adhesion) mechanism for the wall-climbing robot. The general-purpose vibration adhesion mechanism mainly includes the design of cam, spring mechanisms and suction pad. As mentioned in previous chapters, the vibration adhesion mechanism will enable the robot to move on wide range of structure surfaces.

### 3.2.1 Vibration Adhesion Mechanism

The vibration adhesion mechanism is shown in Figure 41. This mechanism includes a servo motor, a cam, spring mechanisms and suction pad, which are installed on a chassis. The cam is driven by the servo motor. It is capable of exerting forces on the rod, which in turn can push the suction pad towards the climbing surface to force out the air between the pad and the surface. Then the compressed spring attached on the rod can provide a pulling force on the pad in the direction opposite to the climbing surface. In a word, the mechanism is able to generate a negative pressure force between the suction pad and the climbing surface by extruding the air and then pulling the pad.

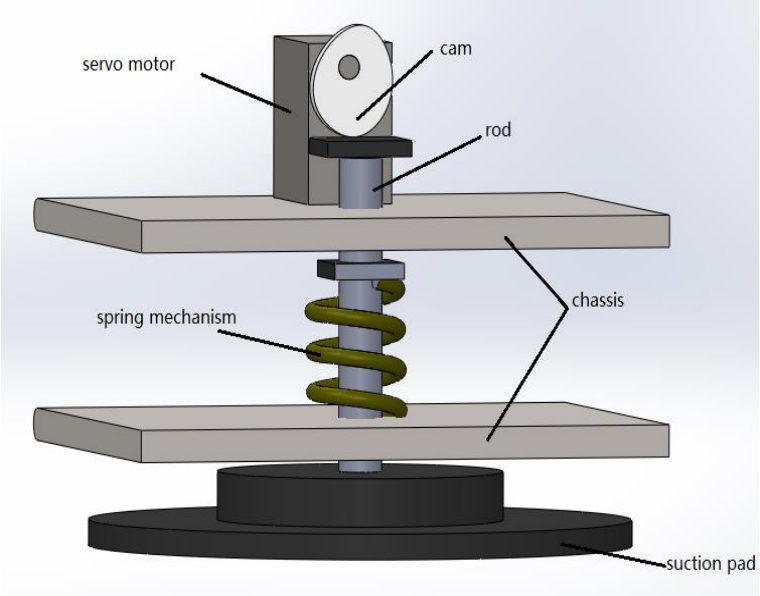


**Figure 41: The vibration adhesion mechanism of the robot.**

The negative pressure force is maintained when the pad forms a ring and seals this pressure area. However, the sealing created by the ring is not long-lasting, and air may leak into the ring area, thus the generated negative pressure will decline. To maintain the negative pressure for the sake of the robot safety, the pads need to be re-primed by extruding the air between the pad and surface unremittingly. The re-priming is fulfilled by forcing the rod against the surface repeatedly by rotating the cam. Therefore constant negative pressure can be generated by the vibration of the suction pad at a certain amplitude and frequency.

The vibration adhesion force is mainly influenced by two factors:

- The spring stiffness. A soft spring may not provide sufficient pulling force, while an over-stiff spring means that the system needs a high torque servo motor to conquer the spring force.
- The vibration amplitude and frequency of the suction pad. The larger the amplitude is, the higher the negative pressure force in suction cup will be achieved. Similarly, the higher the frequency of vibration mechanism is, the higher the negative air pressure is. The vibration amplitude exerts more influence on the negative air pressure than the vibration frequency does.

The main advantage of the vibration suction method is that it does not need a vacuum

pump and a long pipe to generate vacuum force. Thus vibration suction based climbing robots can be compact, and lightweight. In addition, the low power-consumption adhesion mechanism can be powered by battery cells.

This adhesion mechanism can offer required constant suction force on various types of surfaces (including steel, wood, glass and concrete).

### 3.2.2 Suction Pad Design

**Table 1: Average hold force for rubber adhesion pads [12].**

| Adhesion force (kg) | | | |
|---|---|---|---|
| Diameter | 20mm | 30mm | 38mm |
| 1.5 mm insertion rubber | 4.8 | 7.1 | 12.4 |
| 1.0 mm nitrile | 3.1 | 7.4 | 10 |
| 1.5 mm butyl | 6.8 | 11.5 | 16 |
| 3mm natural rubber | 7.2 | 11.7 | 15.9 |

The suction pad plays a critical role in producing the adhesion force for the robot. Table 1 lists the main parameters of the suction pad.

The adhesion force F of the suction pad can be calculated by using Eq. (1), which involves the atmospheric pressure $p_0$, the pressure p inside of the suction cup and the negative pressure area A.

$$F = \Delta p \times A = (p_0 - p) \times A \quad (1)$$

From Eq. (1), it can be seen that the adhesion force F is proportional to the pressure difference ($p_0$-$\Delta p$) and the area A. It implies that, larger suction area A can yield higher suction force F.

In addition, the sealing performance of the pad material also influence the adhesion force F. The suction pads would slide along the climbing surface whilst maintaining the adhesion

force. Low friction coefficient pad can bring low energy consumption in the sliding. High wear-resistance on rough surfaces will enhance the adhesion robustness of the pad. In our case a butyl suction pad with the diameter of 30mm and the thickness of 1.5mm is employed. Such a suction pad can produce the holding force of 11.5 N.

### 3.2.3 Cam Design

This adhesion mechanism adopts a disc cam mechanism, whose follower (i.e. the rod) is plate-bottomed. The cam principle in current concept is illustrated in Figure 42.

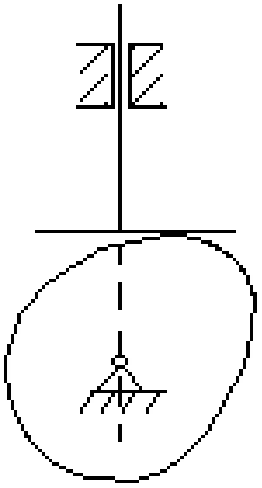

**Figure 42: The cam principle.**

As shown in Figure 43, the rotation of the cam mechanism will induce the simple harmonic motion of the follower, where Disp. in Figure 43 (a) denotes Displacement of the follower, Vel. in Figure 43 (b) denotes Velocity of the follower, and Acce. in Figure 43 (c) denotes Acceleration of the follower. The velocity diagram of the follower in Figure 43 (b) illustrates a smooth trajectory of the follower. The acceleration diagram of the follower, as shown in Figure 43 (c), is a cosine curve. It can be seen from the figure that the maximum acceleration value (vector) is at the initial position, zero is at the mid-position, and negative maximum is at the final position. The profile and the rotating velocity of the cam determine the amplitude and the frequency of the follower reciprocation respectively.

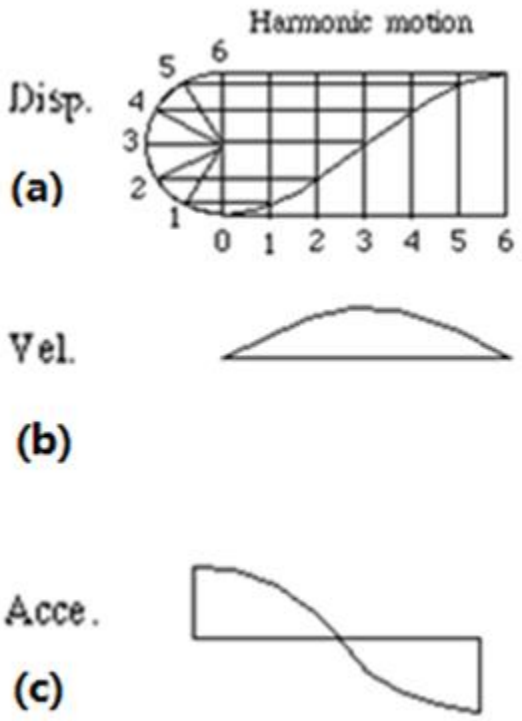


**Figure 43: The movement of follower.**

## 3.3 Structure Design

The structure design of the robot mainly includes the design of the locomotion wheels, the active joints and the balance tail.

### 3.3.1 Locomotion Mechanism

The robot consists of three pairs of wheels made from high friction coefficient material. Two pairs of wheels (front and rear) are driven by two separated servo motors to make turns and move freely on both vertical and horizontal surfaces.

### 3.3.2 Joint Design

Active joints are used to enable the proposed robot to make inter-plane transitions. Figure 44 gives both the section view and exploded view of the joint. Figure 44 (a) also shows the assembly relationship among the two modules, the drive bearing, a set of gears and the motor of the joint.

When the robot encounters an internal plane transition, the motor will be actuated through remote control. The bearing of the joint will rotate to fold the two modules to the desired angle. The bearing also can be driven and rotate reversely to fold the two modules to make an external plane transition.

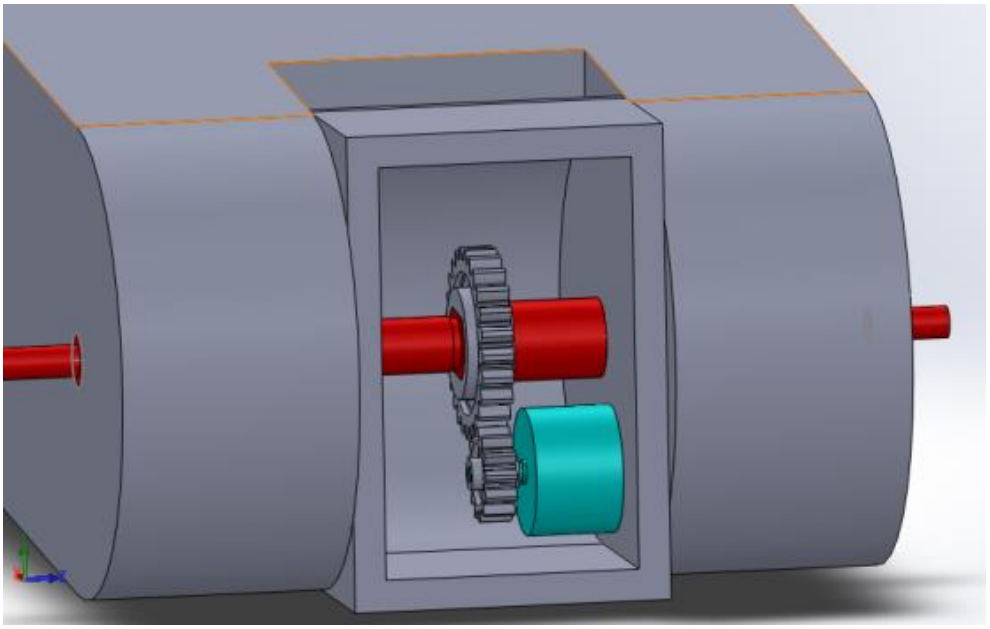

**(a): Section view of the active joint.**

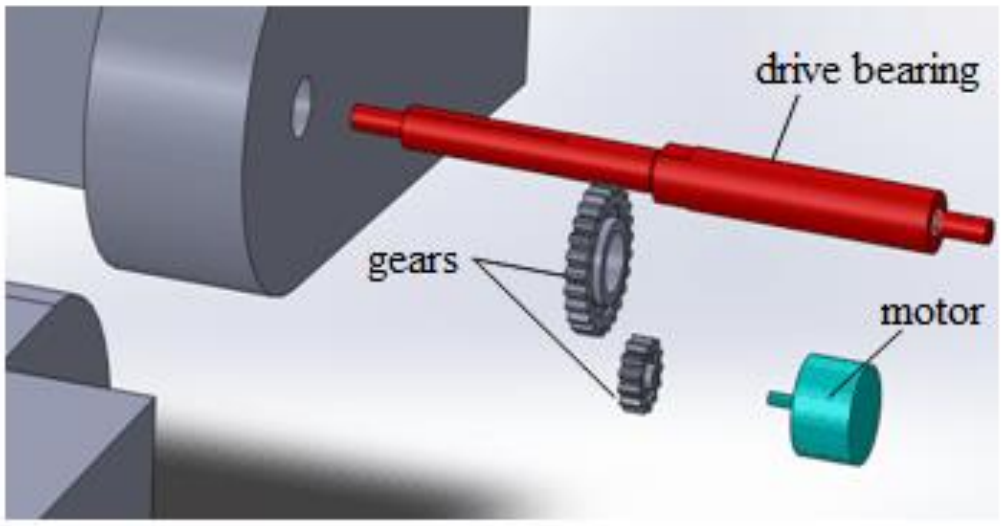


**(b): Exploded view of the joint.**

**Figure 44: The active joint.**

### 3.3.3 Balance Tail Design

A balance tail is jointed to the rear module to provide a preload and prevent the robot from rolling over during its inter-plane transitions.

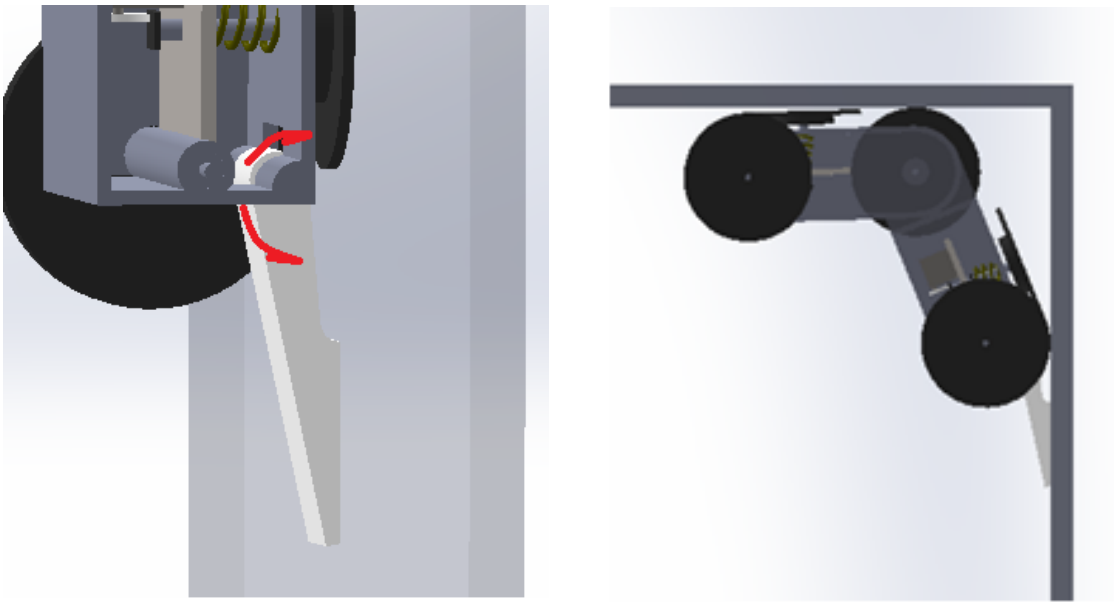

**(a)** **(b)**

**Figure 45: The balance tail (sectional view).**

The balance tail is illustrated in Figure 45(a). It is a level mechanism with an attached torsion spring, which offers 8N preload force. This initial compressive force (i.e. preload) may enhance the adhesion of the robot. In addition, when the robot encounters a plane transition, the tail with the torsion spring can provide a force to prevent the rear module from rolling over, as shown in Figure 45 (b). The red arrows in Figure 45(a) denote the preload directions of the torsion spring. Therefore, to handle the preload and avoid tumbling, the torsion spring with appropriate stiffness is needed. However the stiffness of the spring cannot be too high, since a high stiffness spring may hinder the plane transitions.

## 3.4 Prototyping and Simulation of a Two-Module Robot

Based on above design, the prototyping of a two-module robot is created by using Solidworks. Preliminary simulations have been done to testify the feasibility of the proposed design.

### 3.4.1 Prototyping

Figures 46-49 give the design drawing of the major components of the two-module robot prototype, including two modules and the drive bearing. All the dimensions are in mm (millimetre).

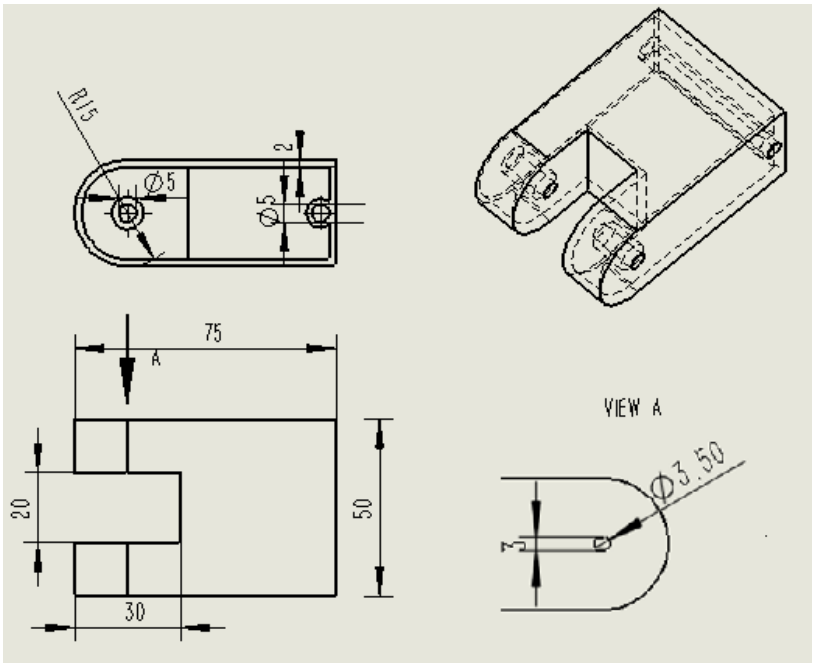


**Figure 46: Design of the front module.**

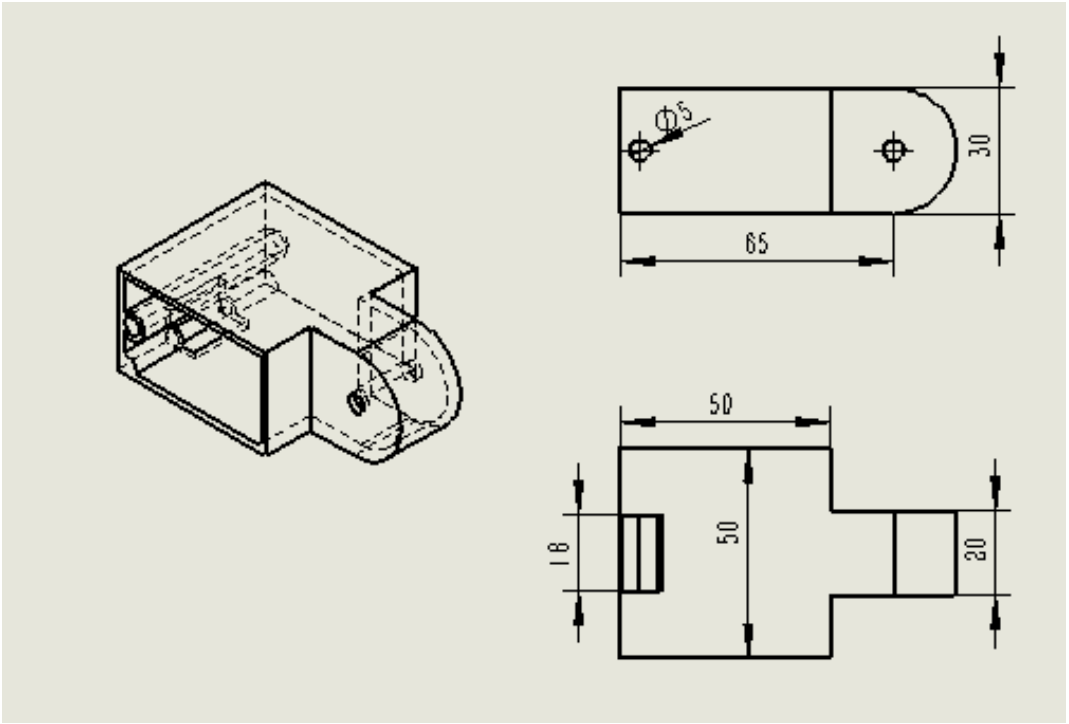


**Figure 47: Design of the rear module.**

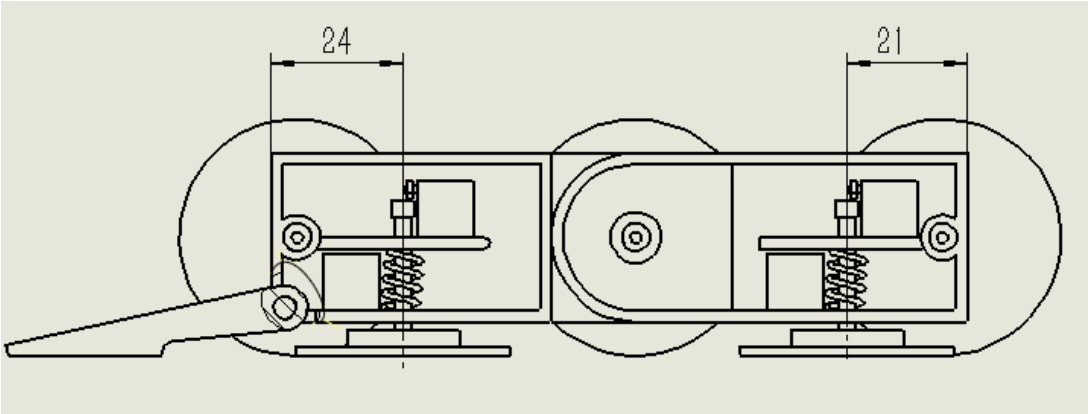


**Figure 48: Sectional view of the robot.**

Front module is shown in Figure 46. It is 50mm in width and 75mm in length. It is a shell part in thickness of 2mm. The “View A” shows the detail of the bore of the drive bearing.

Main dimensions of the rear module are shown in Figure 47. The rear module is 50mm in width and 80mm in length. It is a shell part in thickness of 2mm.

Figure 48 illustrates the detail of the assembly relationship of the robot parts. The distance between the two suction pads is designed carefully to facilitate plane transitions. The drive bearing dimensions are shown in Figure 49.

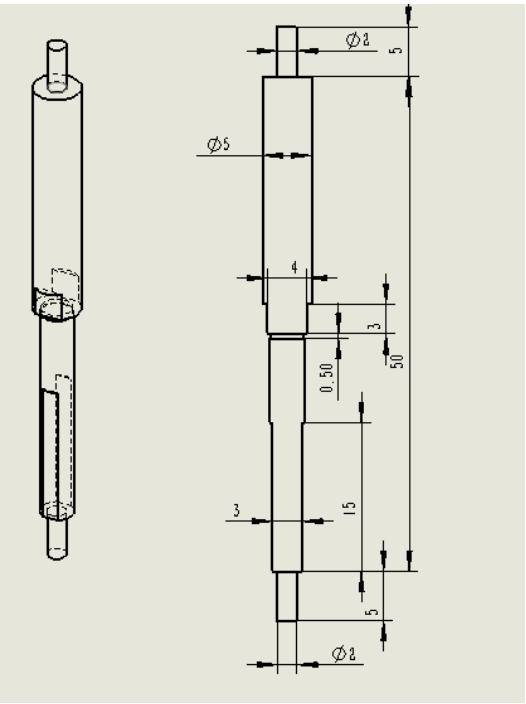


**Figure 49: Design of drive bearing.**

### 3.4.2 Simulation Scenarios

a) Internal Plane Transition

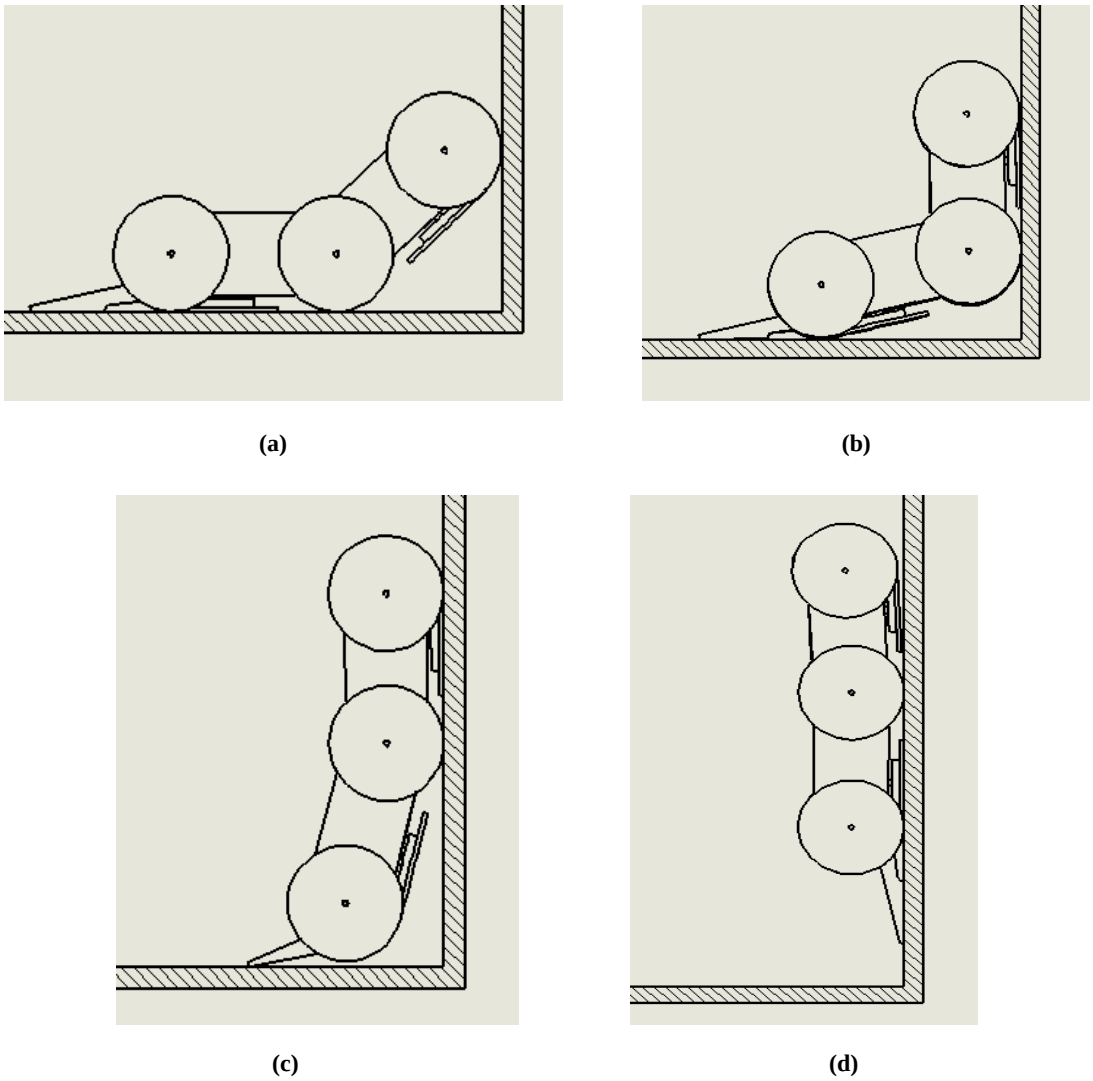

**(a)** **(b)**

**(c)** **(d)**

**Figure 50: Motion scenario of an internal plane transition.**

Figure 50 illustrates the motion scenario of an internal plane transition. When the device travels to an inner corner, the wheels at the front will be pushed against the wall. Meanwhile, the motor of the middle joint will be actuated to lift the front module and fold it to attach to the vertical surface, as shown in Figure 50 (a). As shown in Figure 50 (b), while robot keeps moving ahead, the front module will be folded to the maximum angle, and then the suction pad under the front module fully adheres to the vertical surface. After that, while the front module keeps moving ahead, the motor of the middle joint will rotate reversely to fold the rear module to move toward the

vertical surface, as shown in Figure 50 (c) and (d). Eventually the suction pad under the rear module will lose its adhesion to the horizontal surface and also attach to the vertical surface, and the device completes the internal plane transition.

b) External Plane Transition

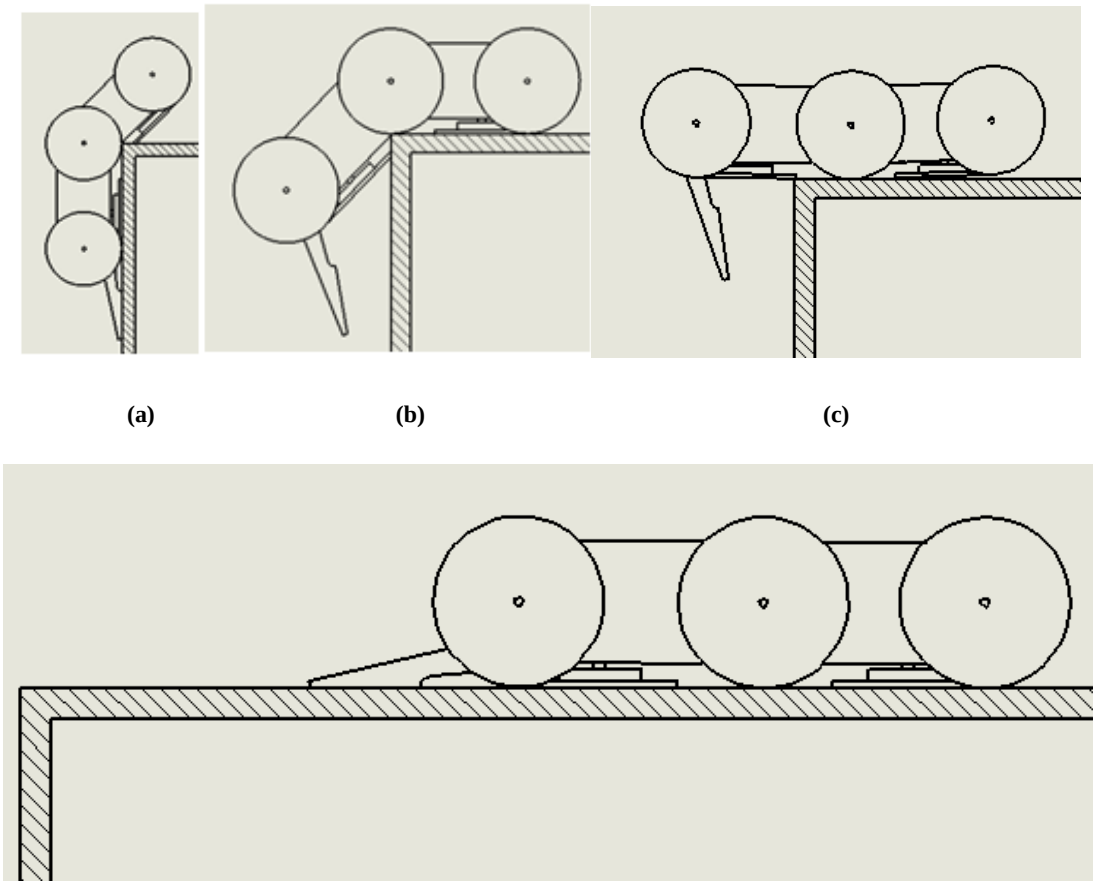

**(a)** **(b)** **(c)**

**(d)**

**Figure 51: Motion scenario of an external plane transition.**

Figure 51 illustrates the motion scenario of an external plane transition. When the device travels to an external corner, the robot mainly driven by the rear module wheels will keep moving ahead on the vertical surface; meanwhile the motor of the middle joint will be actuated to fold the front module to attach to the horizontal surface, as shown in Figure 51 (a). After that, the front module finally adheres to the horizontal surface, and the front wheels will drive the device forward on the horizontal surface. Then the middle joint is actuated reversely to lift the rear module to detach from the vertical surface, as shown in Figure 51 (b) and (c). Eventually the suction pad under

the rear module will lose its adhesion to the vertical surface and also attach to the horizontal surface, and the device completes the external plane transition.

## 3.5 Design Variants

Besides the fundamental two-module wheeled design above, two design variants of the robot are investigated in the following sections.

### 3.5.1 A Three-Module Robot

As mentioned before, the modular design enables the robot to flexibly arrange its shape and distribute its weight, and to be easily scaled by changing the number of jointed modules. Figure 52 shows the CAD model of a three-module robot prototype. This robot comprises of three almost identical modules, namely the front, middle and rear module. The front and the rear modules both have three driven wheels in "Y" configuration. The middle module consists of four non-driving wheels.

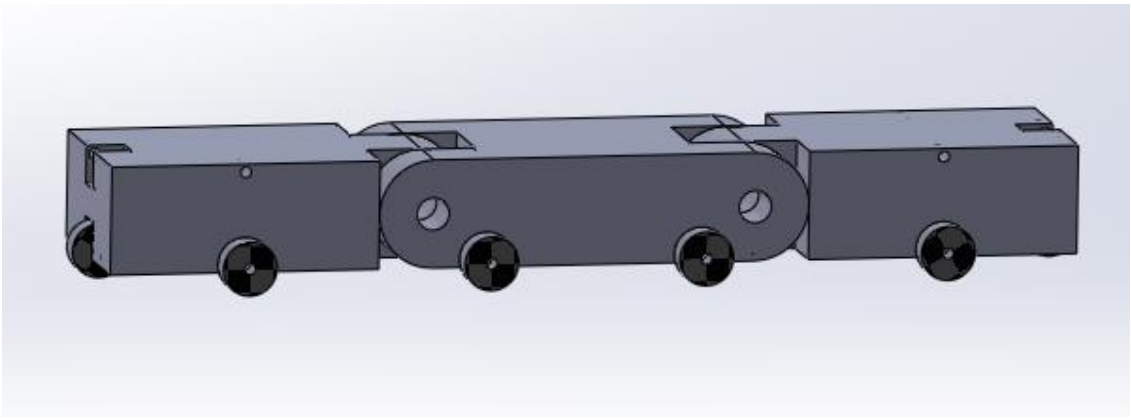

**Figure 52: Three-module robot.**

Figure 53 and Figure 54 illustrate the internal plane transition and the external plane transition of the three-module robot respectively. Figure 53 shows the three-module robot is also good at making internal plane transitions. But the three-module robot has difficulty in making external plane transitions. During the external plane transition, the middle module is not compliant to the corner, and it will be stuck after the front module adheres to the horizontal surface, as shown in Figure 54. Such multiple-module robot design still needs further research in the future.

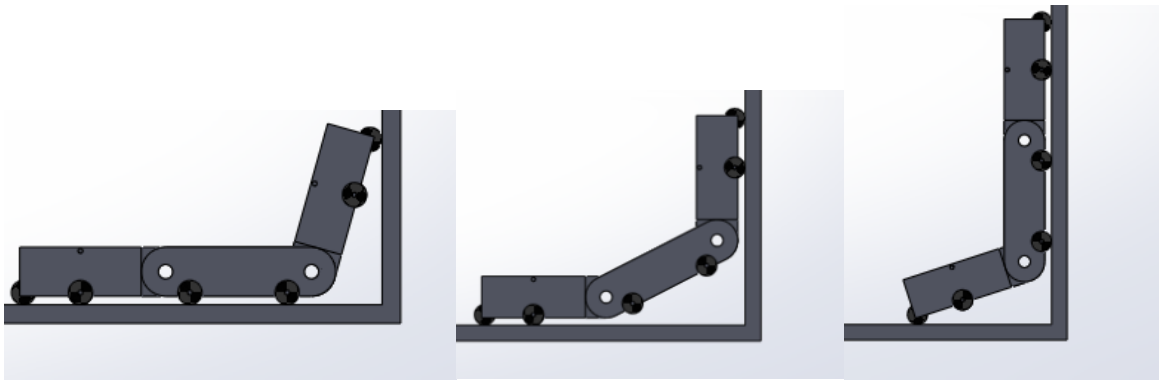

**Figure 53: Internal plane transition stages.**

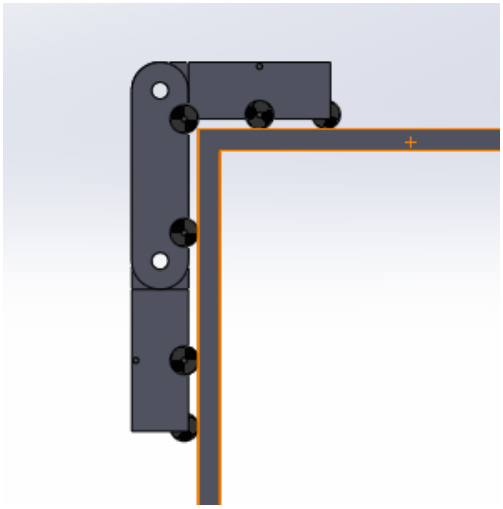

**Figure 54: The middle module is stuck after the front module adheres to the next wall.**

### 3.5.2 An Alternative Joint - Connecting Rods

Figure 55 shows a two-module robot, which employs a new active joint. The new active joint comprises of two connecting rods and three joints with torsion spring. Each module is equipped with one set of adhesion mechanism. The front module adopts a pair of motor-driven fore-wheels. The two wheels, which are made from high friction coefficient material, can obtain a climbing friction force when pushed to a perpendicular wall. It can be seen from the Figure 56 that the front wheels and fore-wheels are configured in an inclining of 85° . By pushing these two pairs of wheels to the new plane, the front module can easily detach the original plane. The rear module consists of two pairs of wheels, the front of which are driven by servo motor.

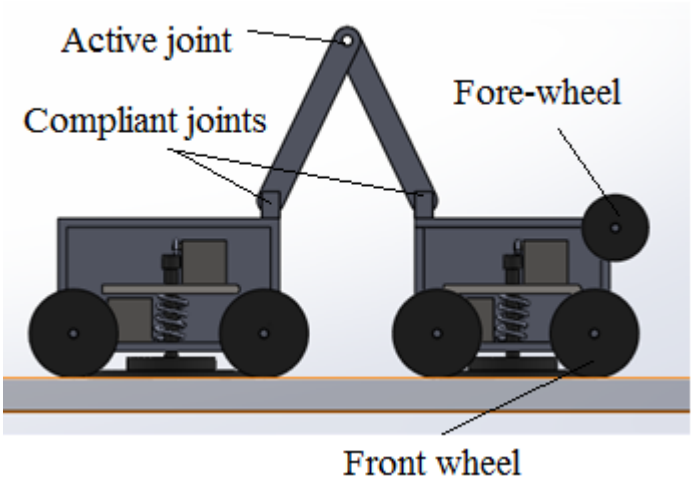


**Figure 55: Two-module with connecting rod robot.**

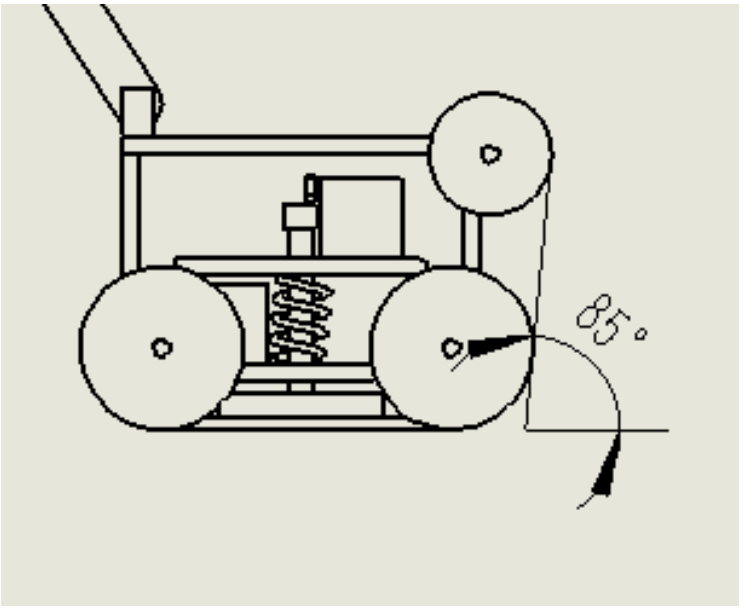


**Figure 56: The front wheels and fore-wheels are configured in an inclining of 85°.**

Since the new connecting rods based active joint can fold the two modules to any desired angle, it significantly enhances the robot's mobility on complex shaped structures. For example, when the robot with the new joint negotiates a large obstacle, the distance between suction pads of two modules can be adjusted to enable the robot to secure sufficient adhesion force by folding the rods during the plane transitions. Furthermore, the new active joint provides a solution to the difficult problem of complex plane transitions of the multiple-module robot. For example, when the new active joint is applied to the three-module robot in subsection 3.5.1, the middle module may become compliant to the

corner during the external plane transition.

However, this concept is more complex in design and control: the two rods have more than two degrees of freedom; the robot should adopt tracks to prevent getting stuck during external plane transition; the plane transitions need to be designed carefully as the active joint and compliant joints will act together on the modules. To make the design and control more efficient, this promising concept also needs a further study in the future.

### 3.5.3 Alternative Vibration Mechanism

Liner servo motor, which is shown in Figure 57, can be employed to replace conventional servo motor in vibration adhesion mechanism. Compared with conventional servo motor, liner motor will allow much accurate control of vibration amplitude and frequency of the suction pad. In addition, adopting liner motor can make the device more compact and simple as it does not need spring mechanism and cam. However, the big disadvantage of liner motor lies in its limited power and force densities.

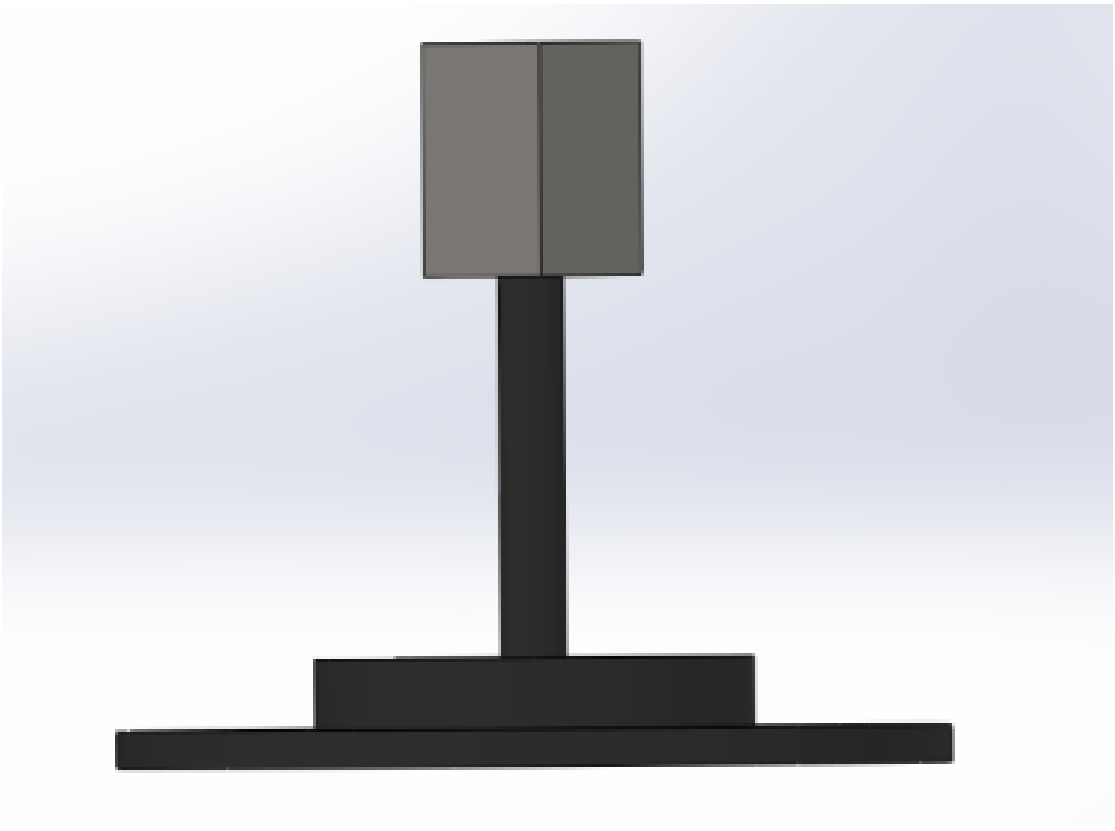

**Figure 57: Vibration mechanism with liner servo motor**

## 3.6 Summary

In this chapter, a modular wall-climbing wheeled robot, which employs general-purpose adhesion mechanism for adhering to various structure surfaces, is proposed. The design, prototyping and simulation of the two-module robot prototype are investigated to demonstrate the feasibility of the proposed robot design. Several design variants, such as a three-module robot, connecting rods based new active joint, and linear motor driven vibration adhesion mechanism, are also explored. The outstanding features of the proposed two-module wall-climbing robot include:

1) High mobility on complex shaped walls. The robot can freely negotiate (up to 90 °) convex and concave obstacles;
2) Simple structure and easy control. Wheeled locomotion and modular design significantly simplify the structure and control of the robot;
3) General-purpose inspection. Vibration adhesion mechanism enables the robot to adhere to various structure surfaces, such a plastic, woods, glass, metals and concrete walls;
4) Scalable. Upon specific requirements, the modular robot can be flexibly scaled by changing the number of jointed modules.

# Chapter 4 Kinematic Analysis of Two-Module Robot

## 4.1 Introduction

Aiming to enable the two-module robot to have high mobility on complex shaped walls, this chapter focuses on the mechanical kinematic analysis of the two-module robot in different typical scenarios of inter-plane transitions. Kinematic analysis includes primary design methods for the adhesion force, the motor force, the joint force and the balance tail force. Simulation case studies of inter-plane transitions are carried out to illustrate the feasibility of the kinematic analysis.

## 4.2 Kinematic Analysis

### 4.2.1 Adhesion Force Analysis

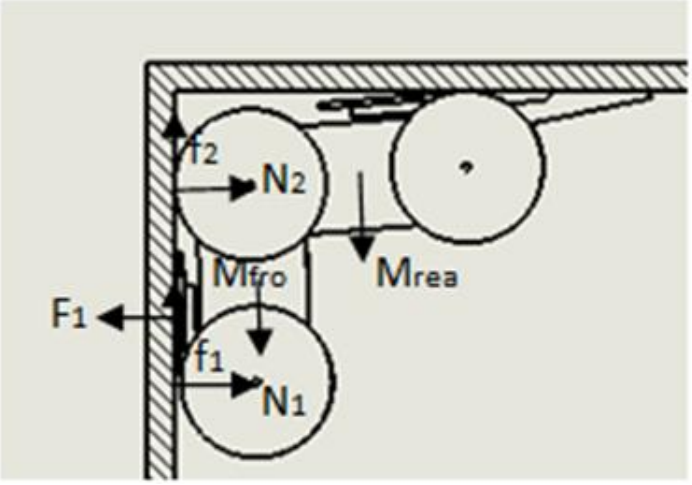


**Figure 58: The robot transits from ceiling to wall.**

For the two-module robot, the front and rear suction pads provide suction force $F_1$ and $F_2$, respectively. Figure 58 shows one worst scenario for the adhesion force analysis. As shown in Figure 58, the robot is transiting from the ceiling to the vertical wall, the rear pad should provide adhesion force to hang the whole device there. When the rear pad begins to lose its suction force, the front pad should afford sufficient force to adhere the robot to the wall. Therefore we will have

$$\mu F_1 > M \tag{2}$$

And then

$$F_1 > M / \mu \qquad (\mu<1) \tag{3}$$

where M is the total weight of the robot, μ is the coefficient of sliding friction between the wheel and wall.

### 4.2.2 Motor Force Analysis

The rolling friction force of a rubber wheel can be written as:

$$f = \delta N \tag{4}$$

where $\delta$ ($\delta < 1$) is the coefficient of rolling friction of the wheel and wall, r is the wheel radius, and N is the force on the wheel and perpendicular to the contact surface.

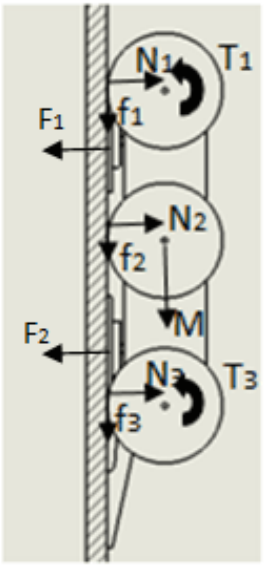


**Figure 59: The robot climbs up a vertical wall.**

As shown in Figure 59, when the robot climbs up a vertical wall, it needs to overcome the maximum resistance in climbing. The corresponding rolling friction is:

$$f = f_1 + f_2 + f_3 = \delta(F_1 + F_2) \tag{5}$$

To drive the robot with weight of M, the motors of the wheels need to provide torque:

$$T_1 + T_3 \geq r\left[\delta(F_1 + F_2) + M\right] \tag{6}$$

where $T_1$, $T_3$ are the torque of front motor and rear motor, respectively.

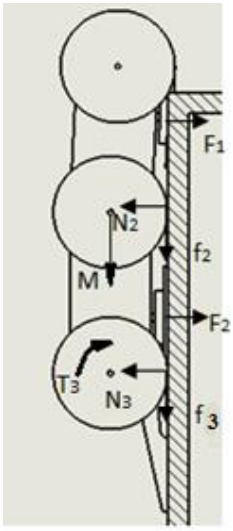


**Figure 60: The front pad begins to lose the suction force at an extern corner.**

When the front pad begins to lose the suction force during inter-plane transition at an extern corner, as shown in Figure 60, the drive torque should obey:

$$f_2 + f_3 = \delta\left(F_1 + F_2\right) \tag{7}$$

$$T_3 / r - (f_2 + f_3) - M \geq 0 \tag{8}$$

From (7) and (8), we can get:

$$T_3 / r - \delta\left(F_1 + F_2\right) - M \geq 0 \tag{9}$$

As a result:

$$T_3 \geq r\left[\delta(F_1 + F_2) + M\right] \tag{10}$$

When the front module adheres to the front surface during plane transition at an internal corner, as shown in the Figure 61, we will have:

$$f_2 + f_3 = \delta\left[(f_2 + f_3) + M + F_2\right] \tag{11}$$

$$N_2^{'} + N_f = T_3 / r - (f_2 + f_3) + F_1 \tag{12}$$

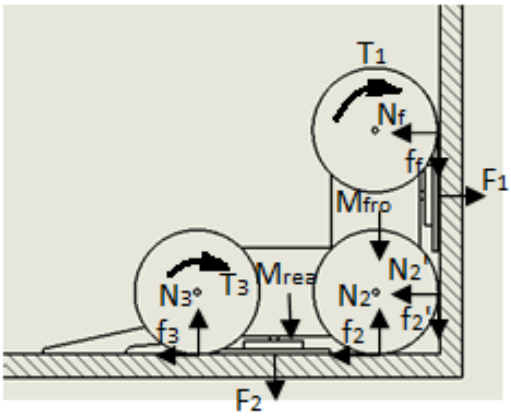


**Figure 61: The front module adheres to the front surface.**

From (11) and (12), we can obtain:

$$f_f + f_2^{'} = \delta(N_2^{'} + N_f) = \delta[T_3 / r - (f_2 + f_3) + F_1] = \\ \delta(T_3 / r + F_1) - \delta^2 \left(M + F_2\right) - \delta^2 (f_f + f_2^{'}) \tag{13}$$

As a result:

$$f_f + f_2^{'} = [\delta(T_3 / r + F_1) - \delta^2 \left(M + F_2\right)] / (1 + \delta^2) \tag{14}$$

To lift the rear module, the following condition should be satisfied:

$$T_1 / r - (f_f + f_2^{'}) - M - F_2 > 0 \tag{15}$$

Substitute (14) into (15):

$$T_1 / r - [\delta(T_3 / r + F_1) - \delta^2 \left(M + F_2\right)] / (1 + \delta^2) - M - F_2 \geq 0 \tag{16}$$

Re-arrange:

$$T_1 > r\{[\delta(T_3 / r + F_1) - \delta^2 \left(M + F_2\right)] / (1 + \delta^2) + M + F_2\} \tag{17}$$

### 4.2.3 Joint Force Analysis

A motor located at the joint can fold modules to the desired direction during the inter-plane transitions. The torque $T_r$ of the joint motor can be calculated as

$$\theta = \alpha t^2 / 2 \tag{18}$$

$$T_r = I_{fro}\,\alpha \tag{19}$$

Substitute (19) into (18), we have

$$\theta = T_r t^2 / 2 I_{fro} \tag{20}$$

where θ is angular displacement, α is angular acceleration. $I_{fro}$ is the moment of inertia of the front module.

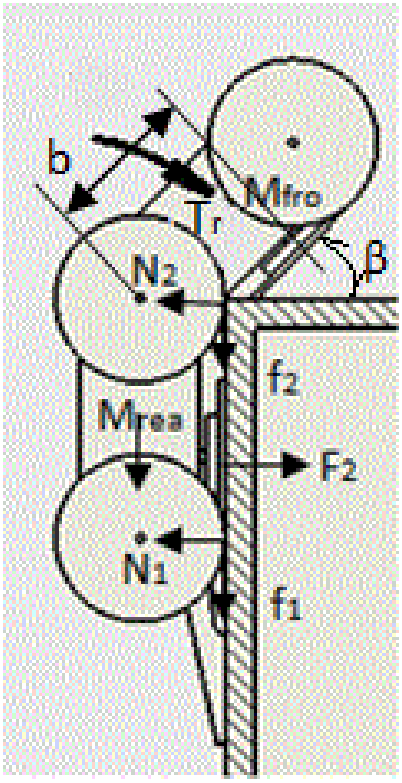


**Figure 62: The front module rotates.**

As shown in Figure 62, β is the angular between the front module and the new surface, r is the distance the robot has moved up, c is the radius of the suction pad and b is the distance from middle wheel to the front suction pad. We can have

$$\beta = \sin^{-1}\frac{\sqrt{r^2 + c^2}}{b} \tag{21}$$

When the speed of the robot is 0.1m/s

$$t = r / 0.1 \tag{22}$$

$$\theta = \beta \tag{23}$$

The torque $T_r$ of the joint motor should be:

$$T_r > (0.02 I_{fro} \sin^{-1} \frac{\sqrt{r^2 + c^2}}{b}) / r^2 \tag{24}$$

$$\frac{\beta}{t} = \frac{n\pi}{60} \tag{25}$$

Substitute (21) into (25), the rotational speed of the joint motor will be

$$n = 60\beta / \pi t = 6 sin^{-1} \frac{\sqrt{r^2 + c^2}}{b} / \pi r \tag{26}$$

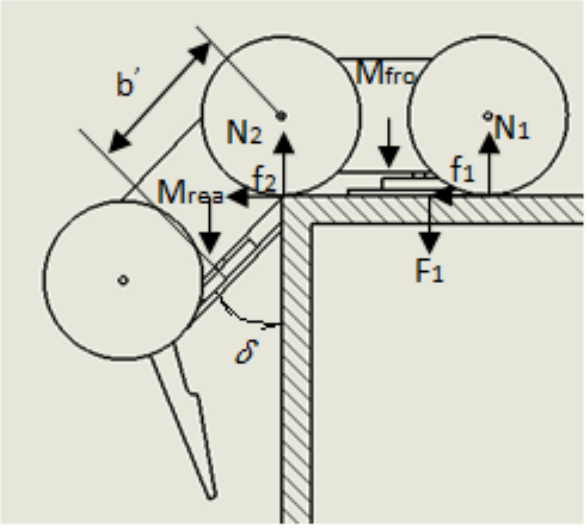


**Figure 63: The rear module rotates.**

The case shown in Figure 63 is similar to the case shown in Figure 62.

The joint motor should generate a torque to overcome the front adhesion and lift the front module during an internal plane transition, as shown in Figure 64. The rolling friction of the robot on the surface is:

$$f = \delta (M + F_1 + F_2) \tag{27}$$

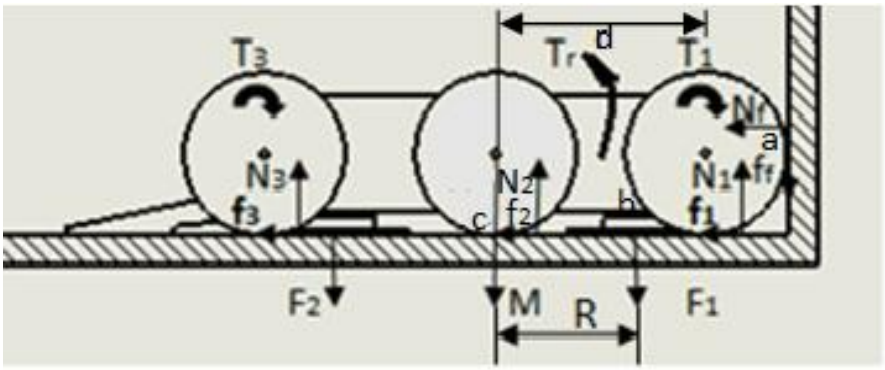


**Figure 64: Joint motor lift the front module.**

The forces provided by the two motors are $T_1$/r and $T_3$/$r$. The driving force of the motors $F_m$ is:

$$F_m = (T_1 + T_3)/r \tag{28}$$

$$N_f = F - f = (T_1 + T_3)/r - \delta(M + F_1 + F_2) \tag{29}$$

The sliding friction force at point "a" is:

$$f_f = \delta \cdot N_f = \delta\left[(T_1 + T_3)/r - \delta\left(M + F_1 + F_2\right)\right] \tag{30}$$

Consider the driving force of the $T_1$, the motive force at point "a" is:

$$F = T_1/r - f_f = T_1/r - \delta[(T_1 + T_3)/r - \delta\left(M + F_1 + F_2\right)] \tag{31}$$

$$T_a = F_a\left(d + r\right) = \left(d + r\right)\left\{T_1/r - \delta\left[\left(T_1 + T_3\right)/r - \delta\left(M + F_1 + F_2\right)\right]\right\} \tag{32}$$

At the point "b", the torque created by suction force and gravity of the front module is $T_b$,

$$T_b = R(F_1 + M_{fro}) \tag{33}$$

To obtain a torque relate to point "c", the torque $T_r$ of the joint motor should be satisfy the following condition:

$$T_r + T_a > T_b \tag{34}$$

Substitute (31) and (33) into (34), we can get:

$$T_r > R\left(F_1 + M_{fro}\right) - \left(d\right)\left\{r_1/T - \delta\left[\left(1 + T\right)_3/T - \delta\left(r + M_1F\right)\right]\right\} \quad (35)$$

### 4.2.4 Balance Tail Force Analysis

During the transition from the vertical wall to ceiling, in the scenario shown in Figure 65, the rear wheel motor should have the torque of $F_3 l_3$ at point "d" to overcome the maximum torque caused by the payload $M_{fro}$ of the front module and the joint force.

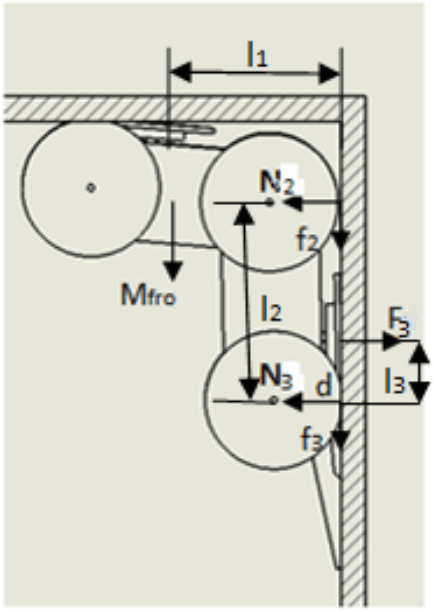


**Figure 65: The force analysis of transition from wall to ceiling.**

The torque $F3l3$ can be calculated as:

$$F_3 l_3 = M_{fro} l_1 + N_2 \quad (36)$$

When $N_2$ is 0, we will have

$$F_3 l_3 = M_{fro} l_1 \quad (37)$$

And then

$$F_3 = M_{fro} l_1 / \quad (38)$$

The preload force provided by spring of the tail ($F_s$) can be calculated as

$$F_s = F_3 - F_p = M_{fro} l_1 / l_3 - F_1 \quad (39)$$

where $F_p$ is the suction force of the pad.

## 4.3 System Specifications

According to the analysis above, the system specifications are given in the following as a case study for the sake of simulations.

**Table 2: Technical Specifications.**

| | |
|---|---|
| Payload | 1 kg |
| Climbing speed of the robot | $s$ = 0.1 m/s |
| Front module(mm) | 50(width)×75(length) |
| Rear module(mm) | 50(width)×80(length) |
| Wheel radius size | $r$ = 21 mm |
| Coefficient of Rolling friction(on plastic) | $\delta$ = 0.6 |
| Coefficient of sliding friction(on plastic) | $\mu$ = 0.8 |
| Negative pressure force | $F_1 = F_2$ =11 N |
| Motor of wheels | $T_3$ = 0.6 N·m |
| | $T_1$ = 1 N·m |
| | $n_1 = n_2$ = 46 rpm |
| | $p_1$ = 5 W |
| | $p_2$ = 5 W |
| Motor of joint | $T_r$ = 0.1 |
| | $n_r$ = 31 rpm |
| | $p_r$ = 1 W |
| Pre load of Balance tail spring | $F_p$ = 8 N |

## 4.4 Motion Simulations

This section illustrates the motion simulations of the two-module wall-climbing robot, and all simulations are completed with SolidWorks. The system specifications and parameters are listed in Table 2. Simulation scenarios include the flat plane moving and inter-plane transitions between vertical and horizontal planes.

### 4.4.1 Flat Plane Moving

Figure 66 shows how to set the type of study as “motion analysis” in Solidworks. This computational kinematic analysis not only can accurately specify the material properties,

mass and inertia of the robot, but also can emulate the effects of gravity, suction forces, motor torque, springs function, and frictions on this robot.

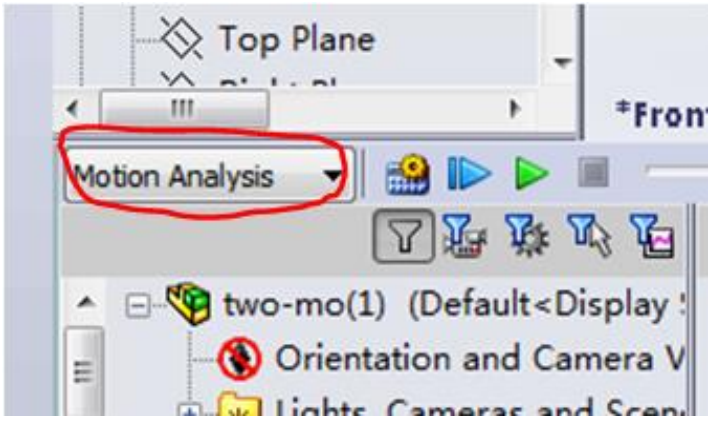


**Figure 66: Set the type of study as "motion analysis" in Solidworks.**

As shown in Figure 67, the adhesion force of suction pad is set as a constant 11N, with the blue arrow indicating the force position and direction.

Figure 68 shows how to set the servo motor of front wheels in Solidworks. The speed of motor is set as a constant 46 rpm. The red arrow denotes the rotate direction of the motor.

Similarly, as shown in Figure 69, the speed the servo motor of the rear wheels is also set as a constant 46 rpm.

Figure 70 shows how to set the robot contact condition. The material of the wall is defined as acrylic, and the material of the wheels is defined as rubber.

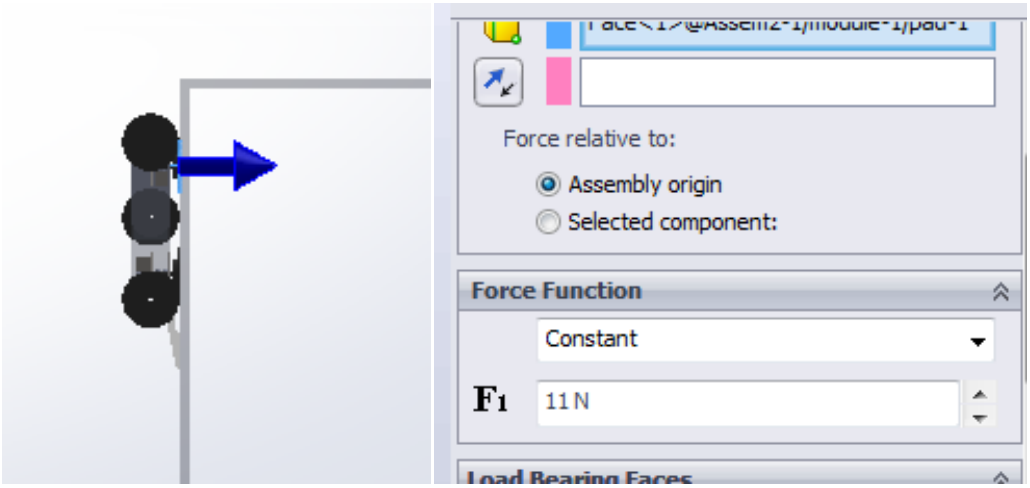


**Figure 67: Set adhesion force.**

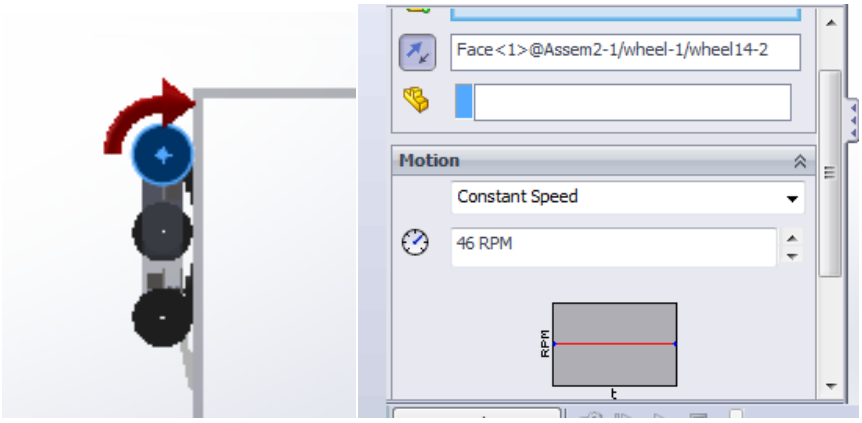


**Figure 68: Set the servo motor of front wheels.**

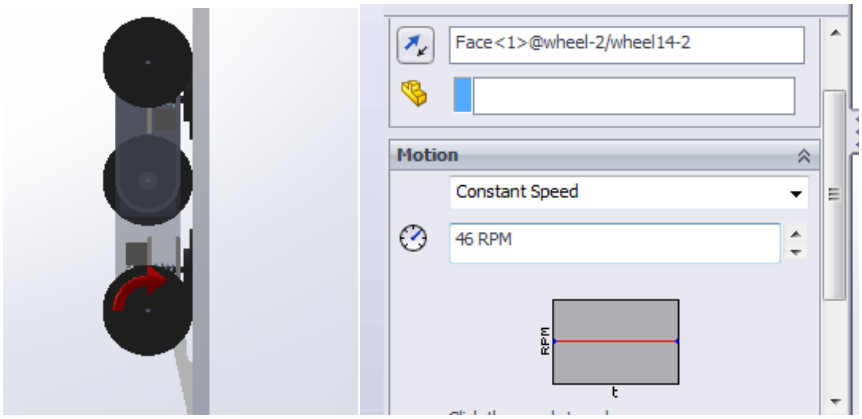


**Figure 69: Set the servo motor of rear wheels.**

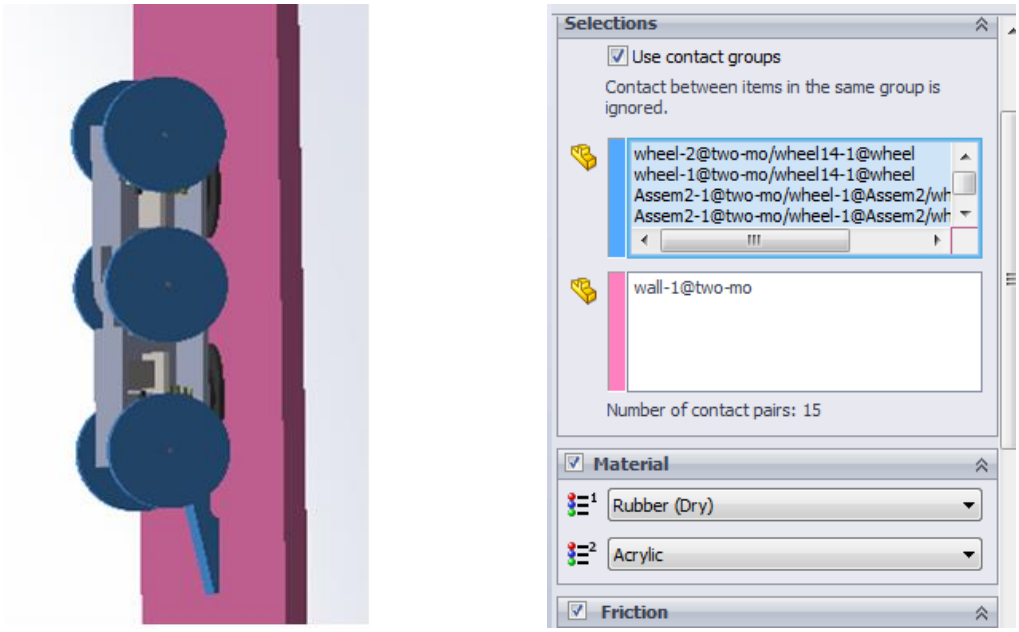


**(a)** **(b)**

**Figure 70: Set the robot contact condition.**

Figure 71 shows how to set the torsion spring of the tail. The tail spring can provide a preload force to enhance the adhesion.

After the settings described above being done, the motion simulations of the robot on flat plane are conducted. The simulation results demonstrate the proposed two-module robot can freely move on the flat planes as expected.

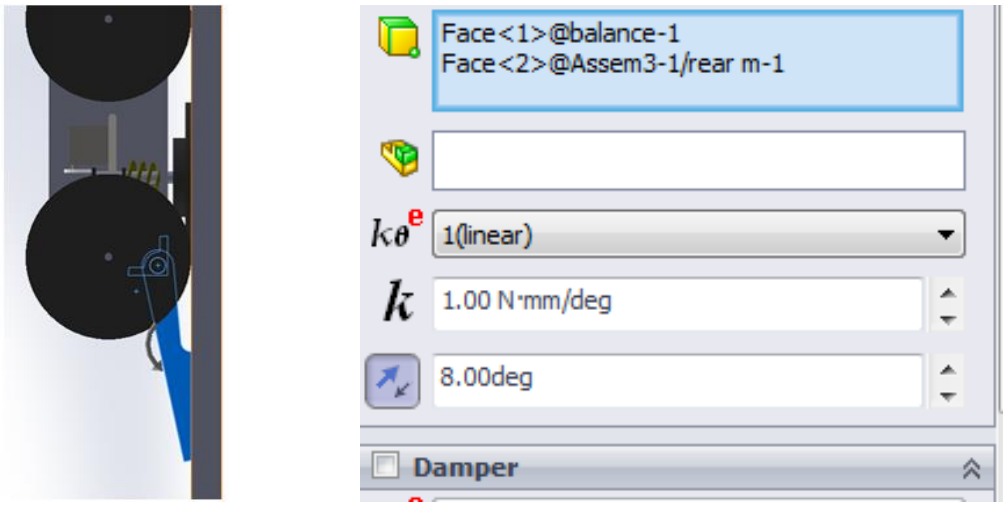


(a) (b)

**Figure 71: Set the torsion spring of the tail.**

### 4.4.2 Inter-Plane Transitions

To testify the mobility of the robot on complex shaped walls, inter-plane transitions between the vertical and the horizontal walls are employed as typical scenarios.

#### 4.4.2.1 The Motion Simulations of the Joint

Figure 72 shows how to set simulation parameters of the joint motor, where the red arrow indicates the rotate direction of the joint motor.

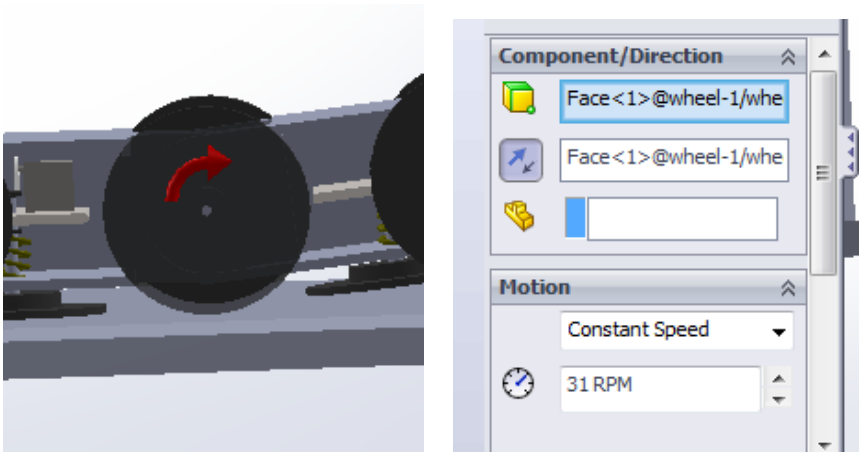


**Figure 72: Set the joint motor.**

Figure 73 show how to set mate of two gears of the joint for motion analysis.

Figure 74 illustrates the simulated operation of the joint motor, where the red arrow in Figure 74 (a) denotes the rotate direction of motor and the parameters of the motor are given in Figure 74 (b).

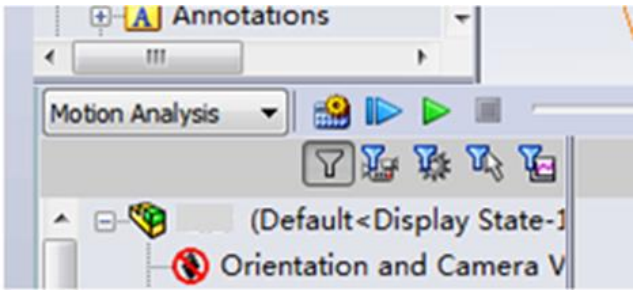


**(a)**

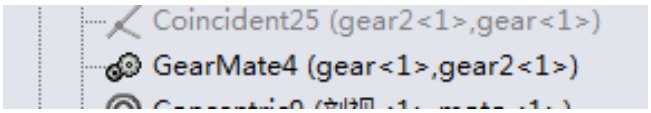


**(b)**

**Figure 73: Set mate of two gears.**

As shown in Figure 75, the red circles show the time of simulations. Figure 75 (a) and (b) indicates that the joint can operated as the expected descriptions in Chapter 3.

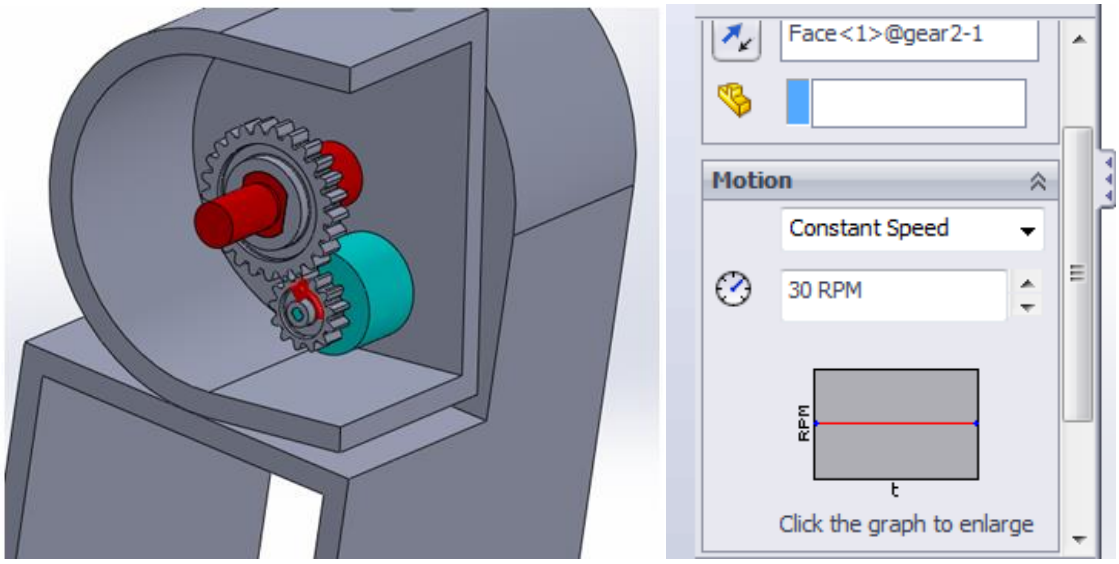


**(a):Sectional view of joint.** **(b): parameter sittings.**

**Figure 74: Simulations of the joint.**

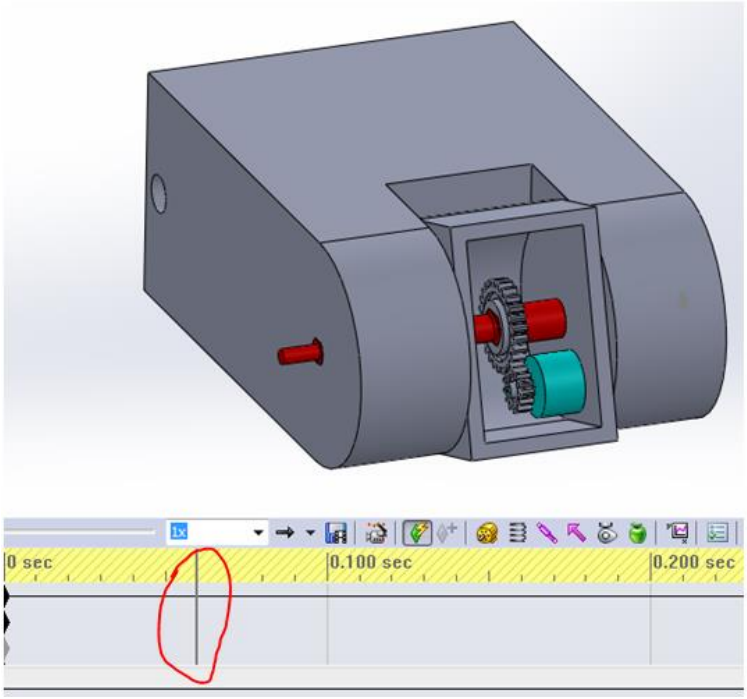


**(a)**

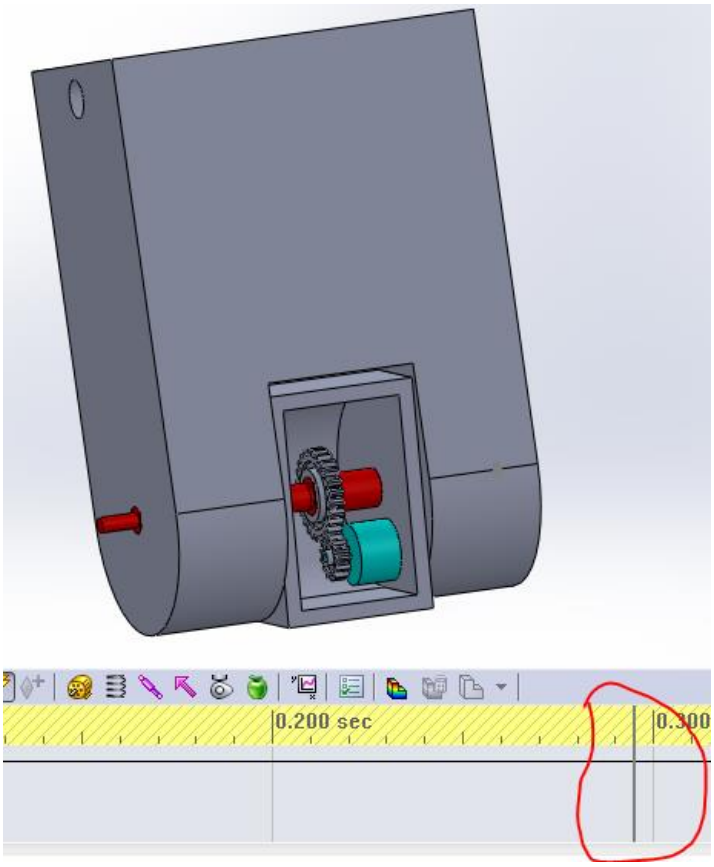


**(b)**

**Figure 75: Simulation results.**

### 4.4.2.2 Inter-Plane Transition Simulations

To illustrate the plane transitions, four situations are simulated, the details will be given in the following:

a) Internal plane transition (concave) from horizontal to vertical wall

The analysis of the joint motor for lifting the modules is given in the previous section. As a result, to simplify the simulations, it is assumed that when the front wheels are pushed to the vertical wall, the adhesion of the front suction pad is lost while robot relies on the rear pad to adhere on the wall. It is also assumed that the front adhesion will recover when it rotates to attach to the vertical wall, and meanwhile the rear pad loses the suction until it finishes the folding.

Figure 76 shows how to set the suction pads functions. Figure 77 shows the simulation snapshots of how the robot makes a successful internal plane transition from

horizontal to vertical,

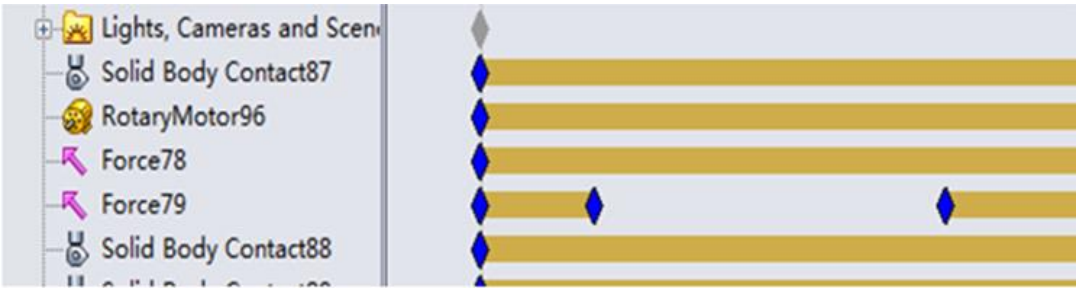


**Figure 76: Set the state of the suction force (on/off).**

b) External plane transition (convex) from vertical to horizontal wall, shown in Figure 79.

Similarly, to simplify the simulations, it is assumed that when the front pad moves ahead and detaches itself from the vertical wall, the adhesion of the front suction pad is lost while robot relies on the rear pad to adhere to the wall. It is also assumed that the front adhesion will recover when it rotates to attach to the horizontal wall, and meanwhile the rear pad loses the suction force until it finishes the folding.

Figure 78 shows how to fulfil the suction pads functions: in the timeline area, set the state of the suction force (on/off) according to the positions of two modules.

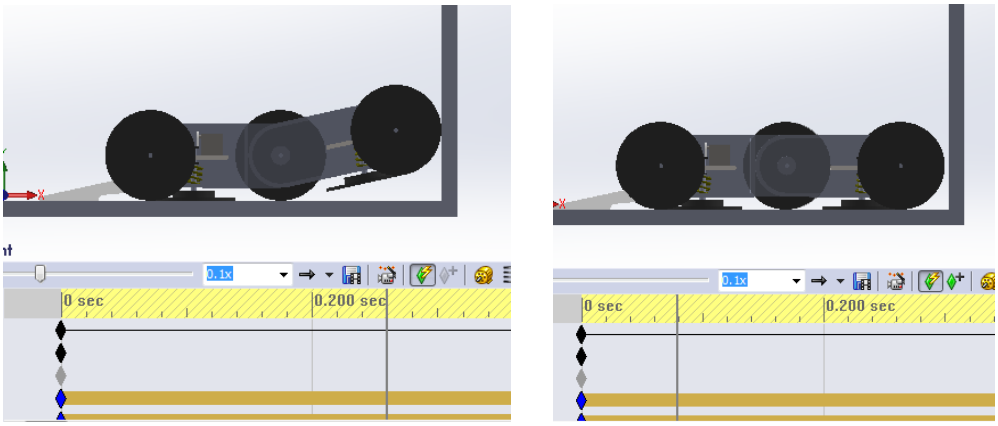


**(a)** **(b)**

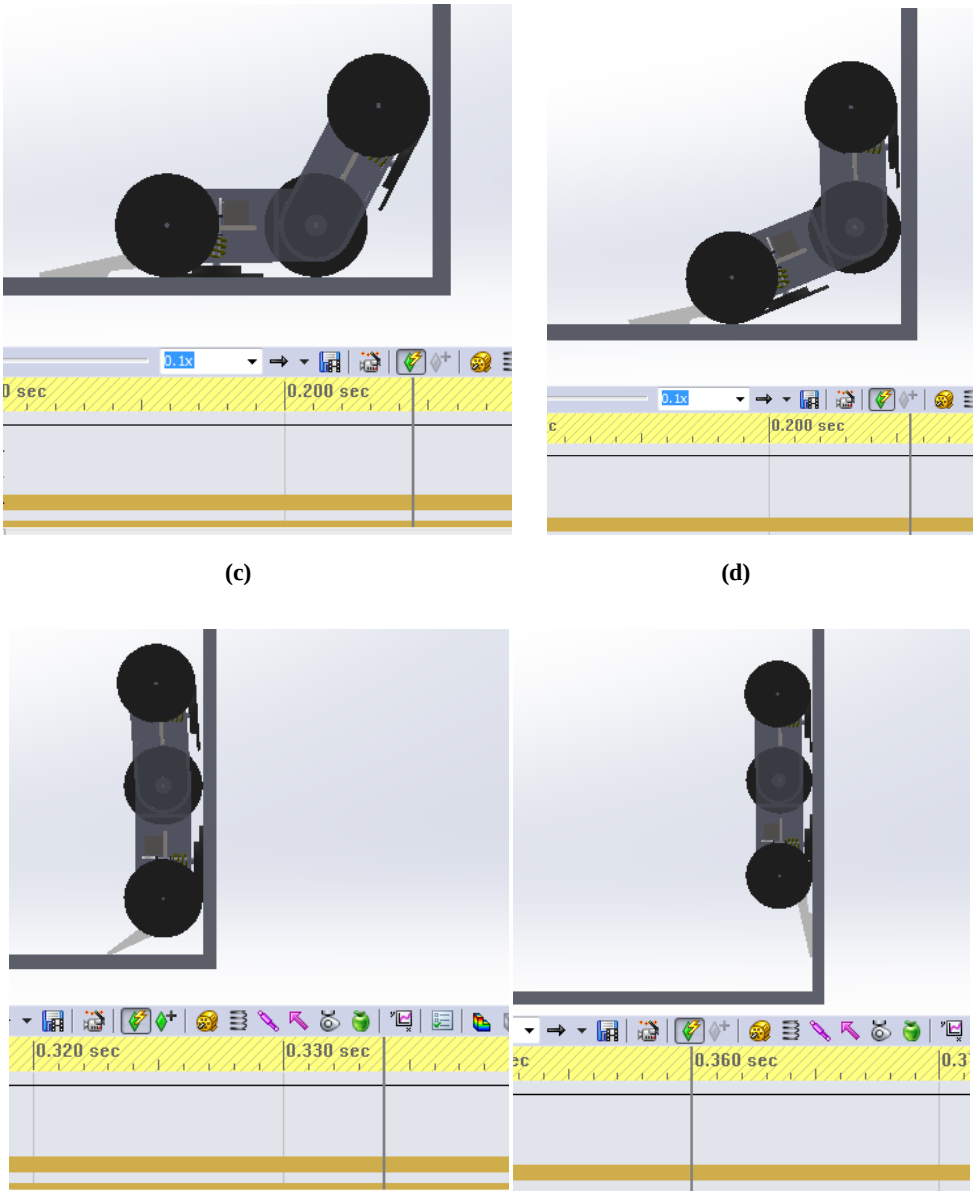


**(c)** **(d)**

**(e)** **(f)**

**Figure 77: Internal plane transition from horizontal to vertical wall Simulations.**

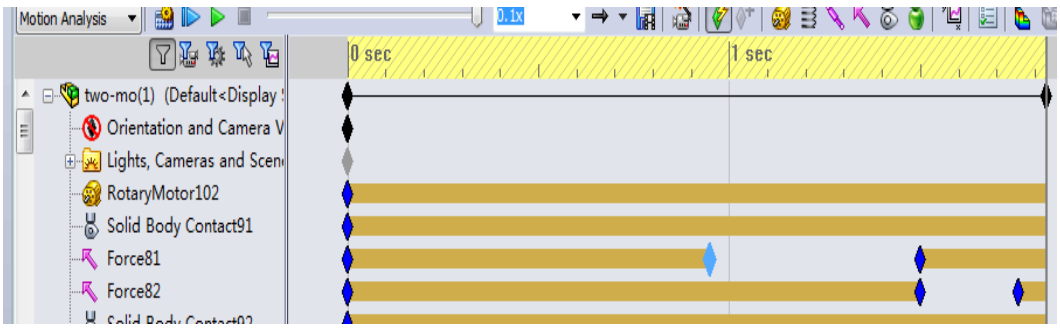


**Figure 78: Set the state of the suction force (on/off).**

Figure 79 shows the simulation snapshots of how the robot makes a successful external plane transition from vertical to horizontal.

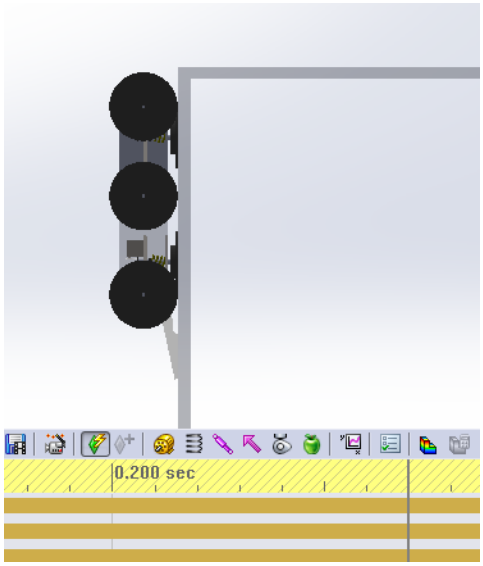


**(a)**

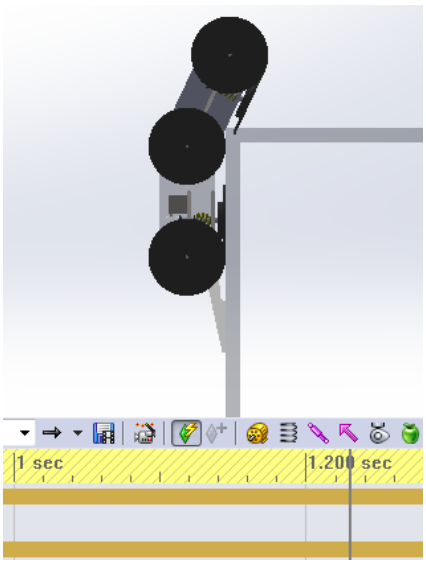


**(b)**

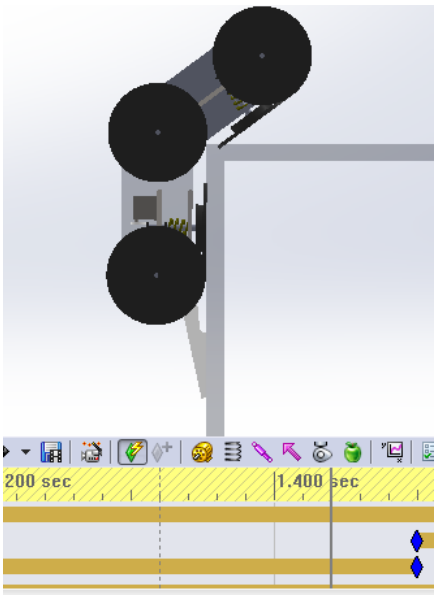


**(c)**

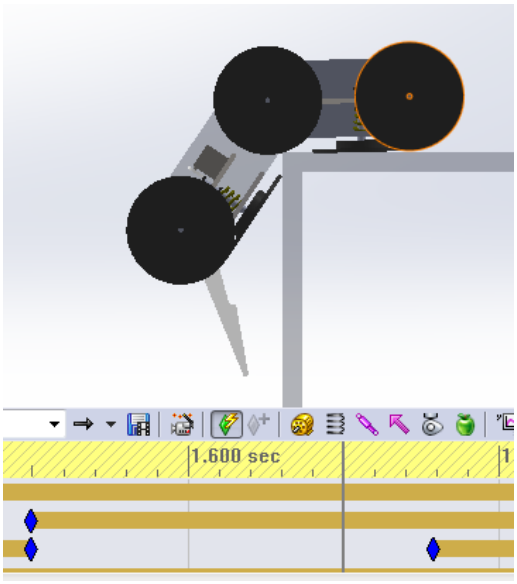


**(d)**

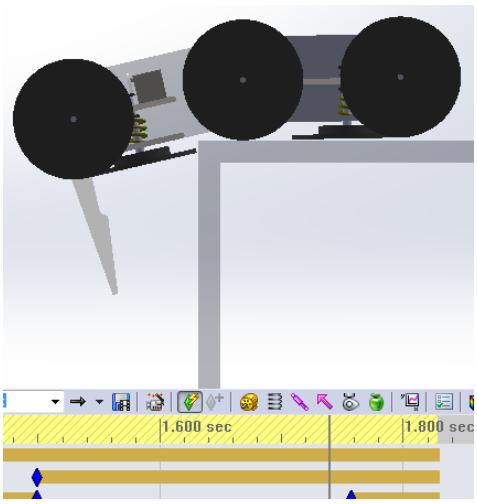


(e)

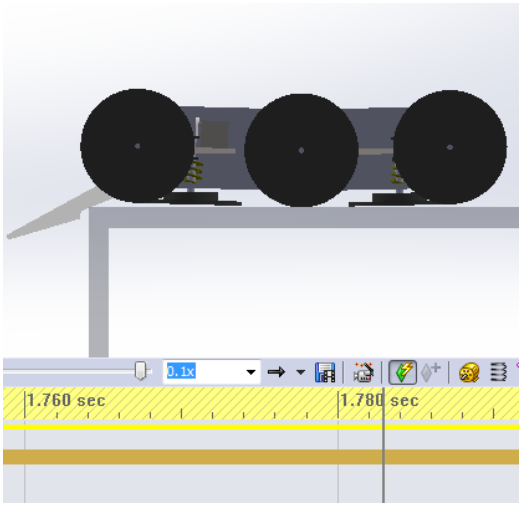


(f)

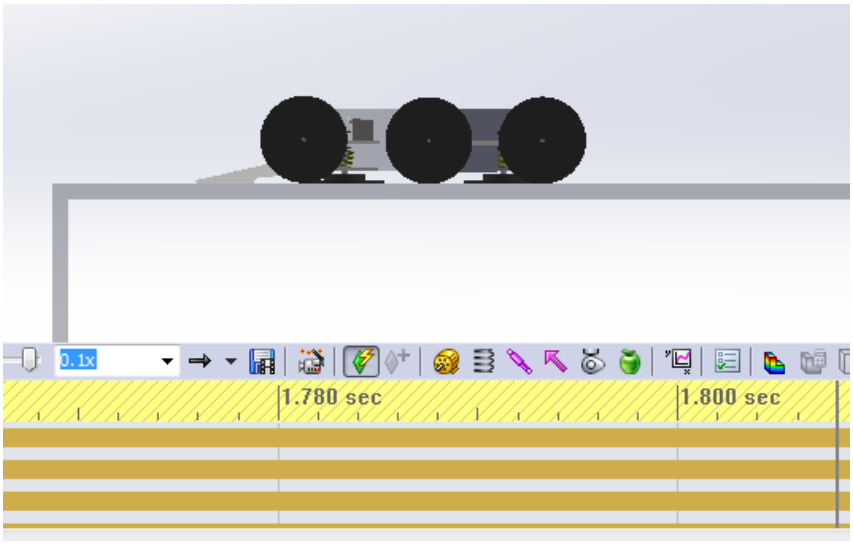


(g)

**Figure 79: External plane transition from vertical to horizontal wall simulations.**

c) External plane transition from horizontal to vertical wall, shown in Figure 81.

It is assumed that when the front pad moves ahead and detaches the horizontal wall, the adhesion of the front suction pad is lost while robot relies on the rear pad to adhere on the wall. It is also assumed that the front adhesion will recover when it rotates to the horizontal wall, and meanwhile the rear pad loses the suction force until it finishes the folding.

As shown in Figure 80, the suction pads functions are fulfilled through: in the timeline area, set the state of the suction force (on/off) according to the positions of two modules.

Figure 81 shows the simulation snapshots of how the robot makes a successful external plane transition from horizontal to vertical.


**Figure 80: Set the state of the suction force (on/off).**

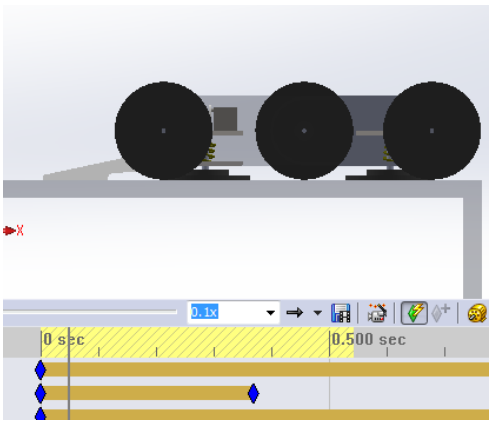


**(a)**

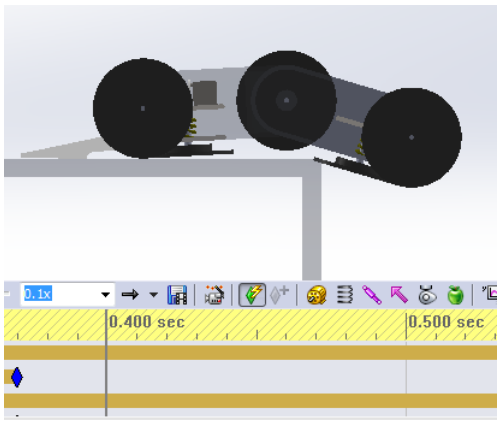


**(b)**

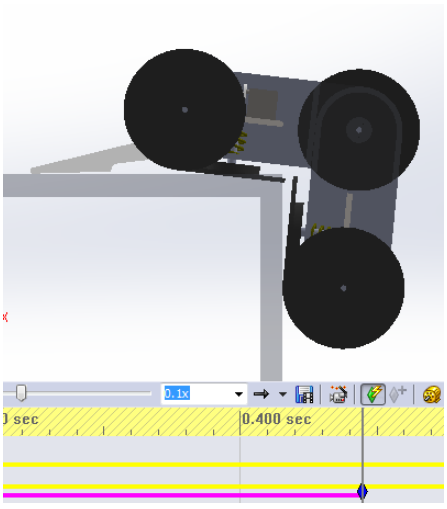


**(c)**

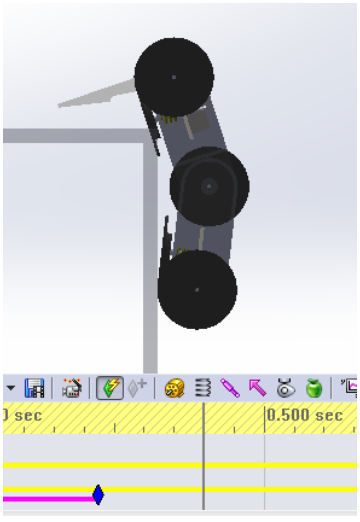


**(d)**

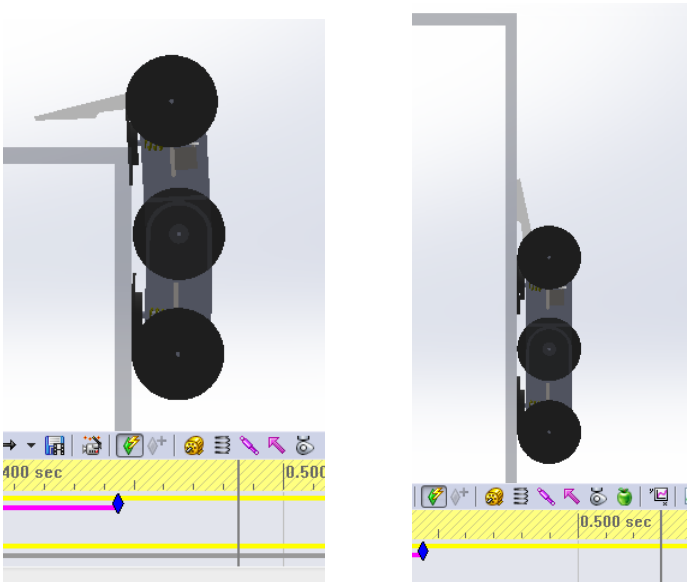


(e) (f)

**Figure 81: External plane transition from horizontal to vertical wall simulations.**

d) Internal plane transition from vertical to horizontal wall, shown in Figure 83.

It is assumed that when the front wheels are pushed on the horizontal wall, the adhesion of the front suction pad is lost while robot relies on the rear pad to adhere on the wall. It is also assumed the front adhesion will recover when it rotates to the horizontal wall, and meanwhile the rear pad loses the suction force until it finishes the folding.

As shown in Figure 82, the suction pads functions are fulfilled through: in the timeline area, set the state of the suction force (on/off) according to the positions of two modules.

Figure 83 shows the simulation snapshots of how the robot makes a successful internal plane transition from vertical to horizontal.

The plane transitions simulations, including internal plane and external plane transitions, are achieved. They are agreeing with the description of expected motion in chapter3.

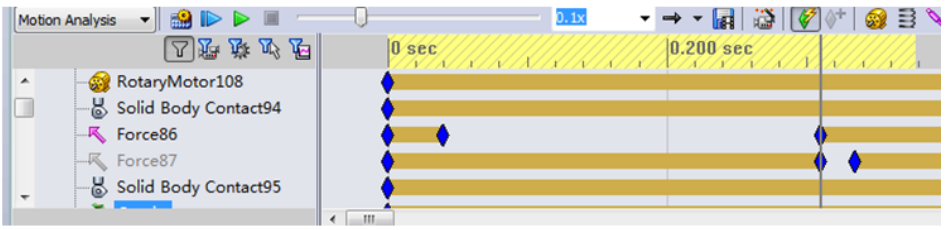


**Figure 82: Set the state of the suction force (on/off).**

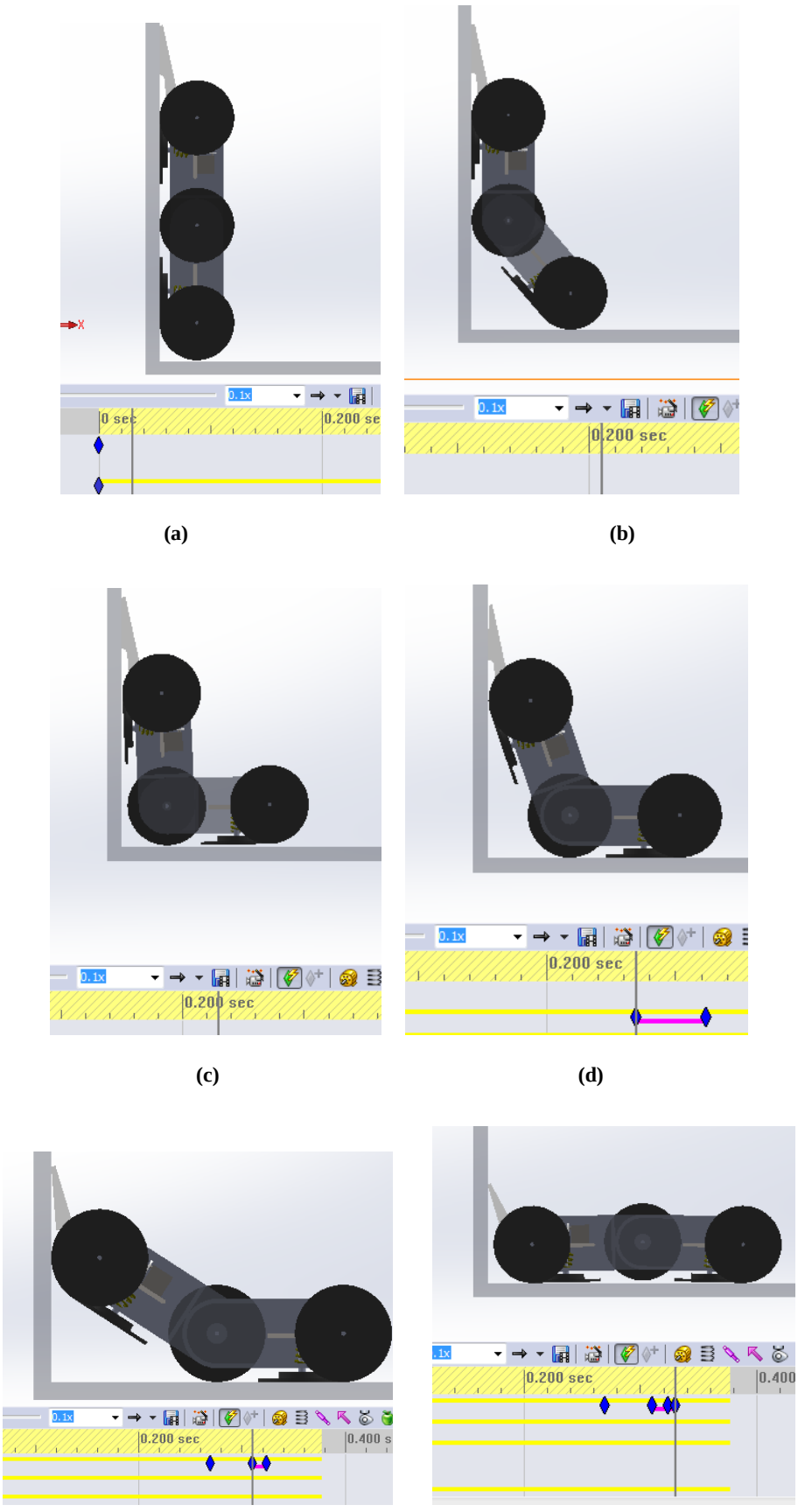


**(a)** **(b)**

**(c)** **(d)**

**(e)** **(f)**

**Figure 83: Internal plane transition from vertical to horizontal wall simulations.**

## 4.5 Summary

In this chapter, kinematics analysis of the two module wall-climbing robot is presented, which illustrates the design and selection of adhesion mechanism, locomotion mechanisms, the active joint and the balance tail. Motion simulations also preliminarily demonstrate the high mobility of the two-module wall-climbing robot.

# Chapter 5 Modular Robot with Electromagnetic Adhesion

## 5.1 Introduction

General-purpose vibration adhesion mechanism may fail to provide robust adhesion force to robots on rough surfaces. Moreover, compared with other adhesion mechanisms, such as dry adhesion and magnetic adhesion mechanism, vibration adhesion mechanism usually consumes more energy. Magnet adhesion using permanent magnets or/and electromagnets is considered the best adhesion solution for ferromagnetic structures in terms of energy efficiency, adhesive force abundance and operation reliability. Therefore an alternative modular climbing robot with electromagnetic adhesion is conceived for the inspection of ferromagnetic structures.

As shown in Figure 84, a two-module robot prototype with magnetic adhesion is developed. It takes almost the same mechanical design as the two-module robot in Chapter 3 and 4, but replaces the vibration adhesion mechanism with magnetic cups. The two-module wall-climbing robot also utilizes wheeled locomotion with three pairs of wheels, the front and rear wheels are driven by two motors respectively. The balance tail for such a robot can be omitted to simplify the robot design.

This chapter focuses on the feasibility study of such a robot variants, which is exclusively developed for ferromagnetic structure inspection.

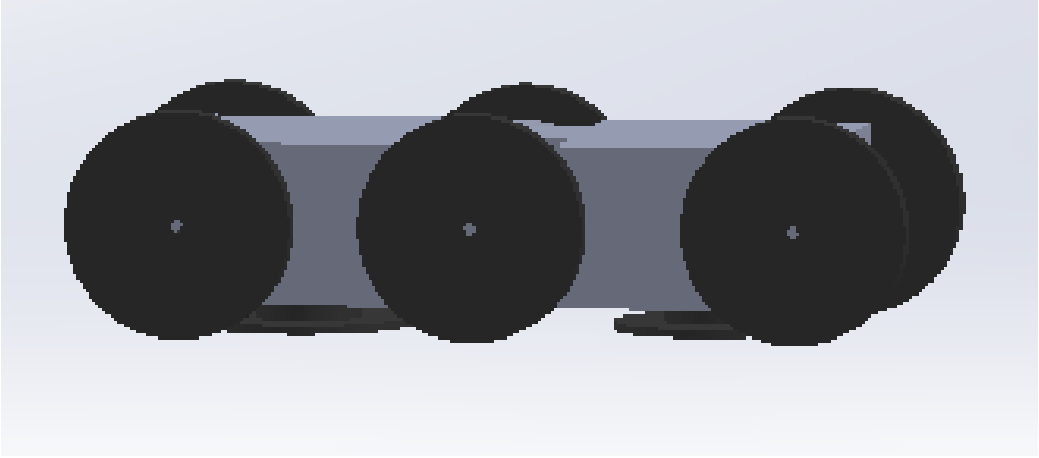

**Figure 84: Configurable climbing robot with magnetic adhesion.**

### 5.1.1 Electromagnetic Adhesion Mechanism

Unlike the previous design, this two-module robot replaces the vibration adhesion mechanism with two magnetic cups. The magnetic cup integrates an array of permanent magnets and electromagnets to obtain a low power consumption but reliable adhesion. Permanent magnets themselves don't consume any power to generate the magnetic force. During the plane transitions, in order to detach the module from a wall and lift it, the electromagnets will be energized to offset the resultant magnetic force of permanent magnets. The electromagnets can also be energized to reinforce the adhesion force of permanent magnets. In addition, the two-module robot with the electromagnetic adhesion mechanism does not need a balance tail to ensure the stability of the robot during its inter-plane transitions.

Figure 85 shows how the resultant adhesion force changes with the distance between the magnetic cup and the metal wall surface. It can be seen from Figure 85 that the adhesive force drops down sharply with increasing distance. Therefore, in order to obtain strong adhesive force, the magnetic cups should be put very near the wall surface. However, the magnetic cups would not touch the wall surface because it will increase the friction resistance to movement of the robot.

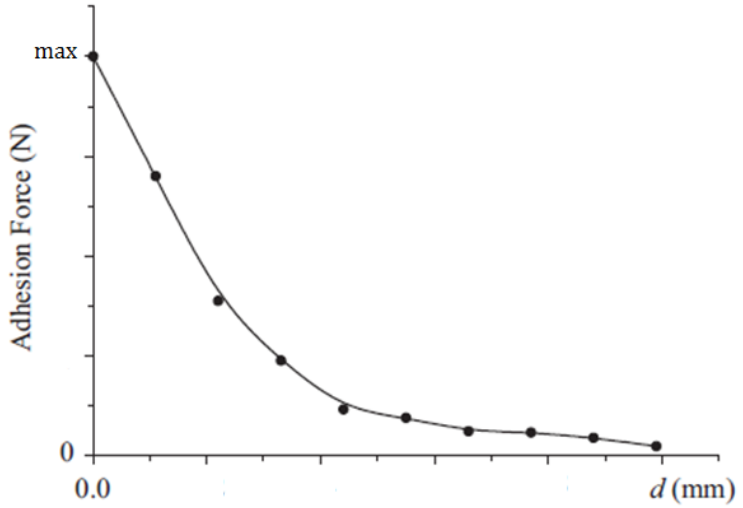


**Figure 85: The relationship between adhesion force and the cup-wall distance.**

### 5.1.2 Wheeled Locomotion Mechanism

The robot consists of three pairs of wheels: one pair of front module wheels, one pair of rear module wheels, and one pair of joint wheels. All the wheels are made from high friction coefficient material. The front and rear wheels which are drive wheels with two separated servo motors, enable the robot to freely move (forward, backward and turn) on flat wall surfaces. The joint wheels are driven wheels without any servo motor.

### 5.1.3 Joint Design

This robot also adopts an active joint, which is manipulated by a servo motor. The joint can actively fold the modules to facilitate the inter-plane transitions of the robot. Figure 86 presents the detail of the active joint - the section view of the joint shown in Figure 86(a) and the exploded view of the joint in Figure 86(b). The active joint mainly comprises of a drive bearing, a set of gears and a servo motor. The active joint can fold the modules to facilitate the inter-plane transitions of the robot by controlling the servo motor.

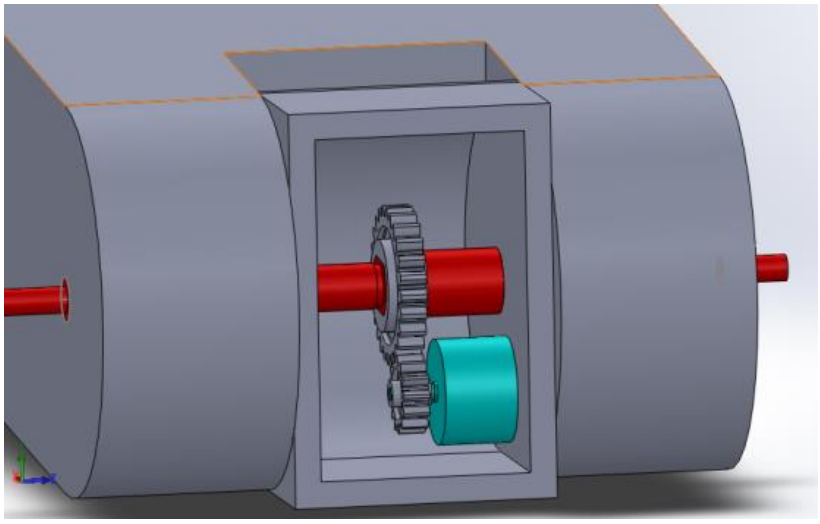

**(a)**

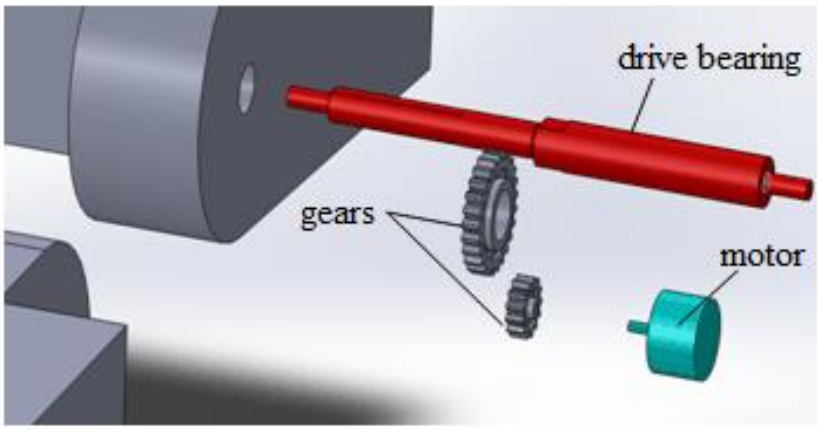


**(b)**

**Figure 86: Active joint design.**

## 5.2 Inter-Plane Transition Motion Scenarios

This section investigates typical scenarios of inter-plane transitions of the robot with electromagnetic wheels.

### 5.2.1 Internal Corner (Concave)

When the device travels to an inner corner, the wheels at the front is pushed against the wall. The electromagnets of front magnetic cups become energized to offset the resultant magnetic force of permanent magnets to detach the front module from its current surface. The motor of the middle joint is actuated to lift and fold the front module to touch the next surface. Meanwhile the rear module is pushing the device to move forward. When the front module touches the next surface, the front magnetic cups will stop offsetting permanent magnetic forces. The permanent magnets will make the front module adhere to the new surface. After that, the front module will keep moving ahead on the new surface, and the electromagnets on the rear magnetic cup are energized to offset the resultant magnetic force to detach the rear module from its current surface. At the same time, the middle active joint will rotate reversely to fold the rear module rotate to touch the new surface. After the robot completes the inter-plane transition, the adhesion cups under the rear module will also stop offsetting permanent magnetic forces, and the permanent magnets will make the rear module adhere to the new surface.

### 5.2.2 External Corner (Convex)

When the device travels to an external corner, the drive wheels on the rear module will push the device to move forward, and the electromagnets of magnetic cups on rear modules become energized to reinforce the magnetic adhesion of the robot to current surface. Meanwhile the middle active joint will fold the front module to touch the new surface. When the front module adheres to the next surface, the rear magnetic cups will start to offset permanent magnetic forces, and the front magnetic cups will be energized to reinforce its magnetic adhesion to the new surface. And then the front drive module will start to pull the device to move forward on the new surface, and the middle active joint will rotate reversely to lift the rear module to be detached from the current surface. After the robot completes this inter-plane transition, the adhesion electromagnetic cup under the rear module will stop offsetting permanent magnetic forces, and the permanent magnets will adhere the rear module to the new surface.

## 5.3 Kinematic Analysis

The kinematic analysis of the new two-module robot is almost the same as previous robot. It mainly involves the analysis of adhesion force and active joint.

### 5.3.1 Adhesion Force Analysis

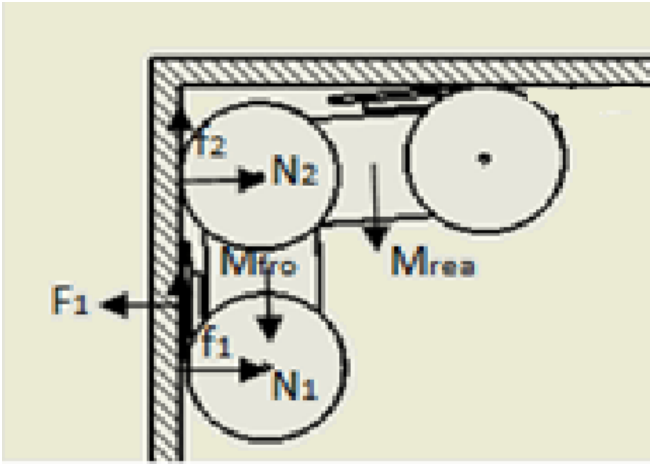


**Figure 87: Force analysis of the robot transiting from ceiling to wall.**

For the two-module robot, the front and rear suction pads provide suction force $F_1$ and $F_2$,

respectively. Figure 87 shows one worst scenario for the adhesion force analysis. As shown in Figure 87, the robot is transiting from the ceiling to the vertical wall, the rear pad should provide adhesion force to hang the whole device there. When the rear pad begins to lose its suction force, the front pad should afford sufficient force to adhere the robot to the wall. Therefore we will have

$$\mu F_1 > M \tag{40}$$

And then

$$F_1 > M / \mu \qquad (\mu<1) \tag{41}$$

where μ is the coefficient of sliding friction of the wheel and wall, and M is the weight of the robot.

## 5.3.2 Motor Force Analysis

A rubber wheel rolls on a surface is considered have friction force of rolling:

$$f = \delta N \tag{42}$$

where $\delta$ ($\delta < 1$) is the coefficient of rolling friction of the wheel and wall, r is the wheel radius, and N is the force on the wheel and perpendicular to the contact surface.

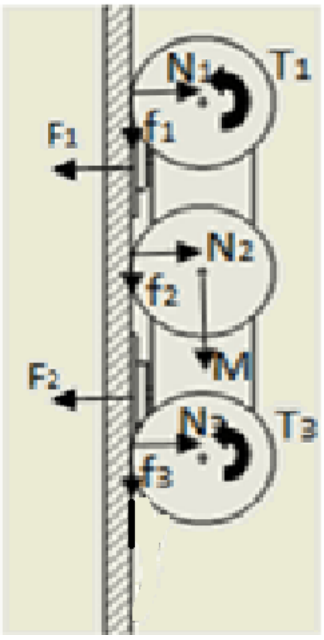


**Figure 88: The robot climbs up the wall.**

As shown in Figure 88, when the robot climbs up the wall, it should overcome the maximum rolling resistance in climbing. The rolling friction is:

$$f = f_1 + f_2 + f_3 = \delta(F_1 + F_2) \tag{43}$$

To drive the robot with weight of M, the servo motors of the wheels need to provide torque:

$$T_1 + T_3 \geq r\left[\delta(F_1 + F_2) + M\right] \tag{44}$$

where $T_1$, $T_3$ are the torque of front motor and rear motor, respectively.

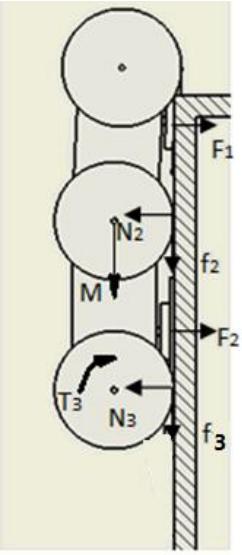


**Figure 89: The front pad begins to lose the suction force at an extern corner.**

As shown in Figure 89, when the front pad begins to lose the suction force at an extern corner, the torque $T_3$ provided by rear wheel should satisfy

$$f_2 + f_3 = \delta\left(F_1 + F_2\right) \tag{45}$$

$$T_3 / r - (f_2 + f_3) - M \geq 0 \tag{46}$$

From (45) and (46), we will have:

$$T_3 / r - \delta\left(F_1 + F_2\right) - M \geq 0 \tag{47}$$

$$T_3 \geq r\left[\delta(F_1 + F_2) + M\right] \tag{48}$$

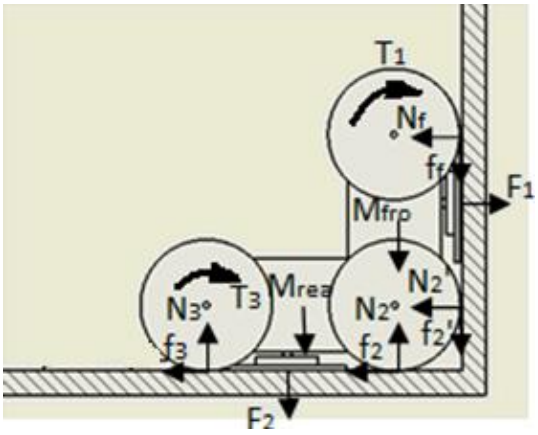


**Figure 90: When the front module adheres to the front surface.**

As shown in the Figure 90, when the front module adheres to the front surface during an internal plane transition from the horizontal wall to the vertical wall, the relationship among the forces can be written as

$$f_2 + f_3 = \delta\left[(f_2 + f_3) + M + F_2\right] \tag{49}$$

$$N_2^{'} + N_f = T_3 / r - (f_2 + f_3) + F_1 \tag{50}$$

From (49) and (50), we can get:

$$\begin{aligned} &f_f + f_2^{'} = \delta(N_2^{'} + N_f) = \delta[T_3 / r - (f_2 + f_3) + F_1] = \\ &\delta(T_3 / r + F_1) - \delta^2\left(M + F_2\right) - \delta^2(f_f + f_2^{'}) \end{aligned} \tag{51}$$

Thus

$$f_f + f_2^{'} = [\delta(T_3 / r + F_1) - \delta^2\left(M + F_2\right)] / (1 + \delta^2) \tag{52}$$

To fold the rear module, the following condition should be satisfied:

$$T_1 / r - (f_f + f_2^{'}) - M - F_2 > 0 \tag{53}$$

Substitute (52) into (53), we have

$$T_1 / r - [\delta(T_3 / r + F_1) - \delta^2\left(M + F_2\right)] / (1 + \delta^2) - M - F_2 \geq 0 \tag{54}$$

And then,

$$T_1 > r\{[\delta(T_3 / r + F_1) - \delta^2\left(M + F_2\right)] / (1 + \delta^2) + M + F_2\} \tag{55}$$

At that moment the rear module begins to energize electromagnetic force to offset the resultant magnetic force of the permanent magnet, that means

$$F_2 = 0 \tag{56}$$

Therefore

$$T_1 > r\{[\delta(T_3 / r + F_1) - \delta^2 M] / (1+\delta^2) + M\} \tag{57}$$

### 5.3.3 Joint Force Analysis

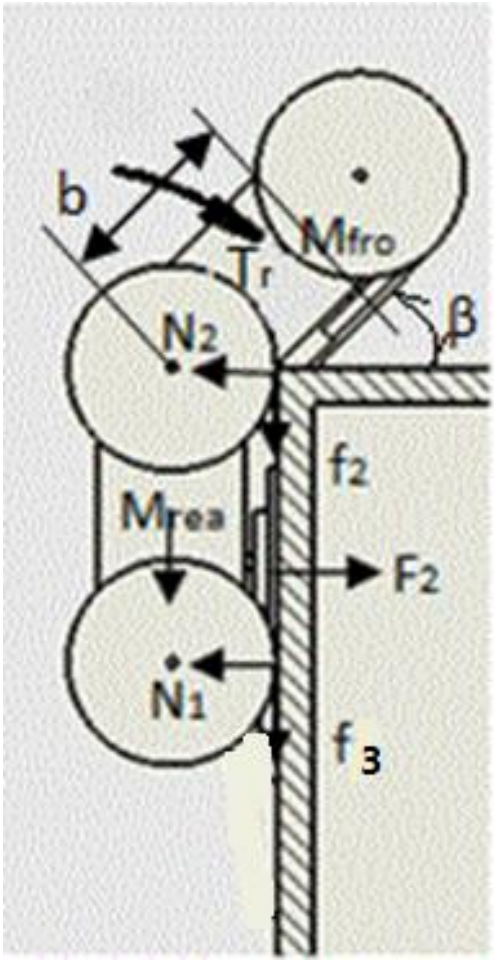


**Figure 91: The front module rotates.**

As shown in Figure 91 and Figure 92, a motor located at the joint is used to fold modules during the inter-plane transitions. The torque of the joint motor can be written as:

$$\theta = \alpha t^2 / 2 \tag{58}$$

$$T_r = I_{fr} \alpha \tag{59}$$

Substitute (59) into (58), we have

$$\theta = T_r t^2 / 2I_{fro} \tag{60}$$

where θ is angular displacement, α is angular acceleration. $I_{fro}$ is the moment of inertia of the front module.

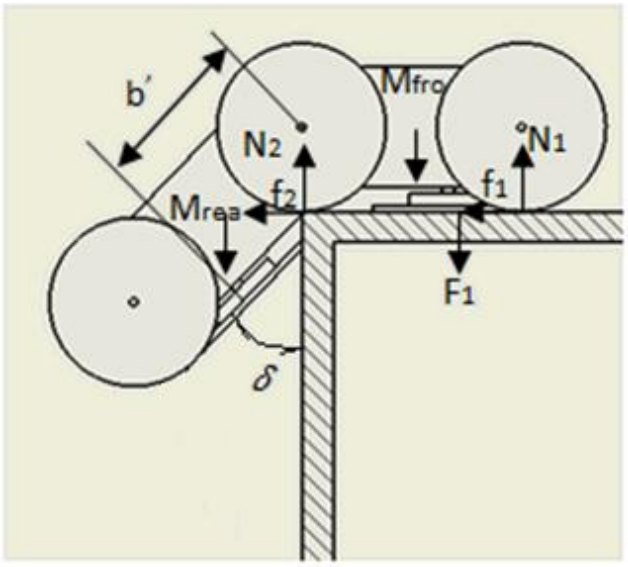


**Figure 92: The rear module rotates.**

As shown in Figure 91, β is the angular between the front module and the new surface, r is the distance the robot has moved up, c is the radius of the suction pad and b is the distance from middle wheel to the front suction pad. We can have

$$\beta = \sin^{-1} \frac{\sqrt{r^2 + c^2}}{b} \tag{61}$$

When the speed of the robot is 0.1m/s, we will have

$$t = r / 0.1 \tag{62}$$

$$\theta = \beta \tag{63}$$

The torque $T_r$ of the joint motor should satisfy

$$T_r > (0.02 I_{fro} \sin^{-1} \frac{\sqrt{r^2 + c^2}}{b}) / r^2 \tag{64}$$

$$\frac{\beta}{t} = \frac{n\pi}{60} \tag{65}$$

Substitute (61) into (65), we can get the rotational speed of the joint motor

$$n = 60\beta / \pi t = 6sin^{-1}\frac{\sqrt{r^2 + c^2}}{b} / \pi r \tag{66}$$

The case shown in Figure 92 is similar to the case shown in Figure 91.

Figure 93 shows one worst scenario which needs maximum joint torque. As shown in Figure 93, at the moment of detaching the rear module from the vertical wall, the gravity of the rear module will yield the torque $T_b$ as

$$T_b = dM_{rea} / 2 \tag{67}$$

The required torque $T_r$ of the joint motor should satisfy:

$$T_r \geq T_b \tag{68}$$

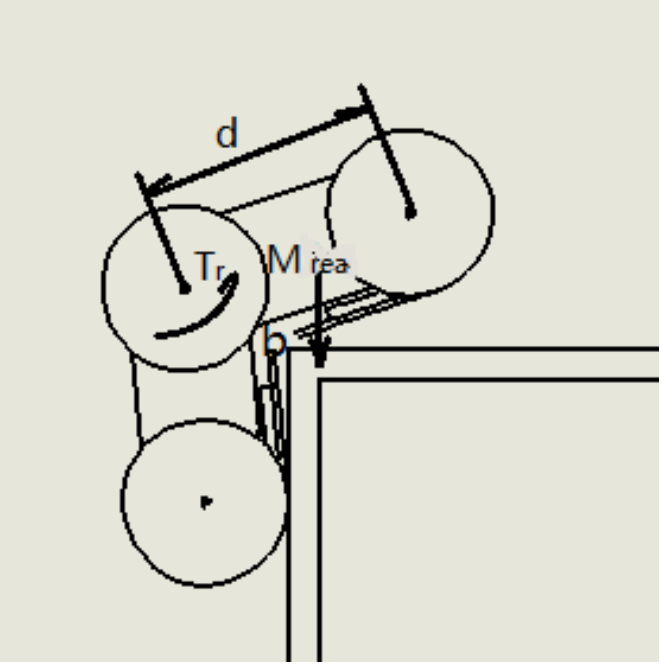


**Figure 93: The rear module begins to be detached from the vertical wall.**

Substitute (67) into (68), we can obtain:

$$T_r \geq dM_{rea} / 2 \tag{69}$$

## 5.4 System Specifications

According to the analysis above, the system specifications are listed in Table 3.

**Table 3: Technical Specifications.**

| | |
|---|---|
| Payload | 1 kg |
| Climbing speed of the robot | $s$ = 0.1 m/s |
| Front module(mm) | 50(width)×75(length) |
| Rear module(mm) | 50(width)×80(length) |
| Wheel radius size | $r$ = 21 mm |
| Coefficient of Rolling friction(on metal) | $\delta$ = 0.6 |
| Coefficient of sliding friction(on metal) | $\mu$ = 0.8 |
| Magnetic adhesion force | $F_1 = F_2$ =10 N |
| Motor of rear wheels | $T_3$ = 0.6 N·m |
| Motor of front wheels | $T_1$ = 1 N·m |
| | $n_1 = n_2$ = 46 rpm |
| | $p_1$ = 5 W |
| | $p_2$ = 5 W |
| Motor of joint | $T_r$ = 0.6 N·m |
| | $n_r$ = 31 rpm |
| | $p_r$ = 1 W |

## 5.5 Summary

In this chapter, an alternative two-module climbing robot with electromagnetic adhesion is investigated. The main characteristic features of this concept include:

1) High mobility on complex shaped walls. The robot can freely negotiate (up to 90 °) convex and concave obstacles;
2) Energy-efficient and reliable adhesion solution for ferromagnetic structures;
3) A simpler structure due to the omission of the balance tail;
4) Simple structure and easy control wheeled locomotion;
5) Scalable modular design.

The shortcoming of such design is that it is only applicable for ferromagnetic structure climbing.

# Chapter 6- Conclusions and Future Work

## 6.1 Conclusions

This thesis investigated the development of a wall-climbing inspection robot with high mobility on complex shaped walls. The robot is applicable for various inspection tasks, such as duct/vessel inspection, bridge maintaining, and so on.

After a comprehensive review of the state-of-the-art wall-climbing robots, a modular wall-climbing wheeled inspection robot is proposed. Firstly a two-module wall-climbing robot with vibration (vacuum) adhesion is investigated. The two robot modules are connected by an active joint. Each robot module has one pair of locomotion wheels for motion and one mounted suction pad for adhesion. The active joint can fold the two modules from -90° to 90°, and enables the robot to pass various obstacles. General-purpose vibration adhesion mechanism is suitable for various structure surfaces (e.g. wood, concrete, steel, etc.). A balance tail is adopted to ensure the stability of the robot during its inter-plane transitions. In addition, several design variants, such as a three-module robot, a connecting rod based active joint, and linear motor driven vibration adhesion, are explored to improve the robot design.

Secondly, for ferromagnetic structure inspections, an optimized two-module wall-climbing robot with magnetic adhesion mechanism is explored. Compared with the robot with vibration adhesion mechanism, the robot with electromagnetic adhesion mechanism consumes less power while offering much reliable adhesion in harsh environments (such as rough and wet structure surfaces), and simplifies the mechanical structure due to the omission of the balance tail.

The comprehensive design, kinematic analysis and simulations of above two different adhesion mechanism robots are performed. All simulation results have demonstrated that the proposed modular wall-climbing robots can agilely move on complex shaped walls,

such as passing 90° convex and concave. Moreover, several design variants, such as a three-module robot, a two-module robot with connecting rods, and linear motor driven vibration adhesion are also investigated.

The major contributions of this thesis include:

- A wall-climbing inspection robot which is of low cost, simple structure, easy control, and scalable capability, is proposed. Modular design and wheeled-locomotion enable the robot to be scalable and simple and reliable.
- To achieve high mobility on complex shaped walls, two types of two-module wall-climbing robot prototypes with different adhesion mechanisms are designed and developed. The robot with general-purpose vibration adhesion mechanism is applicable to the climbing of various structure walls, while the robot with magnetic adhesion mechanism offers an optimal climbing device for ferromagnetic walls.
- Comprehensive design, kinematic analysis and simulations of the two wall-climbing robots are successfully carried out to demonstrate the feasibility of proposed robot.

## 6.2 The Future Work

Due to the time limitation and budget constraints, some tasks are expected to be conducted in the future, such as physical prototyping and adhesion mechanism optimization.

### 6.2.1 Physical Prototyping

In addition to their virtual SolidWorks prototyping models, physical prototypes of the robots should be built for physical tests. For examples, the chassis of prototype can be fabricated by using 3-D printers; the remote control module is needed; comprehensive physical experiments of the prototypes should be done.

### 6.2.2 Adhesion Mechanism Optimization

For various inspection tasks, the optimization of adhesion mechanism is crucial to the performance and reliability of the wall-climbing robots. The further study of vibration adhesion mechanism, such as linear motor driven vibration adhesion, is needed. The array

of permanent magnets and electromagnets also need to be optimized.

# References


[1] D. Schmidt and K. Berns, "Climbing robots for maintenance and inspections of vertical structures—A survey of design aspects and technologies," *Robotics and Autonomous Systems,* vol. 61, pp. 1288-1305, 2013.

[2] L. P. Kalra*, et al.*, "A wall climbing robot for oil tank inspection," in *2006 IEEE International Conference on Robotics and Biomimetics, ROBIO 2006, December 17, 2006 - December 20, 2006*, Kunming, China, 2006, pp. 1523-1528.

[3] J. Shao*, et al.*, "A wall-climbing robot with gecko features," in *2012 9th IEEE International Conference on Mechatronics and Automation, ICMA 2012, August 5, 2012 - August 8, 2012*, Chengdu, China, 2012, pp. 942-947.

[4] D. Schmidt*, et al.*, "Omnidirectional locomotion and traction control of the wheel-driven, wall-climbing robot, CROMSCI," *Robotica,* vol. 29, pp. 991-1003, 2011.

[5] C. Balaguer*, et al.*, "Climbing Robots' Mobility for Inspection and Maintenance of 3D Complex Environments," *Autonomous Robots,* vol. 18, pp. 157-169, 2005/03/01 2005.

[6] Y. Zhao*, et al.*, "Development and applications of wall-climbing robots with a single suction cup," *Robotica,* vol. 22, pp. 643-648, 2004.

[7] P. Sangdeok*, et al.*, "Design of a mobile robot system for automatic integrity evaluation of large size reservoirs and pipelines in industrial fields," in *Intelligent Robots and Systems, 2003. (IROS 2003). Proceedings. 2003 IEEE/RSJ International Conference on*, 2003, pp. 2618-2623 vol.3.

[8] T. S. W. B.L. Luk, D.S. Cooke, N.D. Hewer, G. Hazel, S. Chen, "Climbing Service Robot for Duct Inspection and Maintenance Applications in a Nuclear Reactor," presented at the Proceedings of the 32nd ISR(International Symposium on Robotics), 2001.

[9] T. P. Sattar*, et al.*, "Climbing ring robot for inspection of offshore wind turbines," *Industrial Robot: An International Journal,* vol. 36, pp. 326-330, 2009.

[10] S. S. Mondal, T. P. ; Bridge, B. , "TOFD inspection of V-groove butt welds on the hull of a container ship with a magnetically adhering wall climbing robot " presented at the International conference on climbing and walking robots 5th, International conference on climbing and walking robots, 2002

[11] H. Chen*, et al.*, "Motion Control of a Micro Biped Robot for Nondestructive Structure Inspection," in *Robotics and Automation, 2005. ICRA 2005. Proceedings of the 2005 IEEE International Conference on*, 2005, pp. 478-483.

[12] D. Tom, Ben, S.,&Andrew, T., Liam,S., "Wall Climbing Robot. ," ed. Canterbury: University of Canterbury, 2011.

[13] A. Ariga*, et al.*, "Wall climbing robot in narrow space with pantograph-type structure," in *2010 IEEE International Conference on Robotics and Biomimetics, ROBIO 2010, December 14, 2010 - December 18, 2010*, Tianjin, China, 2010, pp. 1507-1512.

[14] F. Tache*, et al.*, "Compact magnetic wheeled robot with high mobility for inspecting complex shaped pipe structures," in *Intelligent Robots and Systems, 2007. IROS 2007. IEEE/RSJ International Conference on*, 2007, pp. 261-266.

[15] R. L. Houxiang Zhang, Guanghua Zong and Jianwei Zhang, "A Novel Autonomous Climbing Robot for Cleaning an Elliptic Half-Shell," *Mobile Robots: towards New Applications,* 2006.

[16] H. Albitar*, et al.*, "New concept of in-water surface cleaning robot," in *Mechatronics and Automation (ICMA), 2013 IEEE International Conference on*, 2013, pp. 1582-1587.

[17] H. Zhang, *et al.*, "A novel approach to pneumatic position servo control of a glass wall cleaning robot," in *Intelligent Robots and Systems, 2004. (IROS 2004). Proceedings. 2004 IEEE/RSJ International Conference on*, 2004, pp. 467-472 vol.1.

[18] Y. Zhengyao, *et al.*, "Development of a wall climbing robot for ship rust removal," in *Mechatronics and Automation, 2009. ICMA 2009. International Conference on*, 2009, pp. 4610-4615.

[19] J. X. a. A. Sadegh, "City-Climber: A New Generation Wall-Climbing Robots," *Climbing and Walking Robots: towards New Applications,* 2007.

[20] W. Guo, *et al.*, "Design of a six legged wall-climbing robot," in *IEEE International Conference on Advanced Robotics and its Social Impacts, ARSO 2008, August 23, 2008 - August 25, 2008*, Taipei, Taiwan, 2008, p. IEEE Robotics and Automation Society.

[21] M. Wu, *et al.*, "Design and optimal research of a non-contact adjustable magnetic adhesion mechanism for a wall-climbing welding robot," *International Journal of Advanced Robotic Systems,* vol. 10, 2013.

[22] M. Taylor, *et al.*, "TigBot - A Wall Climbing Robot for TIG Welding of Stainless Steel Tanks," in *Mechatronics and Machine Vision in Practice, 2008. M2VIP 2008. 15th International Conference on*, 2008, pp. 550-554.

[23] A. Faina, *et al.*, "Development of a climbing robot for grit blasting operations in shipyards," in *Robotics and Automation, 2009. ICRA '09. IEEE International Conference on*, 2009, pp. 200-205.

[24] W. Chuan-sheng, *et al.*, "Study of the Wall-Climbing Robot for Hull Painting," in *E-Product E-Service and E-Entertainment (ICEEE), 2010 International Conference on*, 2010, pp. 1-4.

[25] X. Jizhong, *et al.*, "Modular wall climbing robots with transition capability," in *Robotics and Biomimetics (ROBIO). 2005 IEEE International Conference on*, 2005, pp. 246-250.

[26] S. TaeWon and M. Sitti, "Under-actuated tank-like climbing robot with various transitioning capabilities," in *Robotics and Automation (ICRA), 2011 IEEE International Conference on*, 2011, pp. 777-782.

[27] W. Shanqiang, *et al.*, "Design of a sliding wall climbing robot with a novel negative adsorption device," in *Ubiquitous Robots and Ambient Intelligence (URAI), 2011 8th International Conference on*, 2011, pp. 97-100.

[28] Y. Fu, *et al.*, "Development of a wall climbing robot with wheel-leg hybrid locomotion mechanism," in *2007 IEEE International Conference on Robotics and Biomimetics, ROBIO, December 15, 2007 - December 18, 2007*, Yalong Bay, Sanya, China, 2008, pp. 1876-1881.

[29] Z.-h. Wang, *et al.*, "Development and control of flexible pneumatic wall-climbing robot," *Journal of Central South University of Technology,* vol. 16, pp. 961-970, 2009/12/01 2009.

[30] K. W. W. W. H. Zhang, "The Mechanical Properties of a Wall-Climbing Caterpillar Robot Analysis and Experiment," *International Journal of Advanced Robotic Systems;,* vol. Vol. 10, , 2013.

[31] J. Zhu, *et al.*, "Development of a Tracked Climbing Robot," *Journal of Intelligent and Robotic Systems,* vol. 35, pp. 427-443, 2002/12/01 2002.

[32] H. Kim, *et al.*, "Development of a wall-climbing robot using a tracked wheel mechanism," *Journal of Mechanical Science and Technology,* vol. 22, pp. 1490-1498, 2008/08/01 2008.

[33] M. Wang, *et al.*, "Research on omni-directional moving adsorption mechanism and its application in wall-climbing robot," in *Information Science and Technology (ICIST), 2013 International Conference on*, 2013, pp. 220-225.

[34] X. Daijun, *et al.*, "Suction Ability Analyses of a Novel Wall Climbing Robot," in *Robotics and Biomimetics, 2006. ROBIO '06. IEEE International Conference on*, 2006, pp. 1506-1511.

[35] M. Elliott*, et al.*, "City-Climbers at Work," in *Robotics and Automation, 2007 IEEE International Conference on*, 2007, pp. 2764-2765.

[36] Y. Yoshida and M. Shugen, "A wall-climbing robot without any active suction mechanisms," in *Robotics and Biomimetics (ROBIO), 2011 IEEE International Conference on*, 2011, pp. 2014-2019.

[37] H. Na Shun Bu*, et al.*, "A mini multi-joint wall climbing robot based on the vibrating suction method," in *Robotics and Biomimetics, 2007. ROBIO 2007. IEEE International Conference on*, 2007, pp. 1861-1865.

[38] H. Yang*, et al.*, "A miniature multi-joint wall-climbing robot based on new vibration suction robotic foot," in *IEEE International Conference on Automation and Logistics, ICAL 2008, September 1, 2008 - September 3, 2008*, Qingdao, China, 2008, pp. 1160-1165.

[39] H. Qingfeng*, et al.*, "Principle and application of Underwater Vibration Suction Method," in *Robotics and Biomimetics (ROBIO), 2009 IEEE International Conference on*, 2009, pp. 1609-1614.

[40] H. Qingfeng*, et al.*, "Wall climbing robot enabled by a novel and robust vibration suction technology," in *Automation and Logistics, 2009. ICAL '09. IEEE International Conference on*, 2009, pp. 331-336.

[41] R. L. X. Y. Zhao, K. Wang, J. H. He, "Analysis and Experiments on Pulse Vibrating Suction Method for Wall Climbing Robot," *Advanced Materials Research,* vol. Vols 201-203, pp. pp. 1837-1844, Feb. 2011.

[42] Z. Bi*, et al.*, "A miniature biped wall-climbing robot for inspection of magnetic metal surfaces," in *2012 IEEE International Conference on Robotics and Biomimetics, ROBIO 2012, December 11, 2012 - December 14, 2012*, Guangzhou, China, 2012, pp. 324-329.

[43] J. C. Grieco*, et al.*, "A six-legged climbing robot for high payloads," in *Control Applications, 1998. Proceedings of the 1998 IEEE International Conference on*, 1998, pp. 446-450 vol.1.

[44] P. Schoeneich*, et al.*, "TRIPILLAR: a miniature magnetic caterpillar climbing robot with plane transition ability," *Robotica,* vol. 29, pp. 1075-1081, 2011.

[45] L. Giuk*, et al.*, "Compliant track-wheeled climbing robot with transitioning ability and high-payload capacity," in *Robotics and Biomimetics (ROBIO), 2011 IEEE International Conference on*, 2011, pp. 2020-2024.

[46] W. Fischer*, et al.*, "Compact magnetic wheeled robot for inspecting complex shaped structures in generator housings and similar environments," in *2009 IEEE/RSJ International Conference on Intelligent Robots and Systems, IROS 2009, October 11, 2009 - October 15, 2009*, St. Louis, MO, United states, 2009, pp. 4116-4121.

[47] M. Eich and T. Vogele, "Design and control of a lightweight magnetic climbing robot for vessel inspection," in *Control & Automation (MED), 2011 19th Mediterranean Conference on*, 2011, pp. 1200-1205.

[48] P. Y. Qiangqiang Zhang, Lisheng Wu, Changshuang Dong,Wei Zhou "Design and Optimization of Variable Magnetic Force Wheel for Wall-Climbing Robot," *International Journal of Advanced Robotic Systems,* vol. Vol. 4, pp. pp. 515 ~ 522,, 2012

[49] J. Shang*, et al.*, "Development of a climbing robot for inspection of long weld lines," *Industrial Robot: An International Journal,* vol. 35, pp. 217-223, 2008.

[50] A. Asbeck*, et al.*, "Climbing rough vertical surfaces with hierarchical directional adhesion," in *Robotics and Automation, 2009. ICRA '09. IEEE International Conference on*, 2009, pp. 2675-2680.

[51] M. Carlo and S. Metin, "A Biomimetic Climbing Robot Based on the Gecko," *Journal of Bionic Engineering,* vol. 3, pp. 115-125, 2006.

[52] J. L. Krahn, Y; Sadeghi, A; Menon, C "a tailless timing belt climbing platform utilizing dry adhesion with mushroom caps," *Smart Materials and Structures,* 2011.

[53] L. Yanwei*, et al.*, "A leg-wheel wall-climbing robot utilizing bio-inspired spine feet," in *Robotics and Biomimetics (ROBIO), 2013 IEEE International Conference on*, 2013, pp. 1819-1824.

[54] K. A. Daltorio*, et al.*, "Mini-Whegs$^{TM}$; climbing steep surfaces with insect-inspired attachment mechanisms," in *Intelligent Robots and Systems, 2007. IROS 2007. IEEE/RSJ International Conference on*, 2007, pp. 2556-2556.

[55] C. Kute*, et al.*, "Adhesion recovery and passive peeling in a wall climbing robot using adhesives," in *Robotics and Automation (ICRA), 2010 IEEE International Conference on*, 2010, pp. 2797-2802.

[56] K. A. Daltorio*, et al.*, "A body joint improves vertical to horizontal transitions of a wall-climbing robot," in *Robotics and Automation, 2008. ICRA 2008. IEEE International Conference on*, 2008, pp. 3046-3051.

[57] P. Boscariol*, et al.*, "Optimal Gait for Bioinspired Climbing Robots Using Dry Adhesion: A Quasi-Static Investigation," *Journal of Bionic Engineering,* vol. 10, pp. 1-11, 2013.

[58] D. Sameoto and C. Menon, "A low-cost, high-yield fabrication method for producing optimized biomimetic dry adhesives," *Journal of Micromechanics and Microengineering,* vol. 19, p. 115002, 2009.

[59] K. H. Koh*, et al.*, "Modeling and simulation of electrostatic adhesion for wall climbing robot," in *2011 IEEE International Conference on Robotics and Biomimetics, ROBIO 2011, December 7, 2011 - December 11, 2011*, Phuket, Thailand, 2011, pp. 2031-2036.

[60] C. Rui*, et al.*, "Design of a double-tracked wall climbing robot based on electrostatic adhesion mechanism," in *Advanced Robotics and its Social Impacts (ARSO), 2013 IEEE Workshop on*, 2013, pp. 212-217.

[61] C. Rui, "A Gecko-Inspired Electroadhesive Wall-Climbing Robot," *Potentials, IEEE,* vol. 34, pp. 15-19, 2015.

[62] W. Hongqiang and A. Yamamoto, "A thin electroadhesive inchworm climbing robot driven by an electrostatic film actuator for inspection in a narrow gap," in *Safety, Security, and Rescue Robotics (SSRR), 2013 IEEE International Symposium on*, 2013, pp. 1-6.

[63] M. Osswald and F. Iida, "Design and control of a climbing robot based on hot melt adhesion," *Robotics and Autonomous Systems,* vol. 61, pp. 616-625, 2013.

[64] A. Sintov*, et al.*, "Design and motion planning of an autonomous climbing robot with claws," *Robotics and Autonomous Systems,* vol. 59, pp. 1008-1019, 2011.

[65] G. Yisheng*, et al.*, "A Modular Biped Wall-Climbing Robot With High Mobility and Manipulating Function," *Mechatronics, IEEE/ASME Transactions on,* vol. 18, pp. 1787-1798, 2013.

[66] H. Zhu*, et al.*, "W-climbot: A modular biped wall-climbing robot," in *2010 IEEE International Conference on Mechatronics and Automation, ICMA 2010, August 4, 2010 - August 7, 2010*, Xi'an, China, 2010, pp. 1399-1404.

[67] J. Xiao*, et al.*, "Intelligent control for wall climbing robot," in *2009 Chinese Control and Decision Conference, CCDC 2009, June 17, 2009 - June 19, 2009*, Guilin, China, 2009, pp. 1336-1341.

[68] R. Liu*, et al.*, "Wall climbing robot using electrostatic adhesion force generated by flexible interdigital electrodes," *International Journal of Advanced Robotic Systems,* vol. 10, 2013.

[69] M. Tavakoli*, et al.*, "OmniClimbers: Omni-directional magnetic wheeled climbing robots for inspection of ferromagnetic structures," *Robotics and Autonomous Systems,* vol. 61, pp. 997-1007, 2013.

[70] X. T. D. Z. Z. L. J. Chen, "An Omni-directional Wall-climbing Microrobot with Magnetic Wheels Directly Integrated with Electromagnetic Micromotors," *International Journal of Advanced Robotic Systems,* 2012.

[71] N. Tunawattana*, et al.*, "Design of an underwater positioning sensor for crawling ship hull maintenance robots," *Proceedings of The Institution of Mechanical Engineers Part M-journal of Engineering for The Maritime Environment,* vol. 224, pp. 115-125, 2010.

[72] L. Jun*, et al.*, "BIT Climber: A centrifugal impeller-based wall climbing robot," in *Mechatronics and Automation, 2009. ICMA 2009. International Conference on*, 2009, pp. 4605-4609.

[73] J. Shang*, et al.*, "Design of a climbing robot for inspecting aircraft wings and fuselage," *Industrial Robot: An International Journal,* vol. 34, pp. 495-502, 2007.

[74] H. Zhang*, et al.*, "Effective Pneumatic Scheme and Control Strategy of a Climbing Robot for Class Wall Cleaning on High-rise Buildings," *International Journal of Advanced Robotic Systems,* 2008.

[75] Y. Wang and Z. Jianhua, "Autonomous Air Duct Cleaning Robot System," in *Circuits and Systems, 2006. MWSCAS '06. 49th IEEE International Midwest Symposium on*, 2006, pp. 510-513.

[76] M. F. Yusoff*, et al.*, "Development of Air Conditional Route Wireless Inspection Robot," *Procedia Engineering,* vol. 41, pp. 874-880, 2012.

[77] A. Ariga*, et al.*, "Wall climbing robot in narrow space with pantograph-type structure," in *Robotics and Biomimetics (ROBIO), 2010 IEEE International Conference on*, 2010, pp. 1507-1512.

[78] A. Nayak and S. K. Pradhan, "Design of a New In-Pipe Inspection Robot," *Procedia Engineering,* vol. 97, pp. 2081-2091, 2014.

[79] A. Gargade*, et al.*, "Modelling and Analysis of Pipe Inspection Robot," *International Journal of Emerging Technology and Advanced Engineering,* vol. 3, pp. 120-126, 2013.

[80] K. Young-Sik*, et al.*, "Design and motion planning of a two-moduled indoor pipeline inspection robot," in *Robotics and Automation, 2008. ICRA 2008. IEEE International Conference on*, 2008, pp. 3998-4004.

[81] M. M. Moghaddam*, et al.*, "IN-PIPE INSPECTION CRAWLER ADAPTABLE TO THE PIPE INTERIOR DIAMETER," *International Journal of Robotics & Automation,* vol. 26, pp. 135-145, 2011.

[82] S. Wakimoto*, et al.*, "A micro snake-like robot for small pipe inspection," in *Micromechatronics and Human Science, 2003. MHS 2003. Proceedings of 2003 International Symposium on*, 2003, pp. 303-308.

[83] S. A. Fjerdingen*, et al.*, "A snake-like robot for internal inspection of complex pipe structures (PIKo)," in *Intelligent Robots and Systems, 2009. IROS 2009. IEEE/RSJ International Conference on*, 2009, pp. 5665-5671.

[84] A. Zagler and F. Pfeiffer, ""MORITZ" a pipe crawler for tube junctions," in *Robotics and Automation, 2003. Proceedings. ICRA '03. IEEE International Conference on*, 2003, pp. 2954-2959 vol.3.

[85] M. R. A. M. Zin*, et al.*, "Development of a Low Cost Small Sized In-Pipe Robot," *Procedia Engineering,* vol. 41, pp. 1469-1475, 2012.

## List of Publications


1. Yuan Chang, Xiao-Qi Chen. “Design of A Scalable Wall Climbing Robot for Inter-Plane Traversing,” The 4th International Conference on Robotic Welding, Intelligence and Automation (RWIA’2014), Shanghai, China, Oct. 25-27, 2014.
2. Chang Y., Chen, X.Q. (2015), "Design of a Scalable Wall Climbing Robot for Inter-Plane Traversing", Robotic Welding, Intelligence and Automation, Advances in Intelligent System, Computing, Vol. 363, Springer Verlag, Editors: Tarn, T.-J., Chen S.B., Chen, X.Q, ISBN 978-3-319-18997-0, DOI 10.1007/978-3-319-18997-0, pp.145-158.